UNIVERSITY OF CALGARY

Evaluating Tile Drainage Systems
as a Method of Salt Remediation in Alberta

by

Amanda Dawn Smith

A THESIS
SUBMITTED TO THE FACULTY OF GRADUATE STUDIES
IN PARTIAL FULFILMENT OF THE REQUIREMENTS FOR THE
DEGREE OF MASTER OF SCIENCE

DEPARTMENT OF GEOSCIENCE
CALGARY, ALBERTA
MARCH, 2008

UNIVERSITY OF CALGARY

FACULTY OF GRADUATE STUDIES

The undersigned certify that they have read, and recommend to the Faculty of Graduate Studies for acceptance, a thesis entitled "Evaluating Tile Drainage Systems as a Method of Salt Remediation in Alberta" submitted by Amanda Smith in partial fulfilment of the requirements of the degree of Master of Science.

_____

Supervisor, Dr. Laurence R. Bentley, Department of Geoscience

_____

Dr. Masaki Hayashi, Department of Geoscience

_____

Dr. Gopal Achari, Department of Civil Engineering

_____

Date

Abstract

The effectiveness of tile drainage systems for saline produced water remediation in Alberta has not been thoroughly evaluated, despite their widespread use for this purpose. A density-dependent variably-saturated groundwater flow and transport model was constructed for a well-characterised historical produced water release site with a tile drainage salt remediation system. Site specific information incorporated into the numerical model included soil hydraulic parameters, hydraulic conductivities and hydraulic head data. The historical chloride distribution at the site was used to calibrate the numerical model. The goal of the numerical modeling was to gain an improved understanding of salt transport to tile drains in the shallow subsurface which may ultimately lead to more effective management of salt-impacted sites. The model was found to be sensitive to density-dependent flow and the top time-variable infiltration boundary. Simulations evaluating tile drainage system design parameters suggest that more closely spaced tile drains maximise chloride production and that irrigating the tile drainage area could enhance chloride flushing if the net water deficit at the study site is overcome. The influence of the hydrogeologic and contaminant transport setting on tile drainage system remediation times was investigated by comparing simulation results from flow systems with aquifer support from a underlying contaminated aquifer, an underlying uncontaminated aquifer, and an underlying aquitard. The best-case salt remediation scenario of these was a tile drainage system with water support from an underlying uncontaminated aquifer. The chloride concentrations in this scenario remained lower at depth than the other scenarios and decreased much more quickly over time in the unsaturated zone. This underlines the importance of quick response time for salt releases. The simulation results show that salt remediation with tile drainage systems depends on a complex interaction between the site soil hydraulic properties, the climate and the hydraulic characteristics of the underlying aquifer. Predictive simulations suggest that salt remediation times in the Canadian Prairies are long and likely greater than 100 years due to the low levels of precipitation and low hydraulic conductivity of the soils.

Acknowledgements

> Constant dripping hollows out a stone.
> *-Lucretius*

Table of Contents

List of Tables

List of Figures

Chapter One: Introduction

1.1 Research Objectives

The effectiveness of tile drainage systems for saline produced water remediation in Alberta has not been thoroughly evaluated, despite their widespread use for this purpose. The research objective of this project was to further the understanding of salt transport to tile drains. To this end, a density-dependent variably-saturated groundwater flow and transport model was constructed for a well-characterised historical produced water release site with a tile drainage salt remediation system. Soil samples and monitoring data collected at the site over several years was used to construct the model and evaluate its performance. It is hoped that an improved understanding of salt transport to tile drains will ultimately lead to more effective remediation design and risk assessment for salt-impacted sites.

The contributions of this thesis include new estimates of silt loam soil hydraulic parameters and monthly infiltration values for the site from 1984 to 2006 calculated using historical weather data and the output of a moisture balance model calibrated for Alberta. New results for two classic density-dependent flow and transport problems (the Henry (1964) and the Elder (1967)) were used to benchmark the variably-saturated density-dependent flow simulator MIN3PD (Henderson et al., 2007). Two site-specific 2D variably-saturated numerical groundwater flow and transport models were developed in MIN3PD to better understand the transport behaviour of chloride in the unsaturated and shallow saturated zones. A tile drain boundary condition was used in one of the numerical models to simulate the transport behaviour of chloride in the unsaturated and saturated zones in the context of chloride remediation with tile drain systems. The results of the tile drain simulations contribute to our understanding of chloride remediation from the unsaturated zone and show that the success of chloride remediation using tile drainage systems depends on a complex interaction between the site soil hydraulic properties, the climate and the hydraulic characteristics of the underlying aquifer.

This thesis is organised into chapters starting with a description of the study area in Chapter Two that includes previous investigations and the regional setting of the study area including climate, hydrogeology and groundwater quality at the site. Data collection, methods, analysis and results for new data collected at the site for this study are described in Chapter Three. Chapter Four describes the conceptual groundwater flow and contaminant transport model and water budget developed for the site using new and historical data. Chapter Five includes the results of the density-dependent flow and transport benchmarking problems in MIN3PD. Chapter Six describes the preliminary, large scale numerical model developed for the site and the results of the model sensitivity analysis. Chapter Seven describes the smaller scale numerical model that was developed for the tile drainage simulations and includes the results of the tile drainage system evaluation scenarios. Finally, discussion of the significance of the tile drain simulation results and conclusions that can be drawn from this study including suggestions for future work are included in Chapter Eight.

1.2 Background

1.2.1 The Oil and Gas Economy

The oil and gas industry has been a part of the Alberta economy for almost 125 years when natural gas was accidentally discovered near Medicine Hat in 1883. By 1914, both oil and gas were discovered in Turner Valley, located in the south-west foothills of Alberta, and it became the first major oilfield in Canada. The industry began to expand across northern Alberta with the discovery of oil in Leduc, located just south of Edmonton, by Imperial Oil in 1947. There was such a large influx of labour into the region that the town of Devon was constructed by Imperial for its employees shortly after.

The oil and gas industry has brought great economic benefit to Alberta. The province received $9.8 billion in oil and gas royalty payments in the 2004-2005 fiscal year (Canadian Association of Petroleum Producers, 2006). This was equivalent to 33% of total government revenues. It has been estimated that if Alberta did not have oil and gas

revenues, the province would need a 20% sales tax to make up the difference. Beyond the income earned in royalties, the oil and gas industry has also ensured that Alberta currently has the highest rate of economic growth in Canada, 3.7% over the last 20 years, a provincial GDP per capita that is 20% higher than the rest of Canada, and 275,000 direct and indirect jobs. This has helped to make the unemployment rate in Alberta, 4.6% in 2004, the lowest in Canada. Because the industry depends on highly skilled and educated labour, Alberta also has the most university degrees per capita compared with the rest of Canada (Canadian Association of Petroleum Producers, 2006).

An environmental cost, however, has come with the economic benefit. In the early days of the industry, a seemingly unlimited supply of oil and gas provided little motivation for conservation practices to be implemented. In Turner Valley, for example, a lack of financial market made it standard practice to burn off excess natural gas in the field. It is estimated that approximately 90% of the field's natural gas was wasted in this manner. Accidents associated with oil and gas production, including well blowouts, pipeline breaks and other spills have also resulted in significant localised environmental impact over the years.

1.2.2 Environmental Legislation

The provincial government began to introduce conservation measures with the 1931 Oil and Gas Wells Act. One year later, the Turner Valley Conservation Act was passed; however, both acts were later declared unconstitutional by the federal government. In 1938, the Alberta Petroleum and Natural Gas Conservation Board, later the Alberta Energy and Utilities Board, was successfully established. A major turning point in environmental conservation in Alberta came in 1992 with the introduction of the Environmental Protection and Enhancement Act. The act covers the protection of air, land and water. The purpose of the Act is to support and promote the protection, enhancement and wise use of the environment (Province of Alberta, 1992).

Among other things, the act recognizes the need for Alberta's economic growth and prosperity in an environmentally responsible manner, the importance of preventing and mitigating the environmental impact of development, and the responsibility of polluters to pay for the costs of their actions (Province of Alberta, 1992). Groundwater use and protection is becoming an issue of increasing importance as population growth and industrial and agricultural development are putting more demand on Alberta's water supply. Sustainable groundwater use practices are currently being developed in Alberta to ensure a clean and adequate supply for future generations (Alberta Environment, 2003). Part of this strategy includes protection of groundwater quantity and quality from impact due to oil and gas industry activities.

1.2.3 Environmental Impact of Salts

The primary soil and groundwater contaminants related to the oil and gas industry are hydrocarbons, salts, heavy metals and process chemicals (Marr-Laing and Severson-Baker, 1999). Of these, salts are often the most difficult to deal with due to the fact that they are highly mobile and do not biodegrade over time. The salts originate from the oil-water-gas emulsion that is produced at an oil or gas well. At a processing facility, the emulsion is separated into oil, produced water and gas phases. The produced water is typically a sodium-chloride (NaCl) type water and can have a chloride concentration ranging from 23,000 mg/L up to 150,000 mg/L or greater (Hitchon et al., 1998). Typical environmental impacts associated with excess salt in soil and surface or groundwater include degradation of soil chemical properties and impaired vegetative growth, degradation of soil physical properties caused by excess sodium, and degraded water quality (Alberta Environment, 2001).

One major source of salt contamination is pipeline failures. As of the end of 1997, there were approximately 266,000 km of energy-related pipelines under the jurisdiction of the Alberta Energy and Utilities Board (Alberta Energy and Utilities Board, 1998). Between 1980 and 1997, a total of 12,137 pipeline failures were reported, or an average of 674 failures per year (Alberta Energy and Utilities Board, 1998). Failures of fresh and/or salt

water pipelines occurred twice as frequently, 16.9 failures per 1,000 km, as the next highest category of line failure which was multiphase pipelines at 8.1 failures per 1,000 km (Alberta Energy and Utilities Board, 1998). Although statistics on the individual breakdown of fresh versus salt-water pipeline breaks were not available, because 66.5% of the fresh or salt-water pipeline failures were caused by internal corrosion of the line (Alberta Energy and Utilities Board, 1998), it is reasonable to assume that the majority of the water pipeline failures involved salt-water since it is much more corrosive than fresh water. Despite a widespread reform towards a higher standard of environmental awareness in the industry in recent years, it is likely that well blow-outs, pipeline breaks and tank leakages will continue to occur and the clean-up of many historical spills has yet to be completed.

1.2.4 Salt Remediation

An adverse effect is defined in the Environmental Protection and Enhancement Act as impairment of, or damage to, the environment, human health, or safety or property (Province of Alberta, 1992). When it is determined that a salt-release has caused an adverse effect, then remedial measures must be taken with the goal that contaminant concentrations must meet or exceed remediation objectives (background levels, generic guidelines or site-specific risk-based objectives), any residual contamination must not adversely affect current or potential future receptors under the existing land use, and that capability of the affected area must be the same after remediation as before the impact occurred (Alberta Environment, 2001).

The chemical behaviour of NaCl largely dictates soil and groundwater salt remediation techniques. Chloride behaves as a conservative species in groundwater and does not participate in chemical reactions, such as biodegradation, that would cause a reduction of source-mass over time. To reduce the mass of chloride in soil or groundwater, the soil or groundwater containing the mass of chloride must be removed from the system or diluted with clean soil or groundwater. When Na^+ from the soil porewater replaces Ca^{2+}, the relative amount of Na^+ can become greater than $[Ca^{2+} + Mg^{2+}]$ in the soil minerals. This

can cause the structure of medium and fine textured soils to degrade, especially if the EC of the soil is relatively low. This phenomenon is known as clay dispersion and it ultimately leads to a decrease in the hydraulic conductivity of the soil (Aringhieri and Giachetti, 2001) which further complicates remediation efforts.

When a salt release occurs, the most highly impacted soil is generally excavated, trucked to an approved landfill facility for disposal and clean fill is brought in. If this action is undertaken soon after the salt release occurs, it is likely that the majority of impact to groundwater quality will be mitigated. Installation of groundwater monitoring wells and initiation of an annual groundwater monitoring program may be sufficient to address any residual salt concentrations. This may only be economically feasible when a salt release is relatively small and shallow since costs associated with excavation, trucking and disposing of very large volumes of soil can be considerable. In cases where salt releases occur over larger areas, in-situ salt remediation is generally pursued.

For in-situ remediation, first remedial efforts are generally focused on restoring the structure and drainage capability of the soil due to the tendency of sodium to cause clay dispersion and soil swelling once the preferential leaching of chloride begins to occur. Calcium amendments such as liquid calcium-nitrate ($Ca(NO_3)_2 \cdot 4H_2O$) or gypsum ($CaSO_4 \cdot 2H_2O$) are usually applied and incorporated into the soil. Excavation of the worst-impacted soil is often undertaken in conjunction with in-situ remediation. The remaining salts are then removed from the soil by passive leaching with natural precipitation or by enhanced leaching with irrigation and precipitation. Where there is a risk of salts moving into groundwater or hydraulic conditions prevent the salts from being leached out of the soil root zone, for example under groundwater discharge conditions, tile drainage systems must be installed to collect the NaCl leachate (Alberta Environment, 2001). Although in widespread use, an exact figure is not available regarding the number of tile drainage systems currently in operation in Alberta. Historically these systems were often installed and then largely forgotten resulting in

poor monitoring and reporting. It is estimated that the number is quite large, however, given the current and historical prevalence of produced water spills.

1.2.5 Tile Drainage Systems

Tile drainage systems are subsurface conduits for removing excess water. The conduits were historically were made of clay or concrete but today are more commonly made of perforated corrugated plastic. The drainage lines are often installed in the subsurface using specialised trenching equipment or tractor mounted plows. The systems are designed such that each drainage line is installed at slight grade to allow the water to drain to a central outlet area. If the water quality is good, the drainage effluent may be discharged directly at the ground surface or into a network of drainage ditches. If the drainage effluent contains a high concentration of dissolved salts or other contaminants, the water is generally collected onsite in tanks and either deep well injected or treated prior to surface discharge.

Tile drainage systems are traditionally installed for agricultural purposes to enhance crop yields on poorly drained but highly productive soils and to reduce annual variability in crop yields. These systems are in widespread use in both the United States (U.S.) and Canada. In the U.S., it is estimated that 34% of all cropland has been tile drained (Skaggs et al., 1994). In Ontario, 43% of land classified as crop land as been tile drained (OMAFRA, 1996). Tile drainage for agricultural purposes is primarily used for wetland drainage and is not as widespread in Alberta due to a continental climate characterised by low levels of precipitation (Wilson et al., 2001).

1.2.6 Solute Transport

Solute transport through the unsaturated zone has received increasing attention in recent years as the U.S. Department of Energy funds research to determine if the unsaturated zone at Yucca Mountain, Nevada, is a suitable repository for high-level nuclear waste. Indeed, any attempt to protect groundwater from contamination usually requires an understanding of the rates and volumes of solute movement through the unsaturated zone

(Richard and Steenhuis, 1988). Although our capacity to accurately measure and model multi-dimensional field-scale water flow and solute transport under variably-saturated conditions is still limited, tile drainage systems have recently become the focus of many investigations as it has been recognised that tile drains are good spatial integrators of field-scale flow and chemical transport processes, including matrix and preferential flow (Mohanty et al., 1998). Tile drains collect water near the surface of the groundwater table, can drain areas on a spatial scale of well over 10 m and have outlets where water samples can easily be retrieved (Richard and Steenhuis, 1988).

A rather substantial body of research exists evaluating nitrate-nitrogen leaching in the U.S. in connection with tile-drained agricultural land, fuelled by concerns about the hypoxic zone in the Gulf of Mexico and other areas worldwide (Kladivko et al., 2004). A similar body of work is present for pesticide transport processes in connection with tile-drained agricultural fields (Boivin et al., 2006). Much of the previous research applicable to salt remediation has focused on evaluation and optimisation of pump and treat techniques (Guan and Aral, 1999). The objective of pump and treat techniques is to create a zone of hydraulic capture to remove salt-impacted groundwater from the saturated zone and prevent impact to downgradient receptors. Little research has been done on the use of tile drainage systems to remove salts from the unsaturated zone, although some work examining the use of tile drain systems in semi-arid regions to keep naturally occurring saline water from rising into agricultural crop rooting zones is currently being done (Hornbuckle et al., 2007). The focus of this research is in reducing the removal of excess saline water from below the rooting zone and minimising the salinity of the drainage system effluent thereby reducing the salt load to drainage water receptors. This is in contrast to the goal of a tile drainage salt remediation system which is to remove as much of the salt mass from the site as possible. No peer-reviewed literature could be found on the use of tile drainage systems for salt remediation in Alberta.

Chapter Two: Study Area

2.1 Site Description

The study area is located at former oil and gas battery, southwest of Edmonton, Alberta. A battery is an intermediate oil and gas production facility, normally located between a group of wells and a gas plant, where the multi-phase effluent produced at a well is separated into oil, gas and water phases. The oil, gas and water are then measured, re-combined with production from other wells, and shipped to a processing plant.

The site began operations sometime in the mid to late 1960s and a major pipeline release is believed to have occurred at the site sometime in the 1980s; however, the exact year is unknown. A large volume of saline produced water and hydrocarbons were released at the site; however, the volume and the total dissolved solids (TDS) concentration of the produced water release is also unknown. Over the operating history of the site, other smaller scale produced water spills and leaks likely have also contributed to the currently observed salt plume at the site.

The facility was decommissioned and the majority of aboveground and underground facilities were removed in the mid 1990s. Former site facilities included separator equipment, an injection plant, a pump station, above ground and underground tanks and underground pipelines. Two flare pits and two production wells were also historically located adjacent to the battery.

2.2 Previous Site Investigations

In 1998, WorleyParsons Komex (formerly Komex International Ltd.) was retained to conduct a phase I environmental investigation to identify potential impacts to soil and groundwater quality at the site (WorelyParsons Komex, 2005a). The site investigation results indicated that approximately 33,085 m^3 of soil onsite contained salinity/sodicity levels above the regulatory guidelines (WorelyParsons Komex, 2005a). Approximately 6,085 m^3 of soil containing hydrocarbons and salts was excavated and placed in a biopile

for hydrocarbon remediation. The remaining 27,000 m^3 of salt-impacted soil was left in place for in-situ remediation using a tile drainage system that was installed at the site and commissioned in March 2003 (WorelyParsons Komex, 2005b). Work conducted at the site by WorelyParsons Komex, AMEC and others between 1998 and 2006 has included the following:

- Electromagnetic (EM) geophysical surveys conducted in 1998, 1999, 2003 and 2004.
- Borehole drilling, collection and laboratory analysis of soil samples and installation of seven shallow groundwater monitoring wells in 1998.
- A groundwater sampling event was conducted in 1998.
- Borehole drilling, collection and laboratory analysis of soil samples and installation of three deeper groundwater monitoring wells in 1999.
- Excavation of both flare pits and the hydrocarbon-impacted soil in the vicinity of the well centres in 2001.
- Application of calcium amendments (gypsum and liquid calcium-nitrate) to the soil and installation of a tile drainage system to address salinity levels in the soil and groundwater in March 2003. Monitoring wells installed prior to 2003 were destroyed during installation of the tile drainage system.
- Borehole drilling, collection and analysis of soil samples and installation of seven new shallow groundwater monitoring wells in August 2004.
- Monitoring of the tile drainage system including measuring water levels in the monitoring wells and collecting drainage effluent samples and groundwater samples for laboratory analysis in 2004, 2005 and 2006.
- Establishment of a research plot at the site to evaluate phytoremediation of salts.

Work conducted at the site by the University of Calgary under the direction of Dr. Laurence Bentley has included the following:

- Six, three-dimensional (3D) electrical resistivity imaging (ERI) surveys were conducted over two zones in July and November 2004, May and October 2005, and May and October 2006.

- Push tool electrical conductivity profile surveys were conducted in November 2004, October 2005 and October 2006.
- Soil coring was conducted in November 2004, October 2005 and October 2006.

A site plan showing the locations of the tile drainage system lines as well as borehole, coring and monitoring well locations is included in Figure 2.1.

2.3 Regional Setting

2.3.1 Physiography and Climate

The study area is located within the Central Parkland Natural Region of Alberta at an elevation of 724 m above mean sea level and contains aspen woodlands, fescue grasslands, shrublands and wetlands. Topography in the area is characterised by undulating plains and hummocky uplands (Alberta Community Development, 2004). Based on site topography, surface water at the site likely drains northwest toward an unnamed creek located 1.75 km north of the site. The study area is extensively cultivated. The main vegetation consists of aspen interspersed with grasslands dominated by plains rough fescue (Alberta Community Development, 2004). The predominant land uses in the area are oil and gas production, agriculture and grazing.

The study area is characterised by severe winters and cool summers. The nearest Environment Canada weather monitoring station to the study site is located in Calmar, Alberta. The maximum daily average temperature based on Calmar Climate Normals for the period 1971-2000 (Environment Canada, 2007a) occurs in July (16.2°C), while the minimum daily average temperature occurs in January (-2.9°C). Total annual precipitation in the area based on Calmar Climate Normals for the period 1971-2000 is 521 mm, of which approximately 25% occurs during the winter months as snowfall (Environment Canada, 2007a).

Figure 2.1. Site plan of study area.
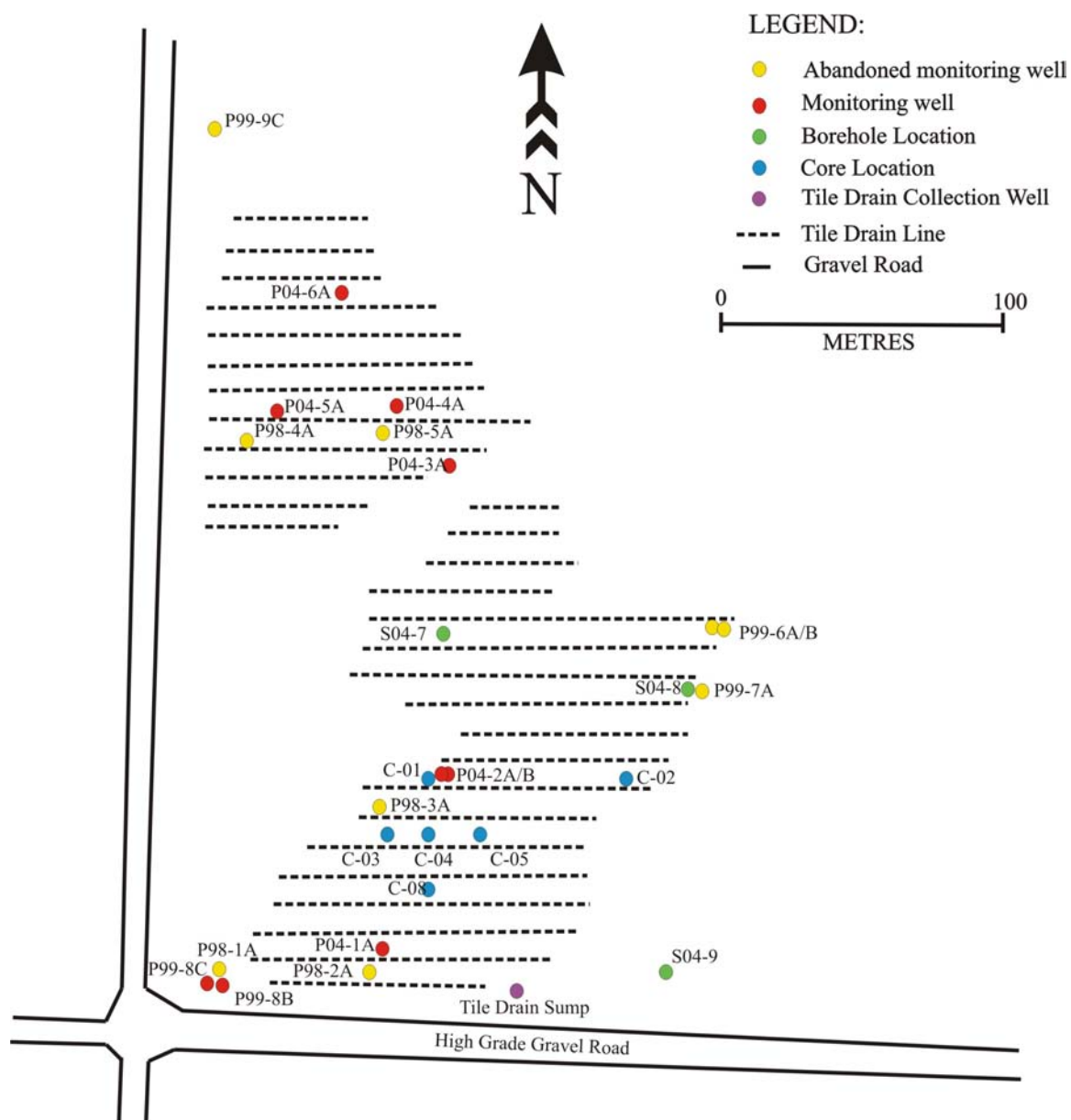
Monthly precipitation over the period 1971-2000 ranged from a minimum of 17.3 mm in February to a maximum of 104.2 mm in July (Environment Canada, 2007a). The extreme daily rainfall event in the area was 132 mm of rainfall recorded on July 3, 1999 (Environment Canada, 2007a).

2.3.2 Geology
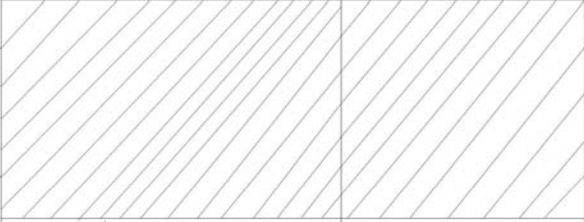
2.3.2.1 Tectonic Setting and Bedrock

The study area is located within the Western Canadian Sedimentary Foreland Basin. During the foreland basin stage, the Western Canadian Sedimentary Basin was subsiding due to isostatic flexure of the North American lithosphere under the weight of the tectonically thickened supracrustal rocks of the foreland thrust and fold belt (Mossop and Shetsen, 1994). The foreland basin was formed by a migrating moat that trapped the detrital outwash eroded from the emerging foreland thrust and fold belt (Mossop and Shetsen, 1994).

A regional stratigraphic column is included in Figure 2.2. The uppermost bedrock unit in the study area is the Cretaceous Upper Horseshoe Canyon Formation which is part of the Edmonton Group (Mossop and Shetsen, 1994). The Upper Horseshoe Canyon Formation has a maximum thickness of 100 m (Prairie Farm Rehabilitation Administration, 1999). The lowermost Horseshoe Canyon sandstones represent the leading edge of a late Cretaceous/Tertiary eastward prograding clastic wedge (Mossop and Shetsen, 1994). The remainder of the Horseshoe Canyon Formation consists primarily of fluvial channel sandstones, floodplain siltstones and shales as well as coals and carbonaceous shales (Mossop and Shetsen, 1994). Because of the low-energy environment in which deposition occurred, the sandstones, when present, tend to be finer grained (Prairie Farm Rehabilitation Administration, 1999). The lower 60 to 70 m and the upper 30 to 50 m of the Horseshoe Canyon Formation can include coarser grained sandstone deposits (Prairie Farm Rehabilitation Administration, 1999). The Bearpaw Formation underlies the Horseshoe Canyon Formation and consists primarily of laminated shale and siltstone with some sandstone beds and lenses of kaolinitic claystone deposited in a marine

environment. The Belly River Formation underlies the Bearpaw Formation and is primarily of fluvial origin consisting of light grey to buff, medium to fine grained sandstone and siltstone with minor mudstone and coal. The Lea Park Formation underlies the Belly River Formation and consists of dark grey to brown mudstone and siltstone (Mossop and Shetsen, 1994).

Figure 2.2. Regional stratigraphy.

Period	Formation		Thickness in Study Area
Quaternary	Laurentide Drift		20 m
Tertiary			
Cretaceous	Edmonton Group	Horseshoe Canyon	>170 m
		Bearpaw	20 m
		Belly River	300 m
		Lea Park	60 m

2.3.2.2 Surficial Sediments and Soils

Surficial sediments in the study area consist mainly of glacial till with lacustrine, fluvial, and eolian deposits. Soils in the area are mapped as Chernozems and consist of Chernozemic Navarre Silty Clay Loam and Malmo Silty Loam (Bowser et al., 1962). Navarre Silty Clay Loam is described as an orthic black soil developed on slightly saline lacustrine material. The Malmo Silty Loam is described as eluviated black soil developed on lacustrine material (Bowser et al., 1962). The soil capability for agriculture in the area is class 1 where soils in this class have no significant limitations in use for crops (Agricultural and Rural Development Act, 1967). The thickness of the surficial deposits in the study area is approximately 20 m (WorelyParsons Komex, 2005b).

2.3.3 Hydrogeology

The regional shallow groundwater flow direction in the study area is north, toward the North Saskatchewan River. The regional aquifer in the study area consists of the sandstone deposits of the Upper Horseshoe Canyon Formation. Groundwater within the Upper Horseshoe Canyon Aquifer is mainly a sodium-sulphate or sodium-bicarbonate type with TDS concentrations between 500 and 1,000 mg/L (Prairie Farm Rehabilitation Administration, 1999). Background chloride concentrations within the Upper Horseshoe Canyon Aquifer are expected to be less than 100 mg/L (Prairie Farm Rehabilitation Administration, 1999).

The apparent yields for water wells completed within the Upper Horseshoe Canyon Aquifer range from less than 10 m³/day to more than 100 m³/day (Prairie Farm Rehabilitation Administration, 1999). The majority (69%) of the apparent yield values that were available are between 10 and 50 m³/day (Prairie Farm Rehabilitation Administration, 1999). The highest well yields would be expected where the Upper Horseshoe Canyon Formation subcrops under the surficial deposits. This is due to weathering processes that increase the secondary permeability of the formation (Prairie Farm Rehabilitation Administration, 1999).

2.3.4 Groundwater Use

A search was performed of Alberta Environment's Groundwater Information Centre Water Well Drilling Report database for six sections surrounding the site to identify nearby groundwater users (Groundwater Information Centre, 2007). The search yielded a total of 43 records. The majority of the water wells in the records were identified as being for domestic or stock purposes. Four wells were identified as test or exploration wells and two wells were identified as being for industrial use (Groundwater Information Centre, 2007). The total depths of the wells ranged from 6.10 to 91.44 m; however, the majority of the wells had total depths ranging between 30 and 45 m and were interpreted to be completed in the Upper Horseshoe Canyon sandstone aquifer.

2.4 Groundwater Quality

Historical groundwater quality data prior to the construction of the tile drainage field is available from November 1998, and March and June 1999 (Table 2.1). Groundwater quality results from 2004, 2005 and 2006 at two indicator monitoring wells are included in Table 2.2. Monitoring wells P04-2A and P04-2B were chosen as indicator wells for this study since they are nested wells and are located in the middle of the south tile drainage field, which was the area of interest for this study. Both the nested wells are completed with 1.52 m screen intervals with the base of screen reaching a depth of 3.10 m for the shallow well (P04-2A) and 8.08 m for the deeper well (P04-2B).

The 1998-1999 chloride concentrations in monitoring wells completed within the shallow surficial sediments ranged from 7,050 mg/L at P98-5A, located within the current north half of the drainage field to 19,000 mg/L at P99-6A, located within the former flare pit area in the east half of the site (Table 2.1; Figure 2.1). Sodium concentrations in 1998-1999 within the surficial sediments ranged from 1,500 mg/L at P98-5A, located within the current north half of the tile drainage field, to 4,170 mg/L at P98-1A, located in the southwest corner of the current drainage field area.

Table 2.1. Site groundwater quality in 1998 prior to the installation of the tile drainage system.

Monitoring Location	Date	Ca (mg/L)	Mg (mg/L)	Na (mg/L)	K (mg/L)	Fe (mg/L)	Mn (mg/L)	Cl (mg/L)	SO_4 (mg/L)	NO_3+NO_2-N (mg/L)	HCO_3 (mg/L)	Hardness (mg/L)	TDS (mg/L)
Shallow Glacial Till													
P98-1A	10-Nov-98	5,510	820	*4,170*	23.9	<0.003	*0.052*	*18,700*	*615*	7.07	274	---	*32,700*
P98-2A	10-Nov-98	4,050	759	*3,250*	31.1	*1.740*	*18.80*	*13,700*	439	0.63	299	---	*25,000*
P98-3A	10-Nov-98	1,240	303	*2,980*	32.5	0.008	*2.80*	*8,110*	464	3.64	471	---	*15,300*
P98-4A	10-Nov-98	2,710	492	*2,990*	46.7	0.012	*5.98*	*11,900*	428	5.95	364	---	*22,100*
P98-5A	10-Nov-98	1,480	391	*1,500*	13.6	0.032	*4.61*	*7,050*	*517*	3.46	310	---	*13,600*
P99-6A	10-Mar-99	---	---	---	---	---	---	*19,000*	---	---	---	---	---
P99-7A	10-Mar-99	3,470	805	*2,400*	29.2	*3.57*	*10.9*	*11,000*	---	---	---	---	---
Lower Glacial Till/ Upper Horseshoe Canyon													
P99-8B	17-Jun-99	240	62	*254*	7	<0.005	*1*	21	*804*	0	579	855	*1,880*
P99-8C	10-Mar-99	16.6	3.2	*320*	2.0	*0.350*	0.033	17.2	140	0.04	727	55	---
P99-9C	10-Mar-99	339	83.8	*371*	7.7	0.144	*0.571*	4.6	*1,380*	0.41	653	---	---
Canadian Drinking Water Guidelines*		NG	NG	200(AO)	NG	0.3(AO)	0.05(AO)	250(AO)	500(AO)	10(MAC)	NG	NG	500(AO)

--- - denotes parameter not analyzed

NG - no guideline specified

AO - aesthetic objective

MAC - maximum acceptable concentration based on health effects for NO_3

^ - Summary of Guidelines for Canadian Drinking Water Quality (Health Canada, 2006)

Italics - indicates values do not meet drinking water guidelines

Data Source (WorleyParsons Komex, 2005a)

In 1998, chloride and sodium concentrations exceeded water quality guideline values of less than 250 and 200 mg/L, respectively, at each shallow monitoring well (Health Canada, 2006). Each of the shallow monitoring wells was destroyed during the construction of the tile drainage system in 2003.

Groundwater at deep and bedrock monitoring wells P99-8B and P99-9C is a sodium-sulphate type with a total dissolved solids (TDS) concentration of approximately 2,000 mg/L (Table 2.1). Groundwater at deep monitoring well P99-8C is a sodium-bicarbonate type with a TDS concentration of approximately 1,000 mg/L (Table 2.1). The low chloride concentrations each of these wells (5 to 21 mg/L) indicate that the deeper bedrock aquifers at the site have not been impacted by oilfield activity and that the elevated sodium and sulphate concentrations are most likely naturally occurring.

In 2004, chloride concentrations at shallow well P04-2A ranged from 7,700 to 8,970 mg/L while chloride concentrations at deeper well P04-2B ranged from 7,580 to 9,140 mg/L. In 2006, after 3 years of operation of the tile drainage system, chloride concentrations at P04-2A ranged from 4,970 to 7,310 mg/L while chloride concentrations at P04-2B ranged from 7,030 to 7,750 mg/L (Table 2.2). Sodium concentrations at the shallow well (P04-2A) ranged from a maximum of 4,600 mg/L in 2004 to a minimum of 3,080 mg/L in 2006 (Table 2.2). Sodium concentrations at the deeper well (P04-2B) are considerably lower and ranged from a maximum of 1,650 mg/L in 2004 to a minimum of 1,230 mg/L in 2006.

Table 2.2. 2004, 2005 and 2006 groundwater quality results at selected monitoring wells.

Monitoring Location	Date	Ca (mg/L)	Mg (mg/L)	Na (mg/L)	K (mg/L)	Fe (mg/L)	Mn (mg/L)	Cl (mg/L)	SO$_4$ (mg/L)	N0$_3$+NO$_2$-N (mg/L)	HCO$_3$ (mg/L)	Hardness (mg/L)	TDS (mg/L)
Shallow Glacial Till													
P04-2A	5-Aug-04	1,050	230	*3,170*	118.00	0.022	*0.867*	*8,970*	*673*	*20.6*	794	3,570	*16,900*
	7-Oct-04	876.0	182.0	*4,160*	96.3	0.108	*0.083*	*7,700*	*785*	*36.2*	852	2,940	*14,100*
	30-Nov-04	1,140	214	*4,600*	98.60	0.021	*0.610*	*8,930*	*648*	*40.7*	697	3,730	*15,800*
	15-Apr-05	856	224	*3,960*	83.40	0.175	*0.240*	*8,160*	*658*	*30.7*	726	3,100	*15,400*
	29-Jun-05	1,030	219	*4,440*	78.10	*24.6*	*2.730*	*8,520*	*767*	*41.0*	655	3,500	*13,200*
	16-Sep-05	778	155	*3,470*	81.30	*2.84*	*0.81*	*7,380*	*646*	*1.60*	749	2,600	*12,500*
	12-Dec-05	863	170	*4,070*	70.00	*0.70*	*1.28*	*8,440*	*671*	*35.2*	721	2,900	*13,200*
	7-Jun-06	706	164	*3,780*	71.00	*16.40*	*0.49*	*7,310*	*693*	*46.0*	701	2,400	*12,200*
	19-Oct-06	506	113	*3,080*	74.90	*3.50*	*0.19*	*4,970*	*497*	*33.3*	810	1,700	*10,100*
P04-2B	5-Aug-04	2,290	726	*1,650*	49.7	*16.9*	*11.95*	*9,140*	*504*	<0.2	405	8,710	*17,500*
	7-Oct-04	2,340	604	*1,550*	38.6	*61.6*	*10.98*	*7,630*	479	<0.2	485	8,330	*13,300*
	30-Nov-04	2,400	633	*1,420*	36.2	*65.1*	*9.68*	*7,580*	*567*	0.12	368	8,600	*12,800*
	15-Apr-05	2,480	670	*1,250*	31.3	*36.6*	*8.72*	*7,340*	*494*	0.09	408	9,000	*14,000*
	29-Jun-05	2,660	870	*1,280*	30.4	*54.2*	*8.80*	*8,230*	*534*	<0.2	269	10,000	*11,900*
	16-Sep-05	2,460	664	*1,100*	29.6	*47.5*	*7.18*	*8,030*	*487*	<0.2	401	8,900	*12,100*
	12-Dec-05	2,520	669	*1,250*	27.0	*72.9*	*9.59*	*8,270*	*552*	<0.2	421	9,000	*13,000*
	7-Jun-06	2,650	779	*1,400*	29.0	*17.5*	*6.70*	*7,750*	*541*	<0.2	335	9,800	*12,000*
	19-Oct-06	2,360	618	*1,230*	28.5	*52.0*	*6.96*	*7,030*	*409*	<0.2	381	8,400	*12,200*
Canadian Drinking Water Guidelines*		NG	NG	200[AO]	NG	0.3[AO]	0.05[AO]	250[AO]	500[AO]	10[MAC]	NG	NG	500[AO]

--- - denotes parameter not analyzed

NG - no guideline specified

AO - aesthetic objective

MAC - maximum acceptable concentration based on health effects for NO$_3$

^ - Summary of Guidelines for Canadian Drinking Water Quality (Health Canada, 2006)

Italics - indicates values do not meet drinking water guidelines

Data Source (WorleyParsons Komex 2005b, 2006 and AMEC, 2007)

Table 2.3. Tile drainage collection sump water quality 2003-2006.

Monitoring Location	Date	Ca (mg/L)	Mg (mg/L)	Na (mg/L)	K (mg/L)	Fe (mg/L)	Mn (mg/L)	Cl (mg/L)	SO$_4$ (mg/L)	N0$_3$+NO$_2$-N (mg/L)	HCO$_3$ (mg/L)	Hardness (mg/L)	TDS (mg/L)
Tile Drain Sump	6-Oct-03	1,380	264	*897*	17.3	0.221	*0.455*	*3,930*	497	*21.8*	347	4,530	*8,320*
	21-Nov-03	1,460	291	*395*	26.3	0.092	*0.455*	*4,800*	*640*	*16.4*	319	4,840	*9,590*
	15-Jan-04	2,050	375	*1,700*	23.2	<0.006	*0.396*	*6,480*	*540*	*11.9*	243	6,660	*18,800*
	26-May-04	1,530	280	*1,240*	18.5	0.022	*0.244*	*4,870*	*515*	*11.9*	347	4,970	*9,940*
	5-Aug-04	1,550	330	*945*	24.3	0.020	*0.463*	*4,860*	*646*	*17.5*	485	5,230	*9,830*
	13-Sep-04	1,540	338	*1,110*	28.0	0.139	*0.666*	*5,710*	*533*	*13.8*	373	5,240	*10,700*
	7-Oct-04	1,700	325	*1,210*	24.1	0.071	*0.838*	*5,120*	495	*10.1*	395	5,580	*11,500*
	10-Nov-04	1,650	307	*986*	20.5	0.071	*0.928*	*4,400*	460	*10.8*	416	5,380	*11,300*
	30-Nov-04	1,570	316	*1,230*	23.0	0.071	*0.892*	*4,990*	489	8.6	403	5,220	*9,070*
	8-Apr-05	1,850	337	*1,140*	19.2	0.255	*0.790*	*5,290*	*729*	*13.0*	390	6,000	*8,380*
	9-May-05	1,590	295	*1,100*	19.1	*0.730*	*0.930*	*4,780*	*536*	*11.3*	406	5,200	*9,310*
	28-Jun-05	2,150	277	*1,410*	15.6	*0.420*	*0.760*	*4,580*	*667*	*10.8*	389	6,500	*8,100*
	19-Jul-05	1,510	281	*987*	17.6	0.048	*1.050*	*4,920*	*518*	9.7	443	4,900	*9,250*
	16-Aug-05	1,420	278	*913*	16.6	0.211	*0.850*	*4,090*	441	9.7	469	4,700	*8,340*
	16-Sep-05	1,470	267	*904*	14.9	<0.006	*0.920*	*4,470*	*715*	9.0	424	4,800	*8,170*
	18-Oct-05	1,660	304	*1,090*	14.0	0.180	*0.960*	*4,570*	*623*	8.2	429	5,400	*8,310*
	22-Nov-05	1,650	331	*1,080*	19.9	0.080	*0.660*	*5,000*	484	7.1	424	5,500	*8,730*
	12-Dec-05	2,160	381	*1,610*	15.8	0.120	*0.210*	*7,380*	*594*	9.8	383	7,000	*12,000*
	7-Jun-06	1,650	349	*1,120*	13.6	*0.770*	*0.540*	*4,900*	*671*	*14.0*	423	5,500	*9,630*
	13-Sep-06	---	---	*1,340*	---	---	---	*5,370*	---	---	---	---	---
	17-Oct-06	1,960	339	*1,420*	23.1	0.210	*1.430*	*5,500*	*523*	6.5	510	6,300	*10,000*
	5-Dec-06	---	---	*1,480*	---	---	---	*5,630*	---	---	---	---	---
Canadian Drinking Water Guidelines*		NG	NG	200$^{(AO)}$	NG	0.3$^{(AO)}$	0.05$^{(AO)}$	250$^{(AO)}$	500$^{(AO)}$	10$^{(MAC)}$	NG	NG	500$^{(AO)}$

--- - denotes parameter not analyzed

NG - no guideline specified

^{AO} - aesthetic objective

^{MAC} - maximum acceptable concentration based on health effects for NO$_3$

^ - Summary of Guidelines for Canadian Drinking Water Quality (Health Canada, 2006)

Italics - indicates values do not meet drinking water guidelines

Data Source (WorleyParsons Komex 2005b, 2006 and AMEC, 2007)

Sodium and chloride concentrations were analysed at the tile drainage collection sump periodically between October 2003 and December 2006 (Table 2.3). Chloride concentrations ranged from a minimum of 3,930 mg/L to a maximum of 7,380 mg/L and sodium concentrations ranged from a minimum of 395 mg/L to a maximum of 1,700 mg/L. The elevated concentrations of calcium and sulphate at shallow monitoring wells and the drainage field sump are likely due to the addition of gypsum and liquid calcium amendments to the soil.

The NaCl concentration of the produced water spill that caused the salt impacts observed onsite is unknown but was likely a sodium chloride brine with a chloride concentration ranging up to 150,000 mg/L or greater, consistent with the chemical composition of other produced waters in Alberta (Hitchon et al., 1998). The elevated concentration of dissolved solutes in the produced water will affect the density of the aqueous solution. As the dissolved solute concentration increases, the density of the aqueous solution will also increase. The relationship between NaCl concentration and solution density is shown in Figure 2.3.

2.5 Summary

The study area is a former battery located southwest of Edmonton, in central Alberta. A pipeline release of unknown volume is believed to have occurred at the site sometime in the mid 1980s. The pipeline release resulted in hydrocarbon and salt impacts to shallow soil and groundwater; however, the deeper bedrock aquifer at the site remains un-impacted. Monitoring wells were first installed at the site in 1998. The 1998-1999 chloride concentrations ranged from 7,050 mg/L, within the current north half of the drainage field to 19,000 mg/L, within the former flare pit area in the east half of the site. The 1998-1999 sodium concentrations ranged from 1,500 mg/L within the current north half of the tile drainage field to 4,170 mg/L in the southwest corner of the current drainage field area.

Figure 2.3. Relationship between NaCl concentration and aqueous solution density.
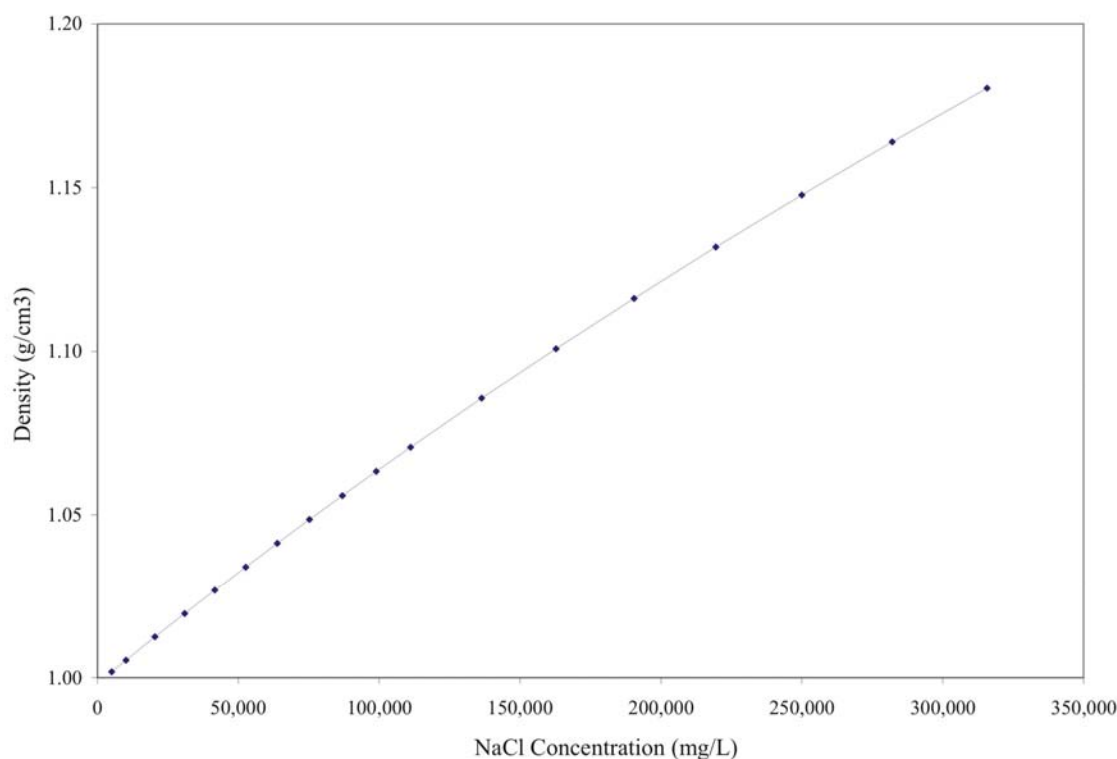
A tile drainage system was installed at the site in March 2003 to address the residual salt impacts at the site. Monitoring of the tile drainage system was conducted at the site in 2003, 2004, 2005 and 2006. Monitoring wells P04-2A and P04-2B were chosen as indicator wells for this study since they are nested wells and are located in the middle of the south tile drainage field, which was the area of interest for this study. Both the nested wells are completed with 1.52 m screen intervals with the base of screen reaching a depth of 3.10 m for the shallow well (P04-2A) and 8.08 m for the deeper well (P04-2B).

In 2004, chloride concentrations at nested shallow monitoring well P04-2A ranged from 7,700 to 8,970 mg/L, while chloride concentrations at deeper nested monitoring well P04-2B ranged from 7,580 to 9,140 mg/L. In 2006, after 3 years of operation of the tile drainage system, chloride concentrations at P04-2A ranged from 4,970 to 7,310 mg/L while chloride concentrations at P04-2B ranged from 7,030 to 7,750 mg/L (Table 2.2). Sodium concentrations at the shallow nested well (P04-2A) ranged from a maximum of

4,600 mg/L in 2004 to a minimum of 3,080 mg/L in 2006 while sodium concentrations at the deeper well (P04-2B) were lower and ranged from a maximum of 1,650 mg/L in 2004 to a minimum of 1,230 mg/L in 2006. Groundwater samples were also taken from the tile drainage sump between 2003 and 2006. Elevated concentrations of sodium and chloride in the collection sump water indicate the tile drainage system is removing sodium and chloride from the subsurface.

To increase the understanding of salt transport in the unsaturated zone at the site and evaluate the effectiveness of tile drainage systems as a method of salt remediation in Alberta, a site-specific numerical model will be developed. The following chapter presents data collection, methodology, analysis and results for parameters that were used in the development of the variably-saturated groundwater flow and transport model for this study.

Chapter Three: Data Collection, Methods, Analysis and Results

3.1 Introduction

Data collection and analysis efforts were guided by the variably-saturated flow and transport model input requirements and were focused on characterising variability in soil texture as a proxy for the variability of site lithology and on obtaining values for unsaturated soil hydraulic parameters (van Genuchten parameters) at the site.

3.2 Data Collection

3.2.1 Soil Cores

New data used in this work was gathered mainly from soil cores collected at the site in November 2004, October 2005 and October 2006. Soil cores were collected in 0.05 m diameter clear plastic tubes in 2004 and in 0.035 m diameter clear plastic tubes in 2005 and 2006. Coring tubes were advanced at each location until soil resistance was encountered and the coring tube could not be advanced further. It was found that the smaller diameter coring tubes were generally able to penetrate the soil to a greater depth than the larger diameter tubes. The core locations are included in Figure 2.1. Table 3.1 is a summary of the cores collected during the field visits and the laboratory analyses performed on the cores for which information was used in this study.

3.3 Methodology

3.3.1 Grain Size Analysis

Discrete soil samples were collected at approximate 0.5 m depth intervals along each core. Standard grain size analysis methodology was followed (Gee and Bauder, 1986). The results of the grain size analysis of the soil samples from each core are summarised in Appendix A.

Table 3.1 Summary of core collected and analyses performed for this study.

Drilling Date	Core	Total Depth (m)	Analysis Conducted
November 2004	C04-01	2.5	GS
	C04-02	5.5	GS
	C04-03	2.5	GS
October 2005	C05-01	4.4	---
	C05-02	4.9	GS, SWRC
	C05-03	4.3	GS, SWRC
	C05-04	4.4	---
	C05-05	4.6	---
	C05-08	6.8	---
October 2006	C06-01	6.2	GS
	C06-02	5.0	GS
	C06-03	3.7	GS
	C06-04	7.6	GS
	C06-05	5.2	GS
	C06-08	3.8	GS

Notes:

GS - grain size analysis

SWRC - soil water retention curve

3.3.2 Soil Hydraulic Parameters

3.3.2.1 Background

Direct measurement of the unsaturated hydraulic conductivity of a soil is difficult to obtain due to extensive variability in the field and because measuring this parameter is generally time-consuming and expensive (van Genuchten, 1980). To overcome this limitation, variably saturated numerical flow models generally incorporate empirical models to calculate the unsaturated hydraulic conductivity of a soil from the much more easily measured soil water retention curve (SWRC). The SWRC describes the relationship between the soil saturation and the soil water pressure potential. The SWRC is dependent on the grain size distribution and the arrangement of the grains in the soil

(Klute, 1986). Popular models used for this purpose include van Genuchten (1980). Van Genuchten (1980) models the SWRC of a soil sample using the following relationship:

$$\Theta = \left[\frac{1}{1 + (\alpha\psi)^n} \right]^m \qquad\qquad 3.1$$

Where Θ is the normalised water content, ψ is the suction head, and α and n are curve fitting parameters that vary based on the soil type. Parameter m is approximated as:

$$m = 1 - \frac{1}{n} \qquad\qquad 3.2$$

3.3.2.2 Procedure

The method used to determine the SWRC for selected site soil samples involved establishing a series of equilibria between the moisture content of the soil sample and a known suction in a pressure chamber. The suction head, volumetric moisture content data pairs were then used to plot the experimental SWRC of the sample. The experimental data is included in Appendix B.

Undisturbed core samples were used, meaning the samples were not repacked since the structure of the sample affects the water retention (Klute, 1986). Repacking soil, even to the original bulk density can not reproduce the field structure and may give results that are not representative of the soil in-situ (Klute, 1986). Four soil samples were analysed, two from core C05-02 and two from core C05-03. A duplicate was also selected for each sample by selecting an additional soil sample immediately below the first sample in the core, ensuring that no visible colour, textural or other differences were present between the two samples. The depth intervals and a visual description of the lithology of each sample are included in Table 3.2.

Table 3.2. Soil samples selected for analysis of soil water retention curves.

Core	Depth Interval (m)	Sample Name	Sample Description
C05-02	0.225-0.055	Sample 1	Light yellow-beige, well sorted, no visible soil structure, some silt, some oxidation staining, some white precipitate. Swelled up when initially saturated.
C05-02	0.255-0.285	Sample 1 duplicate	
C05-03	0.000-0.030	Sample 2	Black, well sorted, organics, some white precipitate, visible soil structure, loose.
C05-03	0.030-0.060	Sample 2 duplicate	
C05-03	0.380-0.410	Sample 3	Light beige, moderately wells sorted, some pebbles up to 3 mm diameter, no visible soil structure, some black mottling
C05-03	0.410-0.440	Sample 3 duplicate	
C05-02	0.165-0.195	Sample 4	Light beige, some white precipitate and black mottling, no visible soil structure, well sorted, compacted.
C05-02	0.195-0.225	Sample 4 duplicate	

The soil samples were 0.035 m in diameter and ranged from 0.025 m to 0.035 m high. The time to reach equilibrium is proportional to the square of the height of the sample and so the height was kept small to reduce the equilibration time (Klute, 1986). The soil samples were wetted with de-aerated tap water and left to saturate by placing the samples in a tub of water at a level just below the top of the soil cores for a period of 12 hours. Standard apparatus set-up as described in Klute (1986) was used to measure the SWRC of the soil samples. The apparatus included:

- ceramic plates with bubbling pressures ranging from 1 to 10 Mbar,
- a pressure-cooker sample chamber,
- an outflow system, which consisted of a small tube in a beaker of water that was attached to the ceramic plate, and
- a suction source which consisted of an air compressor and a series of regulator valves.

The soil-water system was in contact with the exterior of the pressure chamber via a water-wetted porous ceramic plate and a small tube which allowed water to flow out of

the soil samples. The suction in the soil-water system was increased 10 times and allowed to equilibrate. The weight of the soil sample was measured after the sample was allowed sufficient time to equilibrate and recorded along with the suction in the system. In this case, a drainage curve was mapped by establishing a series of equilibria starting from sample saturation at atmospheric pressure and ranging up to a maximum suction head of 45 m (4,500 milibars). Soil textural analysis was also run on the soil samples after the SWRC laboratory experiments were completed according to the methodology outlined in Section 3.3.1 and the results are included in Appendix A.

3.3.2.3 Calculations

The volumetric moisture content (θ) of the soil samples at each equilibrium suction was calculated using the following relationship (Klute, 1986):

$$\theta = \frac{(W_w - W_d)}{(\rho_w V_s)} \qquad\qquad 3.3$$

where W_w is the wet weight of the sample, W_d is the oven dry weight of the sample, ρ_w is the freshwater density of water and V_s is the volume of the soil sample calculated as:

$$V_s = \pi r^2 h \qquad\qquad 3.4$$

where h is the height of the soil core sample and r is the radius of the soil core sample. The pressure was converted to suction head (ψ) and the experimental volumetric water contents were converted to the normalised water content (Θ) using the following relationship:

$$\Theta = \frac{\theta - \theta_r}{\theta_s - \theta_r} \qquad\qquad 3.5$$

where θ_s is the saturated volumetric moisture content of the sample obtained experimentally and θ_r is the theoretical residual moisture content of each sample estimated from ROSETTA (Schaap, Leij and van Genuchten, 2001) based on the soil textural analysis results of the sample. The experimental (Θ, ψ) data pairs were then plotted on the same graph as the theoretical curve modeled using equation 3.1 and the van

Genuchten parameters α, *n* and *m* in equation 3.1 were adjusted manually until the van Genuchten (1980) model curve and the experimental values plotted on the same line.

3.3.2.4 Uncertainty Analysis

The accuracy of the estimated volumetric moisture contents of the soil samples is affected by several sources of uncertainty. If the estimate of *x* depends on a set of variables u_i and the uncertainty in u_i are uncorrelated, then the uncertainty in *x* can be calculated from the uncertainty in u_i as (Bevington, 1969):

$$\Delta x^2 = \sum_{i=1}^{N_u} \Delta u_i^2 \left(\frac{\partial x}{\partial u_i} \right)^2 \qquad 3.6$$

where N_u is the total number of variables. Substituting equation 3.4 into equation 3.3, we obtain the following equation for the volumetric moisture content:

$$\theta = \frac{(W_w - W_d)}{\rho_w \pi r^2 h} \qquad 3.7$$

Variables in equation 3.7 with quantifiable sources of uncertainty include the wet and dry weights of the samples (W_w and W_d), the radius of the soil sample (*r*) and the height of the soil sample (*h*). The estimated uncertainty for each of these variables is included in Table 3.3. The greatest source of uncertainty in the estimate of the volumetric moisture content of the soil samples was the height of the soil sample (*h*). The height of the soil sample was measured at each equilibrium suction at the tallest and shortest part of the soil sample with a ruler and the two measurements were averaged. Because of the uneven top surface of the soil sample, this was relatively difficult to accurately measure. The sample heights required further correction to fit the expected behaviour of a decrease in soil sample height with a decrease in sample moisture content. The averaged soil sample heights were plotted versus time and a decreasing exponential function was fitted to the data. The estimated uncertainty in the corrected average soil sample heights (*h*) was 2 mm.

Table 3.3. Estimated uncertainty associated with volumetric moisture content calculation.

Variable (u_i)	Uncertainty Δu_i
Wet Weight (W_w)	0.1 g
Dry Weight (W_d)	0.1 g
Sample radius (r)	1 mm
Sample height (h)	2 mm

Taking the partial derivative of equation 3.7 with respect to each of the variables in Table 3.3, the following set of partial differential equations was obtained:

$$\frac{\partial \theta}{\partial W_w} = \frac{1}{\rho_w \pi r^2 h} \qquad \qquad 3.8$$

$$\frac{\partial \theta}{\partial W_d} = -\frac{1}{\rho_w \pi r^2 h} \qquad \qquad 3.9$$

$$\frac{\partial \theta}{\partial r} = -\frac{2W_w}{\rho_w \pi r^3 h} + \frac{2W_d}{\rho_w \pi r^3 h} \qquad \qquad 3.10$$

$$\frac{\partial \theta}{\partial h} = -\frac{W_w}{\rho_w \pi r^2 h^2} + \frac{W_d}{\rho_w \pi r^2 h^2} \qquad \qquad 3.11$$

To calculate the uncertainty in the moisture content, equation 3.6 can be re-written as:

$$\Delta\theta^2 = \left[\Delta W_w^2 \left(\frac{\partial \theta}{\partial W_w} \right)^2 + \Delta W_d^2 \left(\frac{\partial \theta}{\partial W_d} \right)^2 + \Delta r^2 \left(\frac{\partial \theta}{\partial r} \right)^2 + \Delta h^2 \left(\frac{\partial \theta}{\partial h} \right)^2 \right] \qquad 3.12$$

Substituting the values in Table 3.3 and equations 3.8 to 3.11 into equation 3.12, the uncertainty in the moisture content was calculated at each equilibrium suction head. The estimated uncertainty in the moisture content at each equilibrium suction head is included in Appendix B.

3.4 Results

3.4.1 Grain Size Analysis

Grain size analysis results for cores collected in 2004 and 2006 are included in Appendix A. The 2004 core textural classes mainly consisted of silt loam and loam, with one occurrence of sandy loam at a depth of 4.0 m at C04-02. The 2006 core textural analysis was consistent with the 2004 results with the majority of textural classes consisting of silt loam and loam, with one occurrence of sandy loam at 1.5 m depth at C05-02, one occurrence of loamy sand at 5.2 m depth at C06-04, and one occurrence of sand at 5.7 m depth at C06-04. Each of the soil samples selected for SWRC analysis also belonged to the silt loam textural class (Appendix A). A comparison of all of the grain size analysis results indicates that out of the 73 soil samples analysed, 59% were silt loam, 36% were loam and the remaining 5% consisted of sandy loam, loamy sand and sand. This suggests that on a larger scale, the shallow lithology at the site can be approximated as a homogeneous silt loam.

3.4.2 Soil Hydraulic Parameters

The experimental and theoretical SWRC are plotted in Figure 3.1. The van Genuchten parameters for each soil sample are summarised in Table 3.4. The experimental data points plotted along the van Genuchten model curve, with the exception of the first experimental data point on each curve (Figure 3.1). At low suction heads, the experimental water content is less than the modeled value in all cases. This may be due to the fact that the secondary porosity (macrostructure) present in the natural soil cores is not accounted for in the van Genuchten model. The macrostructure will act as very large pores that will drain at very low suction heads while the remainder of the smaller, primary pores will remain saturated. This may be why there is less water in the soil sample than would be predicted at low suction heads. In addition, significant soil swelling over the top of the plastic core ring was observed for several of the samples when they were initially water saturated. This made accurate measurement of the height of the soil sample extremely difficult in the higher water content ranges.

Figure 3.1. Experimental and theoretical soil water retention curves for (a) samples 1/1d (b) samples 2/2d (c) samples 3/3d and (d) samples 4/4d.

(a)

(b)

(c)

Sample 3

Sample 3d

(d)
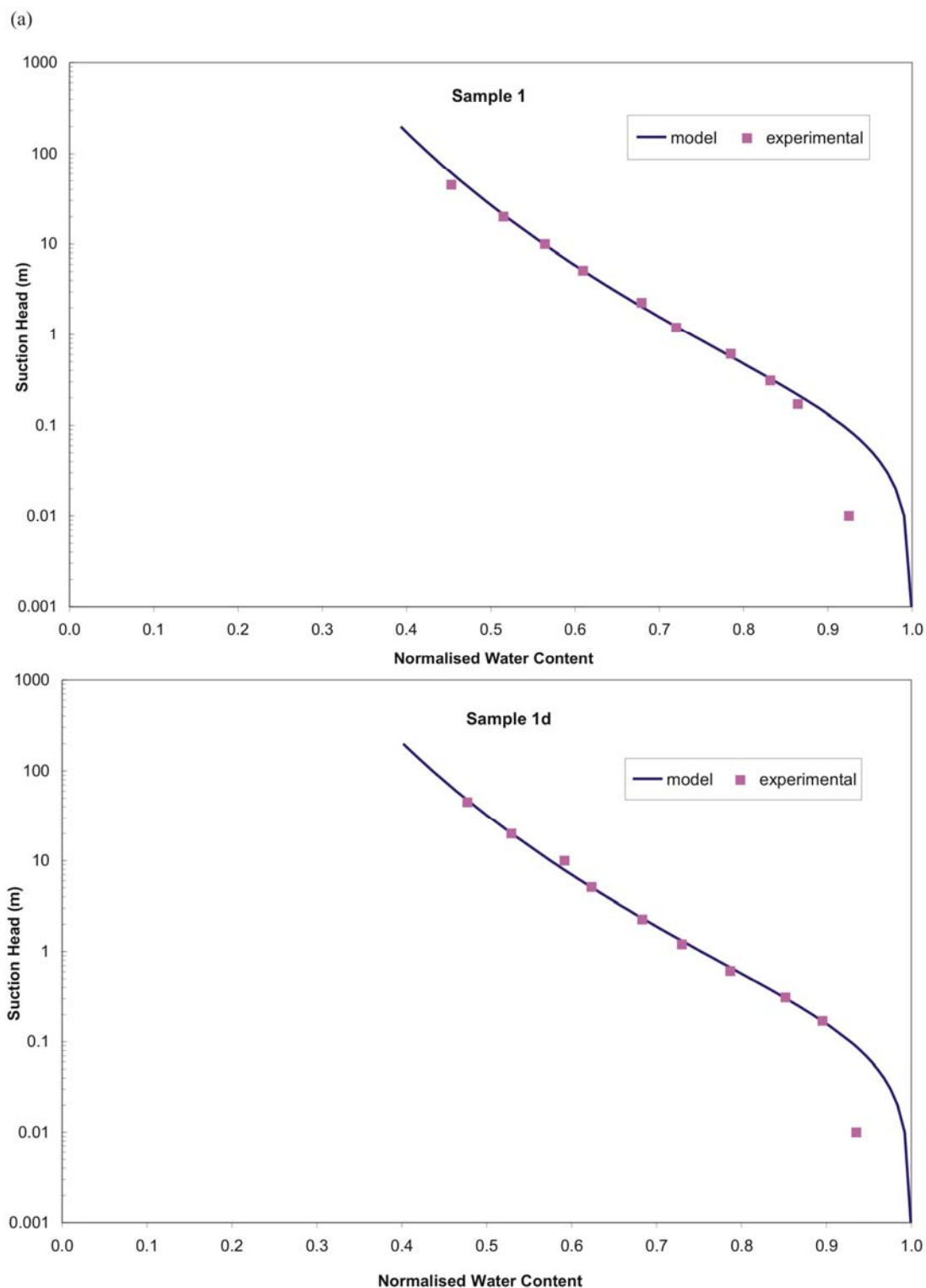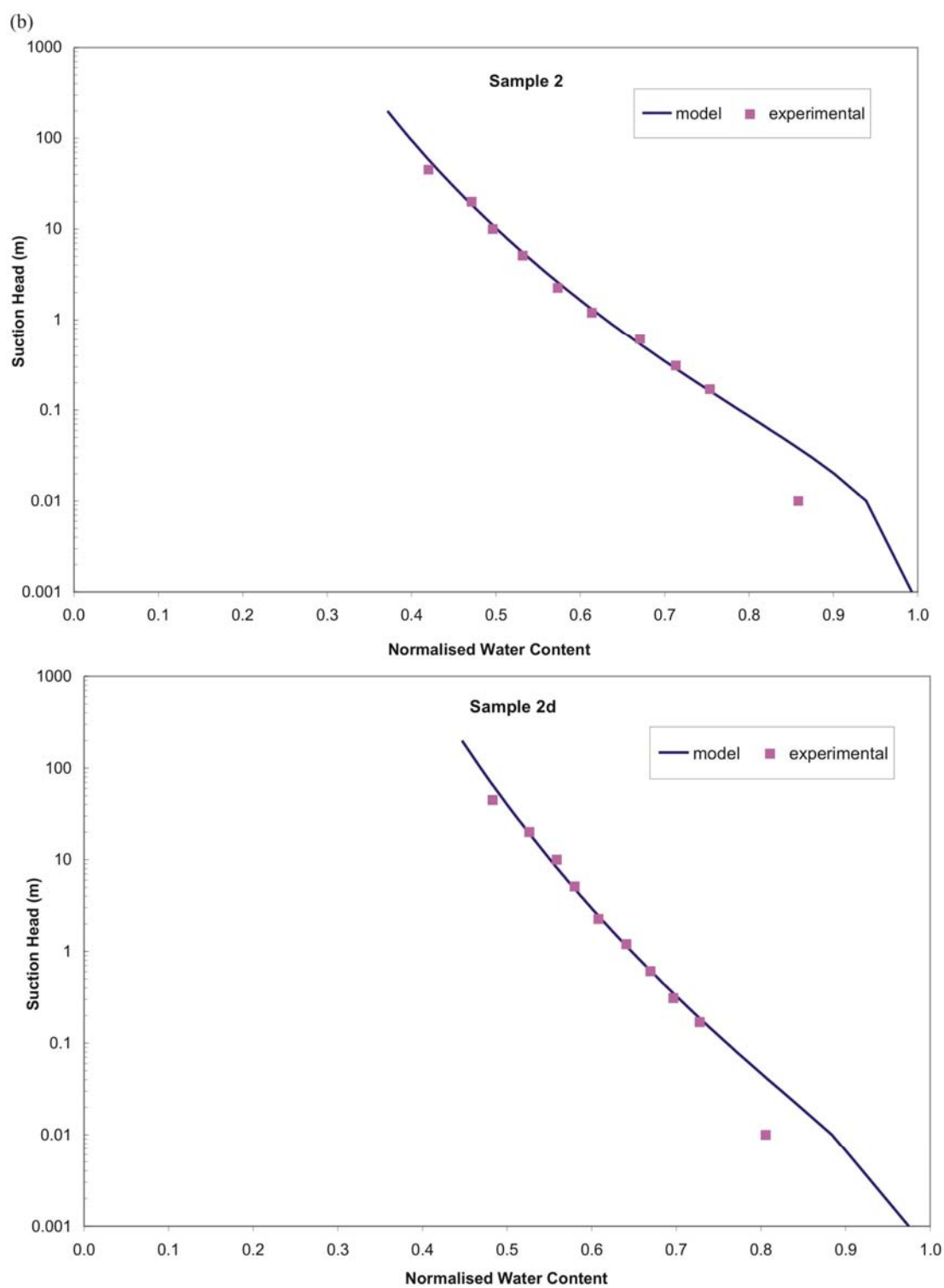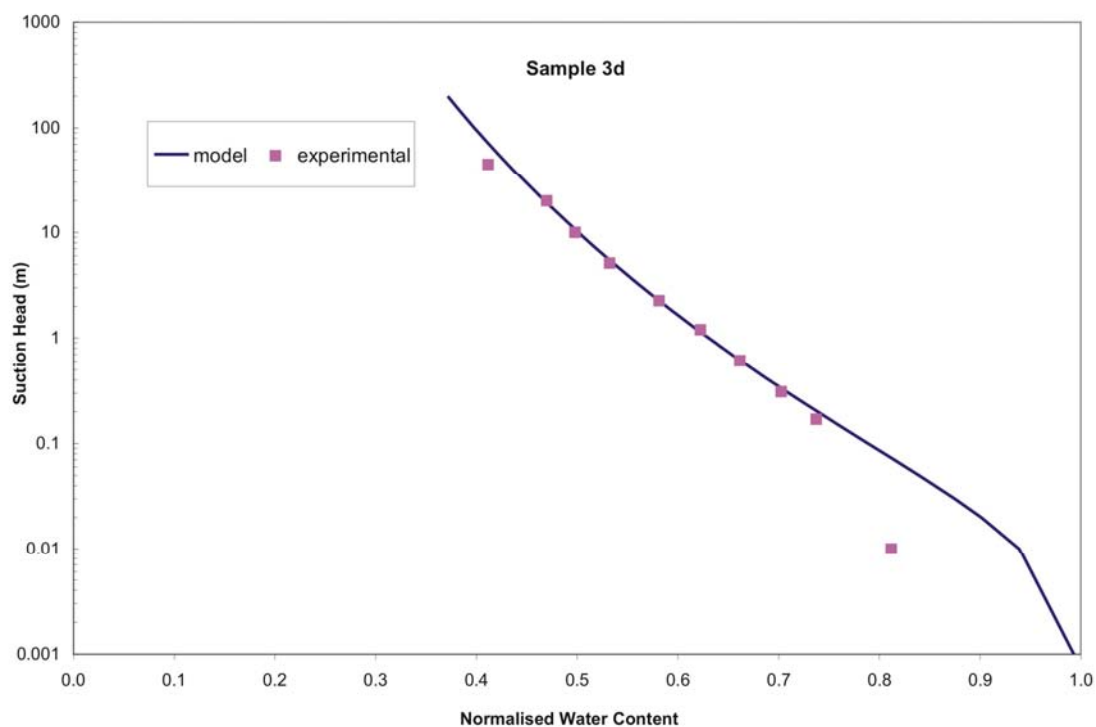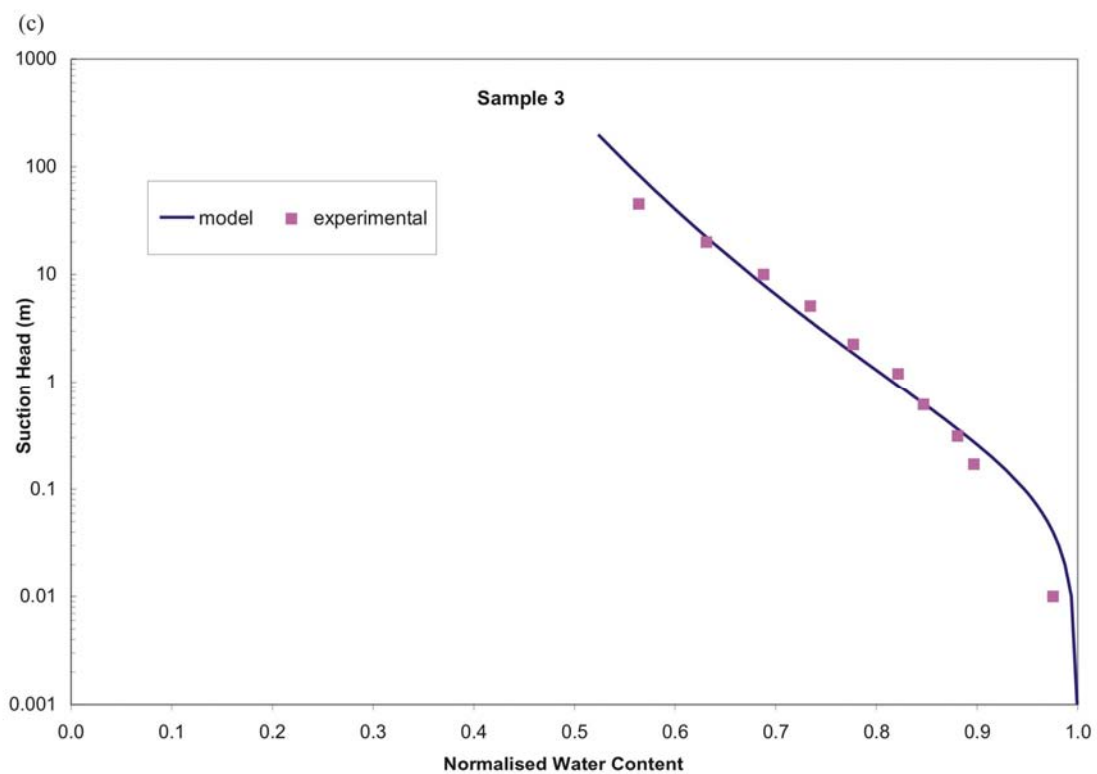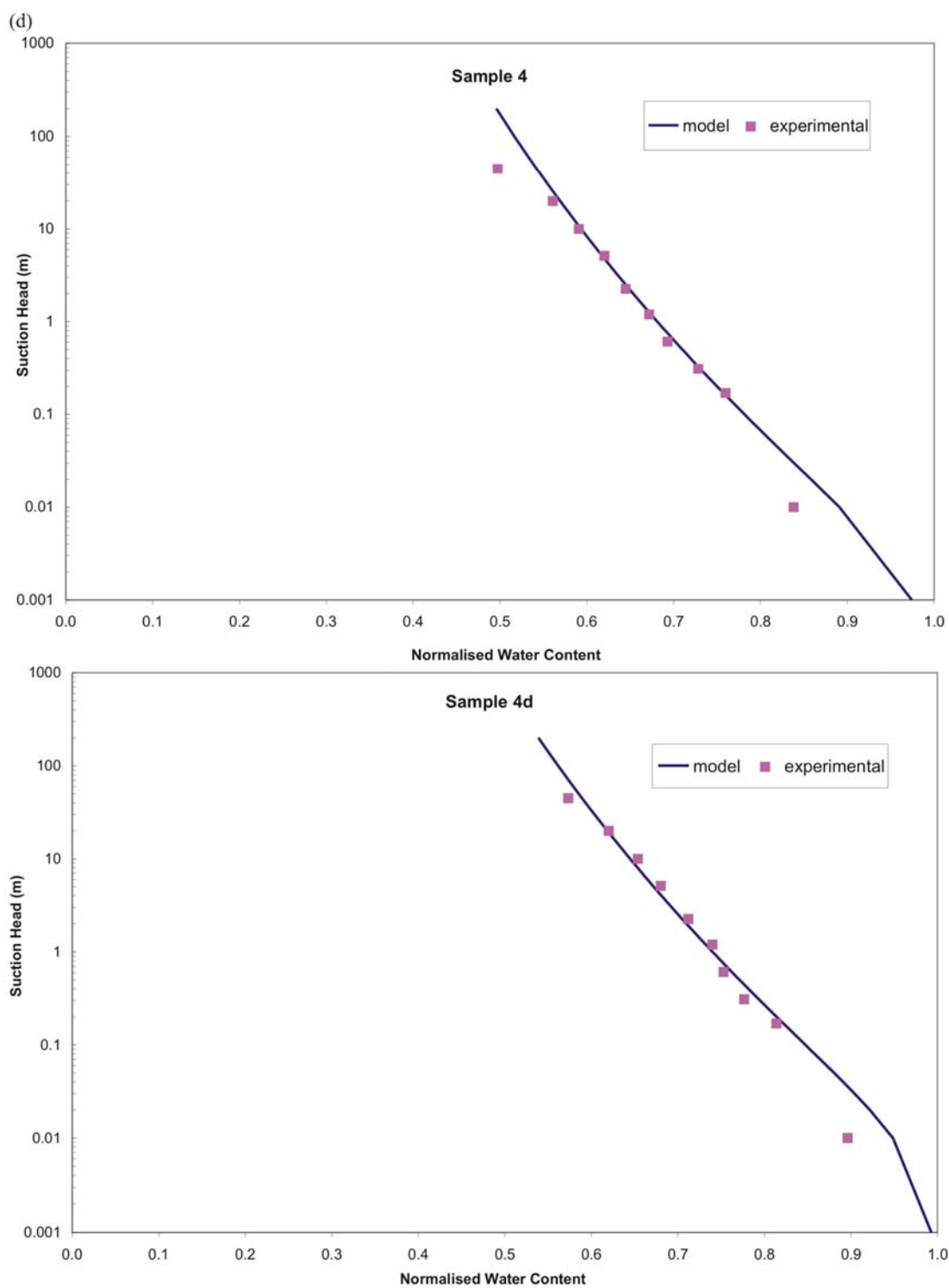
Table 3.4. Summary of van Genuchten parameters for experimental soil water retention curves.

Sample ID	Core	Depth (m)	θ_s	θ_r	α (m^{-1})	n	m
Sample 1	C05-02	0.225-0.255	0.58	0.08	12.0	1.12	0.107
Sample 1d	C05-02	0.255-0.285	0.58	0.07	10.0	1.12	0.107
Sample 2	C05-03	0.000-0.030	0.56	0.06	100	1.11	0.099
Sample 2d	C05-03	0.030-0.060	0.55	0.06	500	1.07	0.065
Sample 3	C05-03	0.380-0.410	0.42	0.07	10.1	1.09	0.078
Sample 3d	C05-03	0.410-0.440	0.52	0.06	100	1.10	0.091
Sample 4	C05-02	0.165-0.195	0.47	0.06	600	1.06	0.057
Sample 4d	C05-02	0.195-0.225	0.42	0.07	150	1.06	0.057
		mean	0.51	0.07	26*	1.09	0.083
		variance	0.004	0.0001	54,038	0.0006	0.0005
		standard deviation	0.07	0.01	232	0.0254	0.02

Notes:
*   - harmonic mean

The saturated moisture content (θ_s) values of three of the samples (sample 3, sample 4 and sample 4d) were consistent with published experimental values for silt loam and ranged from 0.42 to 0.47 m^3/m^3 (Coquet et al., 2005; Shouse et al., 1995). The remaining θ_s were higher than published values for silt loam and ranged from 0.52 m^3/m^3 at sample 3d to 0.58 m^3/m^3 at samples 1 and 1d. If the estimated uncertainty in the saturated moisture content is subtracted from the experimental saturated moisture content for samples 2, 2d and 3d, the resulting saturated moisture contents are more consistent with published results at 0.49, 0.48 and 0.45, respectively (Appendix B). However, if the saturated moisture contents of samples 1 and 1d were 0.07 m^3/m^3 lower than reported, they would still be greater than published results for silt loam at 0.51 m^3/m^3. The elevated saturated moisture content of some of the samples may be related to salt concentrations in the soil core samples given the known elevated salinity at the site. When monovalent-divalent cation exchange occurs and Na$^+$ replaces Ca^{2+} in the clay crystal lattice, the net negative charge attracts hydrated cations to the tetrahedral interlayer. This may have allowed the soil samples to retain more water than through the effective porosity alone. Significant soil swelling was observed for both samples 1 and

1d when they were initially saturated. As the samples were natural and not re-packed, the additional water could also have been due to macropores (earthworm holes and/or root channels), or fractures within the cores that became water saturated and were able to retain more water than via the expected effective porosity of the sample.

Van Genuchten parameter α is related to the inverse of the air entry pressure and is a measure of the pore size of the soil (Wise et al., 1994). A porous medium with small pores will have a smaller value of α and tend to retain more moisture within the unsaturated zone due to capillary forces. The fitted experimental values of α are included in Table 3.4. The values obtained for α were for the most part considerably higher than published experimental results for silt loam soil (Coquet et al., 2005; Schaap and Leij, 1998; Shouse et al., 1995; Simunek et al., 2000; Wessolek et al., 1994). The α values obtained for samples 1, 1d and 3 ranged from 10 to 12 m^{-1} and were similar to values obtained by Coquet et al. (2005) for silt loam soil samples from an agricultural research field. The remaining α values were significantly greater and ranged from 100 to 600 m^{-1}. It is hypothesised that these samples are disturbed samples that contain internal macrostructure that is dominating the flow parameters. This is plausible since very shallow, natural core samples were analysed and the samples were not re-packed. Other studies have also reported that internal structure can dominate the flow parameters when natural core samples are used for SWRC analysis (Meadows et al., 2005). The harmonic mean was calculated for each value of α as suggested by Zhu and Mohanty (2002). The harmonic mean value of α was 26 m^{-1} and the variance and the standard deviation were high. Because of the values of α obtained experimentally were elevated and in poor agreement with published results, they were deemed non-representative of the site silt loam soil. The value of α used in the variably-saturated numerical model for silt loam was 0.48 m^{-1} which is very similar to the average value of α (0.50 m^{-1}) obtained from analysis of 332 silt loam soil samples (Schaap and Leij, 1998).

Van Genuchten parameter n is an inverse measure of the breadth of the pore-size density function (Wise et al., 1994). As n decreases, the relative abundance of smaller pores in comparison to the mean pore size increases in a porous medium. A soil with lower values of n will retain more water in the unsaturated zone than a soil with a higher value of n for the same suction head. The values of n obtained for the site silt loam were relatively low ranging from 1.06 (sample 4 and 4d) to 1.12 (sample 1 and 1d) and were within range of previously published results for silt loam (Coquet et al., 2005). The standard deviation of n for the site silt loam was 0.024 and the arithmetic mean value (Zhu and Mohanty, 2002) was 1.09.

3.5 Summary

New data was gathered for this work through tests conducted on core samples gathered at the site in 2004, 2005 and 2006. Grain size analysis performed on discrete samples from the cores collected in 2004 and 2006 suggest the soil at the site is mainly silt loam. SWRC were measured for selected silt loam core samples from C05-02 and C05-03. The values for the saturated moisture content for three of the samples were consistent with published experimental values for silt loam and ranged from 0.42 to 0.47 m^3/m^3. The remaining θ_s were higher than published values for silt loam and ranged from 0.52 to 0.58 m^3/m^3. Moisture content uncertainty analysis results indicated that the uncertainty decreases with an increase in suction head and that the greatest uncertainty was associated with the saturated moisture content. Decreasing the saturated moisture content by the uncertainty estimate still resulted in samples 1 and 1d having θ_s values greater than published silt loam values. The elevated saturated moisture content of the samples may be related to salt concentrations in the soil core samples given the known elevated salinity at the site. Significant soil swelling was observed for samples 1 and 1d, both of which had elevated θ_s, when they were initially saturated during the experiment, which may support this hypothesis. Additionally, macropores or fractures within the natural cores may also be contributing additional water storage capability.

The values obtained for van Genuchten parameter α were generally elevated and not within range of published experimental values. The α values also varied substantially from sample to sample as evidenced by the high values of the variance and standard deviation. It is hypothesised that the soil samples are likely disturbed samples that contain internal macrostructure that is dominating the flow parameters. This is plausible since shallow, natural core samples were analysed and the samples were not re-packed. Other studies have also reported that internal structure can dominate the flow parameters when natural core samples are used for SWRC analysis. The experimentally determined values of α were therefore judged to be not representative of the site silt loam. The values of n obtained experimentally were relatively consistent between the samples and were within range of previously published results. The mean value of n for the silt loam was 1.09.

The following chapter outlines the conceptual model that will be used to develop the numerical groundwater flow and transport model for the site.

Chapter Four: Conceptual Model

4.1 Introduction

Formulating an appropriate and realistic conceptual model is an important part of the numerical modeling process. The purpose of the conceptual model is to simplify the field problem and organise the associated field data so that the system can be analysed more readily (Anderson and Woessner, 2002). It is critical that the conceptual model incorporate all of the important hydrogeologic conditions and transport processes at the site. The numerical model will be based on the conceptual model, although it may not incorporate each process identified at the site. Any omissions will be identified and may limit the some of the predictions generated by the numerical model. The conceptual model for the site must incorporate both groundwater flow and contaminant transport. As the salt concentrations being considered are relatively elevated, density-dependent flow and transport should also be considered.

4.2 Groundwater Flow

4.2.1 Hydrostratigraphic Units

Textural analysis results for the site indicate that the surficial soils consist mainly of silt loam with lenses of loam and minor thin sandy loam, loamy sand and sand stringers to a depth of 7.6 m bgs (Appendix A). A thicker sand layer was identified at the site between 6.25 and 7.5 m bgs, in the vicinity of nested monitoring well P04-2A/B, which is completed in both the shallow silt loam and the deeper sand (WorelyParsons Komex, 2005b). Very fine-grained, medium grey sandstone interpreted to be part of the Upper Horseshoe Canyon Formation was encountered at a depth of 20 m at P99-8C (WorelyParsons Komex, 2005b).

The site hydrostratigraphy was simplified as a homogeneous silt loam between ground surface and a depth of 6.25 m underlain by a 1.25 m thick sand layer. The base of the hydrostratigraphic model is the bottom of the sand layer at a depth of 7.5 m. The lower

permeability glacial till material encountered underlying the sand will be represented by a no-flow boundary at the bottom of the sand layer. The simplified site hydrostratigraphy is summarised in Table 4.1.

Table 4.1. Study site shallow hydrostratigraphy.

Hydrostratigraphic Unit	Depth Interval (m)	Description
silt loam	0.0-6.25	Shallow unconsolidated variably-saturated aquifer composed of silt loam with some loam.
sand	6.25-7.50	Deeper unconsolidated fully-saturated aquifer composed of very fine grained sand.
glacial till	>7.50	Low permeability aquitard underlying the sand.

4.2.2 Flow System

4.2.2.1 Unsaturated Flow

At the site, unsaturated flow occurs within the silt loam hydrostratigraphic unit. Groundwater elevations were measured in monitoring wells at the site in June 1999 and are included in Table 4.2. The June 1999 groundwater elevations are interpreted to represent background groundwater flow conditions at the site since they were collected prior to installation of the tile drainage system. In June 1999, the depth to the water table water at shallow monitoring wells ranged from 0.76 to 1.16 m bgs (Table 4.2). Overall, groundwater flow is predominantly vertically downward within the unsaturated portion of the silt loam, although during some months of the year, upward flow may also occur. Evidence for upward flow is seen in groundwater elevations measured in November 2004 at nested monitoring wells P04-2A/B where the groundwater elevation was higher at the deep well (P04-2; 723.18 m) than at the shallow well (P04-2A; 723.12 m) indicating a slightly upward vertical groundwater flow gradient (Table 4.3).

Table 4.2. June 1999 background groundwater elevations at the site.

Monitoring Well	Ground Elevation (masl)	29-Jun-99		Total Drilled (m bgs)	Top of Screen (m bgs)	Base of Screen (m bgs)	Hydraulic Conductivity (m/s)
		Depth to Groundwater (m bgs)	Groundwater Elevation (masl)				
Silt Loam							
P98-1A	725.73	0.93	724.81	4.57	1.22	4.57	1.5E-06
P98-2A	725.61	0.76	724.85	4.88	1.22	4.88	5.1E-07
P98-3A	725.62	0.95	724.67	5.15	1.80	5.15	5.4E-07
P98-4A	725.03	0.92	724.11	4.50	1.10	4.50	4.4E-07
P98-5A	725.02	0.88	724.14	5.50	2.15	5.50	8.5E-07
P99-6A	725.53	1.16	724.37	4.40	---	---	5.5E-07
P99-7A	725.72	1.02	724.70	4.37	---	---	4.6E-07
Lower Glacial Till/ Upper Horseshoe Canyon							
P99-6B	725.55	0.93	724.62	---	---	---	---
P99-8B	725.74	0.89	724.85	12.19	7.70	12.19	8.7E-07
P99-8C	725.74	13.78	711.96	21.80	19.22	22.44	3.5E-07
P99-9C	724.98	1.09	723.89	17.05	13.50	19.51	2.1E-07

--- information not available
Data Source (WorleyParsons Komex 2005a)

Table 4.3. 2004 monitoring well summary table.

Monitoring Well	Ground Elevation (masl)	5-Aug-04		30-Nov-04		Total Drilled (m bgs)	Top of Screen (m bgs)	Base of Screen (m bgs)	Hydraulic Conductivity (m/s)
		Depth to Groundwater (m bgs)	Groundwater Elevation (masl)	Depth to Groundwater (m bgs)	Groundwater Elevation (masl)				
Silt Loam									
P04-1A	725.62	dry	---	2.51	723.11	3.75	1.38	2.90	---
P04-2A	725.54	1.72	723.82	2.42	723.12	3.10	1.58	3.10	---
P04-3A	725.07	1.39	723.68	2.17	722.90	3.65	1.53	3.05	---
P04-4A	724.94	1.40	723.54	2.02	722.92	3.50	1.35	2.87	---
P04-5A	725.03	1.35	723.68	1.94	723.09	3.60	1.68	3.20	---
P04-6A	725.00	1.58	723.42	1.98	723.02	3.60	1.53	3.05	---
Sand/Upper Glacial Till									
P04-2B	725.50	1.76	723.74	2.32	723.18	8.25	6.56	8.08	1.5E-07

--- information not available
Data Source (WorleyParsons Komex 2005b)

The site silt loam had relatively low values of van Genuchten parameter α which indicates that the relative abundance of smaller pore sizes, which tend to retain more water, is greater than larger pores, which tend to drain more quickly and retain less water. The low value of n for the site silt loam indicates that there is an increased relative abundance of small pores in comparison to the mean pore size. Small pores are more difficult to drain than large pores due to capillary forces. Once the small number of large pores have drained, the remaining water will be forced to flow through the relatively more abundant smaller pores. This will cause the relative hydraulic conductivity of the unsaturated zone to decrease rapidly with decreasing water content.

4.2.2.2 Saturated Flow

The June 1999 groundwater elevations have been posted and contoured in Figure 4.1. Shallow saturated groundwater flow at the site is to the northwest. The horizontal hydraulic gradient (i) at the site estimated from groundwater elevation contours in June 1999 was calculated using the following relationship:

$$i = \frac{\Delta h}{\Delta x} \qquad\qquad 4.1$$

Where h is the hydraulic head and x is the lateral distance, both in metres. Using equation 4.1, the hydraulic gradient across the site in June 1999 is approximately 0.003 m/m to the northwest. The hydraulic gradient was relatively constant across the site, with the exception of the former flare pit area where it was somewhat steeper.

Water levels were also measured at monitoring wells on August 5, 2004 and November 30, 2004, after the tile drain system has been operational for over 1 year. Groundwater elevations, monitoring well completion information, and estimates of monitoring well hydraulic conductivity are included in Table 4.3. Groundwater elevations exhibited seasonal variation, with higher elevations measured in August than November 2004. Groundwater elevations measured at monitoring wells installed at the site between 1998 and 2006 are included in Appendix C.

Figure 4.1. June 1999 groundwater flow map.
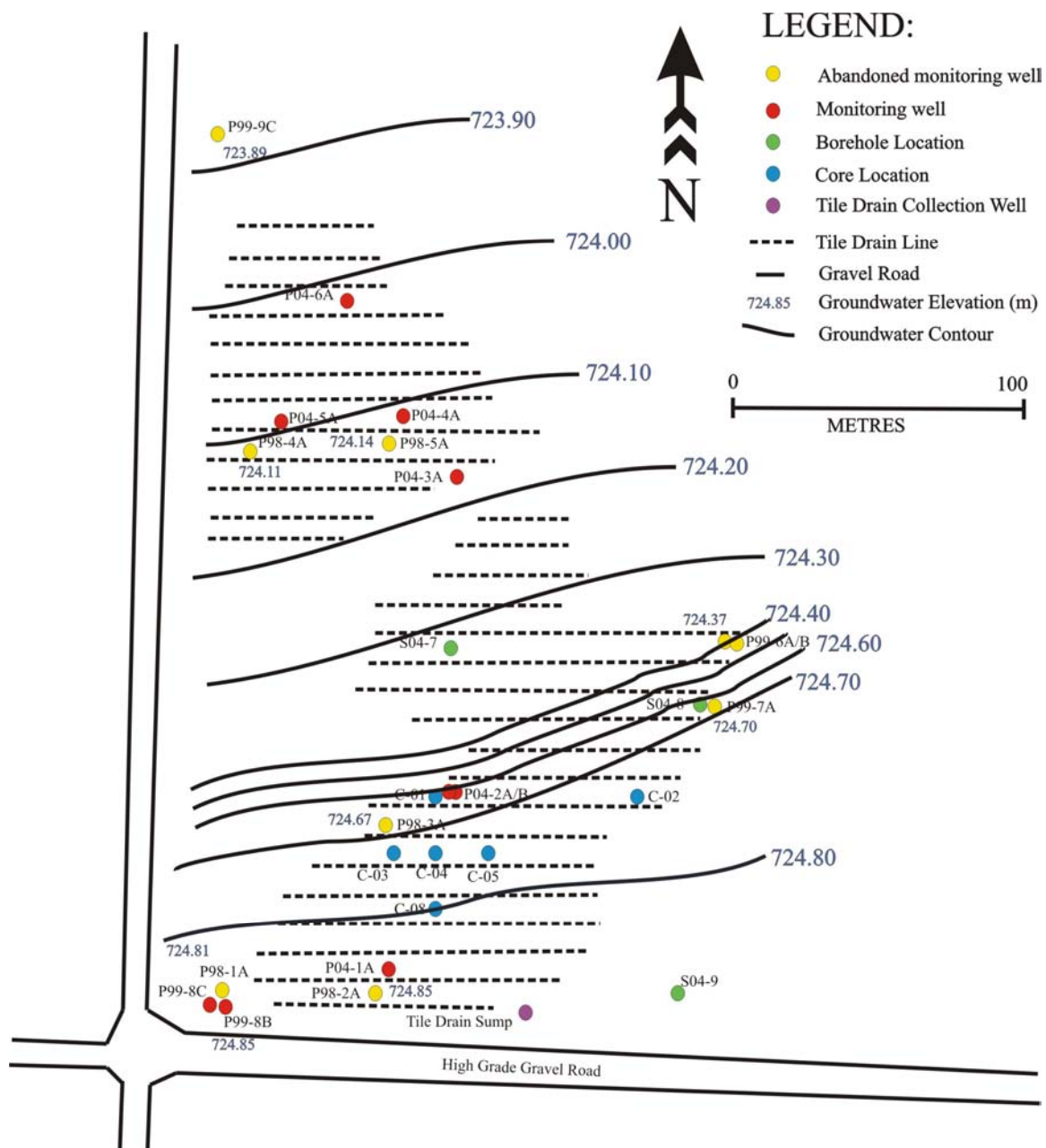
4.2.2.3 Hydraulic Conductivity

Unsaturated soil hydraulic behaviour is characterised by the soil water retention curve.
The soil water retention curve defines the dimensionless water content (Θ) of the soil as
a function of the soil water suction head (ψ) as described in equation 3.1. The
unsaturated soil relative hydraulic conductivity (K_r) can also be defined using the soil
water retention curve (van Genuchten, 1980). The relative hydraulic conductivity of the
unsaturated soil and how it changes with increasing or decreasing water content will
govern the ease with which groundwater will flow in the unsaturated zone. The relative
hydraulic conductivity is given by (van Genuchten, 1980):

$$K_r(\psi) = \frac{\left\{1 - (\alpha\psi)^{n-1}\left[1 + (\alpha\psi)^n\right]^{-m}\right\}^3}{\left[1 + (\alpha\psi)^n\right]^{m/3}}$$
  4.2

The relative hydraulic conductivity of the unsaturated soil will be less than the saturated
hydraulic conductivity K of the same soil and will change in a non-linear fashion with
changes in ψ according by the relationship in equation 4.2.

Saturated hydraulic conductivity tests were conducted at monitoring wells drilled in 1998
and completed within the silt loam. The resulting hydraulic conductivity estimates
ranged from 4.4×10^{-7} to 1.5×10^{-6} m/s (Table 4.2). The geometric mean of the hydraulic
conductivity estimates from monitoring wells P98-2A, P98-3A, P99-6A and P99-7A, all
located in the south half of the site and within the area of interest for this study, is
5.1×10^{-7} m/s. The estimated hydraulic conductivity of the sand layer underlying the silt
loam identified at well P04-2B is likely to be greater than the estimated hydraulic
conductivity of 1.5×10^{-7} m/s since the well was screened across the sand and the glacial
till underlying the sand. The estimated hydraulic conductivity likely represents an
average hydraulic conductivity of the two units. Soil core C06-4 contained sand at a
depth of 5.70 m (Appendix A). The textural analysis from this sand sample yielded an
estimated hydraulic conductivity of 4.4×10^{-5} m/s in ROSETTA (Schaap et al., 2001).

4.3 Water Budget

A water budget defines all inputs, or sources and outputs, or sinks of water for the system of interest. Potential inputs of water within the study area include precipitation and discharge from creeks. Precipitation is expected to be the dominant input of water into the system and can occur in the form of rain or snow, depending on the air temperature. When precipitation occurs as snow, infiltration of liquid water into the subsurface is delayed until temperatures rise, the ground thaws and the snow pack melts, which in the study area generally occurs in late March or April. When precipitation occurs as snow, water may be lost through snow pack sublimation and snow blow-off. When precipitation occurs as rain, generally between the months of April and October, water is more immediately infiltrated into the subsurface. During heavy rain events or during the spring melt, water may pool locally in small depressions and infiltration may be delayed due to water-logged conditions as the hydraulic conductivity of the site silt loam is relatively low.

Potential outputs of water in the system include discharge to rivers and creeks, surface water run-off, evapotranspiration and water loss to the tile drainage system at the site. Discharge occurs to the unnamed creek located northwest of the site. Surface water run-off can occur at the site, but is not estimated to be a significant process due to the relatively flat local topography. Evapotranspiration is water loss due to evaporation of water or transpiration of water by plants and is likely a relatively significant process operating at the site as the area is cultivated. Water loss to the tile drainage system is also a significant process at the site. The tile drainage system produced 3,484 m^3 of water in 2003, 1,658 m^3 of water in 2004, 2,912 m^3 of water in 2005, and 1,320 m^3 of water in 2006 (AMEC Earth and Environmental, 2007; WorelyParsons Komex, 2005b).

4.3.1 Infiltration Boundary

The top infiltration boundary corresponds to the amount of water infiltrating across the ground surface and is a critical boundary within the numerical model. This boundary

controls how much moisture infiltrates down through the unsaturated soil and thereby controls the amount of salt flushing out of the rooting zone that may occur, a feature which is an important element in the remediation of salt-impacted soils using a tile drainage system. A study conducted by Nichols and Freshley (1993) using Monte Carlo simulation concluded that one of the most sensitive parameters in an unsaturated flow model is the infiltration parameter.

The infiltration, or flux, at the top boundary was calculated using daily maximum and minimum temperature and precipitation data. Historical daily precipitation and daily minimum and maximum temperatures from 1979 to 2006 were collected from the Environment Canada online database (Environment Canada, 2007b) for the town of Calmar, located 2 km from the study site. The weather data was input into a version of the Versatile Soil Moisture Budget (VSMB) model (Baier and Robertson, 1996) calibrated for Alberta soils and a spring wheat crop to simulate a cultivated field. The VSMB calculates the water balance through a one-dimensional (1D) soil column 1.20 m thick using the following temperature-dependent water balance equations:

If the average temperature is $>2^{\circ}C$:

$$PCP - AET - RUNOFF - WLEACH = \Delta\theta \qquad 4.3$$

If the average temperature is $<2^{\circ}C$:

$$PCP - AET - RUNOF - WLEACH = \Delta\theta \qquad 4.4$$

where PCP is the amount of liquid water available for infiltration. During the summer months, all water is liquid and PCP = Precipitation. During the winter months precipitation occurs as snow and PCP = Snowmelt. During the spring and fall months, PCP can be a combination of water infiltration due to liquid precipitation and/or snowmelt that varies based on temperature. AET is the actual evapotranspiration which is water loss due to plant transpiration and water evaporation. RUNOFF is surface water runoff due to liquid rain and RUNOF is water loss due to snowmelt runoff. WLEACH is the amount of water that exits the bottom layer of the model that is available for

groundwater infiltration and $\Delta\theta$ is the change is soil moisture storage within the 1.20 m soil column.

The infiltration flux across the top model boundary was calculated using the following equation:

$$\text{Infiltration} = \text{PCP-AET-Runof/Runoff} \qquad\qquad 4.5$$

The VSMB model was first pre-conditioned using climate data from Calmar from 1979 to 1983 to ensure the model had been calibrated. The infiltration between 1984 and 2006 was then calculated on a monthly basis using equation 4.5. A monthly time-variable infiltration flux was calculated since a secondary goal of this research was to investigate the role that seasonal variations in precipitation and water infiltration may play in salt flushing. The monthly infiltration flux calculated with output from VSMB between 1984 and 2006 is included in Appendix D. The monthly infiltration fluxes ranged from a minimum of -80.58 mm in July 1998 to a maximum of +112.85 mm in September 1984. On average, negative fluxes occurred more frequently during the summer months (June, July and August) while positive fluxes occurred more frequently during the spring (March, April and May) and fall (September, October and November) months. Winter fluxes (December, January and February) were generally very small or 0 reflecting the fact that water and the top part of the soil column is mainly frozen during these months.

The net infiltration flux was calculated on an annual basis between 1984 and 2006 for comparison purposes. The annual infiltration flux ranged from -33.15 mm/yr in 1987 to +88.20 mm/yr in 1997. The net annual infiltration flux averaged over the 22 year period from 1984 to 2006 was +17.21 mm/yr, which is approximately 3.3% of the climate normal average precipitation of 521 mm/yr for Calmar (Environment Canada, 2007a). The WLEACH, or amount of precipitation that infiltrates below 1.2 m to become groundwater recharge, averaged over the same 22 year time period from 1984 to 2006 was 13.38 mm/yr or 2.57% of the average annual precipitation. The standard deviation of the annual recharge fluxes was 28.59 mm/yr, indicating that the annual recharge fluxes can vary substantially from year to year.

Plants exert a strong influence on water dynamics and moisture distribution within the shallow unsaturated zone. The VSMB accounts for this influence and calculates the moisture distribution within a 1.2 m column of soil simulating the presence of a crop, in this case spring wheat. The infiltration calculated from the output from the VSMB will be applied across the top model boundary in MIN3PD rather than being spread through the rooting zone as in the VSMB. MIN3PD does not account for the presence of vegetation. The MIN3PD simulated soil moisture distribution in the upper 1.2 m of the model will therefore not be accurate with respect to the actual moisture distribution in the study area, which is covered with grasses.

The water balance was calculated on a daily basis using the relationships in equations 4.3 and 4.4 and the VSMB output file from 1990, selected as a test year. The water balance results were within 0.001 mm, with the exception of the period from July 15 to August 4, 1990 where there appeared to be too little AET to account for the change in soil moisture content. In the output file, the AET was limited to the potential evapotranspiration (PET); however, as the residuals in the water balance show, the actual AET applied in the model was higher. The PET is a reference value for the evapotranspiration based on net solar radiation. Other factors, including crop height and crop type, influence evapotranspiration other than the net radiation and therefore AET can exceed PET estimates. During the period from July 15 to August 4, 1990, the crop stage was relatively advanced (stage 4) and very moist conditions were present in the soil. The AET rate could therefore be expected to be high during that time.

The error in the AET reporting was not discovered until after the numerical modeling had been completed. As shown in equation 4.5, the calculation of the top infiltration boundary used in the numerical modeling included the reported AET term. The magnitude of the error in the AET term ranged from -0.015 to -0.250 mm over a period of 21 days in 1990 resulting in a slight over-prediction of the infiltration term during this time. A small, occasional error in the infiltration term does not affect the results of this study.

4.4 Contaminant Transport

Factors that influence sodium chloride transport at the site include the nature of and depth of the initial release, the physical properties of the hydrostratigraphic units, and the physical properties of sodium chloride. The following is a summary of the main processes that have influenced the transport of sodium chloride at the site.

4.4.1 Release Geometry

Chloride can be a good indicator of groundwater flow direction since the chloride ion behaves conservatively and does not participate in chemical reactions (Appelo and Postma, 1996). Chloride concentrations are reduced through dilution of the plume with ambient freshwater. At the site the NaCl plume likely originated at the ground surface or near ground surface (within the top 1 m of soil) since more elevated chloride concentrations are observed in shallow wells than in deeper wells indicating that the plume moved from the top down. The current NaCl plume is most likely the result of a single, short-lived large-volume release that spread over a large surface area before penetrating into the ground surface. This would include catastrophic tank or large pipeline failures. The plume could have also been the result of many, longer-lived smaller-volume releases spread out across the site. This would include numerous small pipeline or tank leaks that remained undetected and acted as active sources over a period of years. A combination of a large release event and several other smaller volume releases could also have produced the observed plume.

Once the brine was released at the ground surface, NaCl would have infiltrated down through the unsaturated zone until reaching the water table. Once the plume reached the saturated zone, lateral migration of the plume would have occurred in the direction of groundwater flow. However, because the NaCl plume would have had a higher density than the ambient groundwater, there would still have been a significant vertical component to solute migration in the saturated zone. Chloride concentrations detected in bedrock groundwater monitoring wells were less than 22 mg/L and indicate that the

plume has not yet migrated into the bedrock aquifer at a depth of approximately
20 m bgs.

4.4.2 Density, Viscosity and Temperature

The NaCl concentration of the produced water spill that caused the salt impacts observed
onsite is unknown. The source of the salt contamination observed onsite was likely a
sodium chloride brine with a chloride concentration ranging up to 150,000 mg/L or
greater, consistent with the chemical composition of other produced waters in Alberta
(Hitchon et al., 1998). As mentioned in Chapter 2, the elevated concentration of
dissolved solutes in the produced water will affect the density of the aqueous solution.
As the dissolved solute concentration increases, the density of the aqueous solution will
also increase. The relationship between NaCl concentration and solution density is
shown in Figure 2.3.

A dense fluid overlying a less dense fluid, for example an NaCl plume overlying ambient
fresh groundwater, is an unstable system. Density differences will cause the more dense
fluid to propagate vertically downward through the ambient groundwater in the saturated
zone in addition to laterally in the direction of groundwater flow. The density of a fluid
can also be affected by changes in temperature. The density and temperature of water
generally have an inverse relationship where an increase in temperature will result in a
decrease in density. The exception is between 0°C and 4°C where the density of water
actually increases with an increase in temperature. At the study site, however, the
temperature of the ambient fresh groundwater in the subsurface is expected to be the
same as the NaCl plume and therefore a relative difference in the densities of the ambient
fresh groundwater and the NaCl plume due to changes temperature is not expected to
occur.

Dynamic viscosity is a measure of the resistance of a fluid to deform under the shear
stress which is necessary for fluid flow (Fetter, 2001). In other words, dynamic viscosity
describes a fluid's internal resistance to flow. As the aqueous salt concentration

increases, the viscosity of the solution will also be affected. The higher the ionic strength of a solution, the higher the electrical attractions between ions in adjacent fluid layers and therefore the greater the viscosity of the fluid, and the greater the resistance to fluid flow. The relationship between NaCl concentration and the dynamic viscosity of a solution is shown in Figure 4.2. Dynamic viscosity and temperature have an inverse relationship. As the temperature of a fluid decreases, such as in the winter time, the viscosity of the fluid is expected to increase and the fluid will become more resistive to fluid flow. The effects of viscosity and density on solute transport are taken into account in MIN3PD, the numerical mode code used in this study.

Figure 4.2. Relationship between NaCl concentration and aqueous solution viscosity.
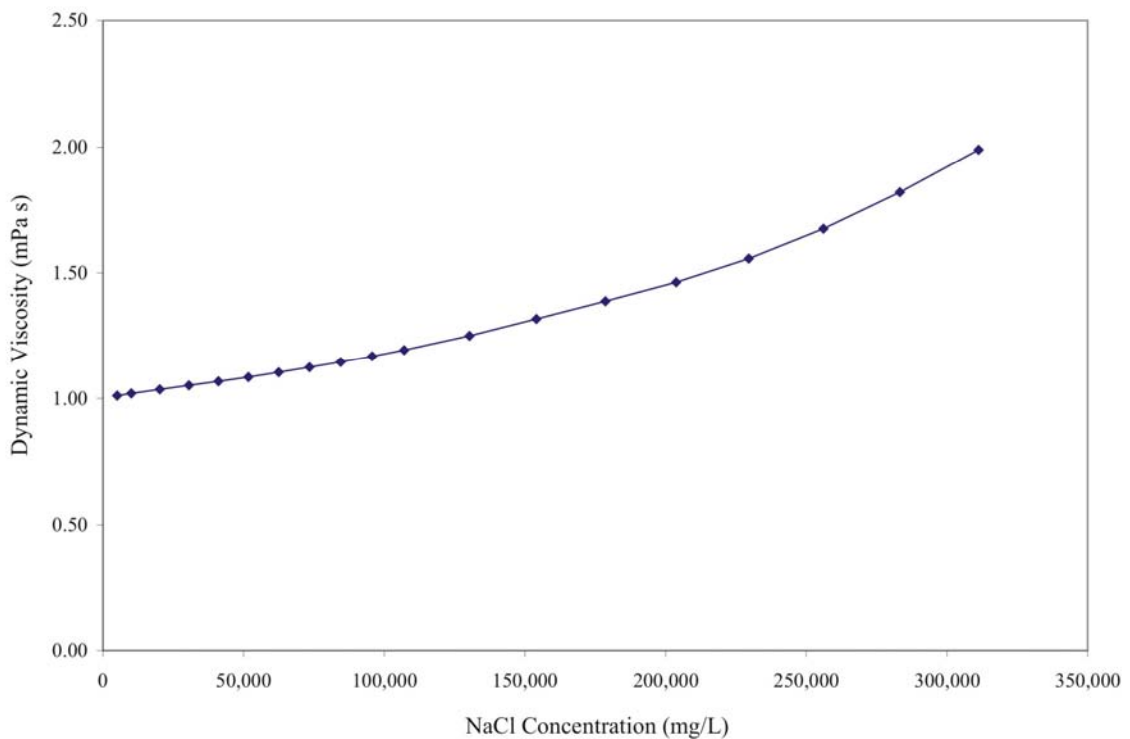
4.4.3 Diffusion, Advection and Mechanical Dispersion

Diffusion is the process by which ionic and molecular species dissolved in water move from areas of higher concentration to areas of lower concentration (Fetter, 2001). Fick's

second law describes the flux of a solute in a 1D system where concentrations change with time:

$$\frac{\partial C}{\partial t} = D\frac{\partial^2 C}{\partial x^2} \qquad\qquad 4.6$$

where C is the solute concentration, t is time, x is distance and D is the diffusion coefficient. Typical values for D for most solutes in water range from 1×10^{-9} to 2×10^{-9} m^2/s (Fetter, 2001). However, in porous media, D is generally lower due to the longer pathways ions must travel around mineral grains. The effective diffusion coefficient D^* can be defined as:

$$D^* = \omega D \qquad\qquad 4.7$$

where ω is an empirical coefficient that has been determined to range from 0.5 to 0.01 (Freeze and Cherry, 1979). The effective diffusion coefficient can therefore be expected to range between 1×10^{-11} and 1×10^{-9} m^2/s. Diffusion is not expected to be a significant process within the saturated zone at the site as solute transport due to groundwater flow, or advection, is likely to be much more dominant process. Within the unsaturated zone, solute transport due to diffusion may be a more significant process due to the low hydraulic conductivity of the unsaturated soils.

The advective mass flux (j_{adv}) is the solute mass crossing a unit area perpendicular to the groundwater flow direction, per unit time and is given by:

$$j_{adv} = u\phi_e c \qquad\qquad 4.8$$

where u is the groundwater velocity, ϕ_e is the effective porosity, and c is the solute concentration.

Mechanical dispersion is the process of uneven solute spreading and dilution within the porous medium due to small-scale aquifer heterogeneity (Gelhar et al., 1992). In a two-dimensional (2D) system, longitudinal dispersion is the mixing that occurs in the direction of groundwater flow and transverse dispersion is the mixing that occurs normal to the direction of groundwater flow. The longitudinal (D_L) and transverse dispersion (D_T) coefficients can be expressed as the product of an intrinsic aquifer property, the

dispersivity (α), and the intrinsic property of the flow field, which is given by the velocity (u). For uniform velocity in a 2D system, the dispersion coefficients are given by (Scheidegger, 1957):

$$D_L = \alpha_L u \qquad\qquad 4.9$$

$$D_T = \alpha_T u \qquad\qquad 4.10$$

For field-scale dispersion, there is a general trend of increasing longitudinal dispersivity with observation scale; however, it is unclear whether dispersivity increases indefinitely with scale or whether the relationship becomes constant for very large scales (Gelhar et al., 1992). Since this study involves transport of chloride, and chloride acts as a conservative tracer, trial and error and a sensitivity analysis was used to determine the dispersivity values that best reproduce the observed chloride plume at the site.

4.4.4 Preferential Flow

Preferential flow refers to the uneven and often rapid movement of water and solutes through porous media characterised by regions of enhanced permeability such that a small fraction of the porous media is responsible for most of the flow. Matrix flow is when water and solutes move through all of the porous media pore space and is a less rapid solute transport process compared to preferential flow. Conditions favourable for preferential flow are present when unsaturated soils contain macropores such as cracks associated with swelling and shrinking clays, plant root tunnels and worm holes. These macropores become preferential flow paths and the relationship between hydraulic conductivity, infiltrations rates and moisture content under conditions of preferential flow is highly complex (Richard and Steenhuis, 1988).

Previous tile drainage studies conducted in agricultural environments have shown that contaminants such as pesticides and newly applied tracers tend to exhibit preferential flow behaviour where concentrations increase as flow rates to the tile drainage system increase (Kladivko et al., 1991; Kung et al., 2000). Chemicals that are well distributed in

the soil tend to move more by matrix flow where at peak flow rates, contaminant concentrations tend to drop as concentrations are diluted by the relatively clean water flowing in the preferential pathways (Hallberg et al., 1986; Smettem et al., 1983). An examination of detailed tile drain sump effluent production data for 2004 (Appendix E) and a comparison of this data with groundwater quality results from the tile drain sump effluent (Table 2.3) shows that during months of peak tile drain production, for example August and May 2004, chloride concentrations in the tile drain sump effluent were lower than during months of lower tile drain production, for example September and October 2004. This may indicate that the chloride at the site tends to move more by matrix flow rather than preferential flow.

The numerical model chosen for this study does not incorporate the effects of preferential flow. A study performed by Richard and Steenhuis (1988) showed that transport times of a chloride tracer applied to a tile drained field exhibiting preferential flow characteristics was on the order of 3 to 4 hours rather than the 3 to 4 weeks predicted by a homogeneous matrix flow model. Neglecting the effects of preferential flow on solute transport at the study site could therefore result in an under-estimation of solute transport times.

4.4.5 Cation Exchange

Ion exchange occurs when ions attracted to a solid surface are exchanged for other ions in an aqueous solution (Fetter, 2001). Monovalent cations such as Na^+ and K^+ and divalent cations such as Mg^{2+} and Ca^{2+} are readily exchanged in natural soils while Cl^- is a conservative anion and does not participate in ion exchange reactions (Fetter, 2001). Ion exchange reactions are limited by the exchange capacity of the solid (Appelo and Postma, 1996). Clay minerals, organic matter and oxides and hydroxides all have a certain ion exchange capacity. The cation exchange capacity (CEC) of the site silt loam has been estimated to be relatively elevated, ranging from 10.2 to 33.1 meq/100 g from laboratory analysis of the CEC of selected soil samples.

When high concentrations of Na$^+$ are present in groundwater, some of the excess sodium may be exchanged onto the solid surface of the porous medium for Ca^{2+} or Mg^{2+} which then go into solution according to the following reversible exchange reaction:

$$Na^+ + Ca_{0.5} - X \leftrightarrow Na - X + \,^1/_2 Ca^{2+} \qquad\qquad 4.11$$
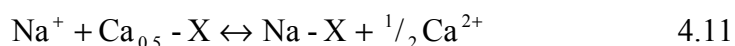
where X$^-$ is the exchange site. Evidence of the exchange of Ca^{2+} for Na$^+$ is present in the groundwater quality analysis from shallow wells at the site. In August 2004, 9,140 mg/L of Cl$^-$ was detected in water from monitoring well P04-2B (Table 2.2). If the plume source consisted predominantly of a NaCl type produced water, then approximately 5,930 mg/L of Na$^+$ would be expected to be present to maintain electroneutrality. In fact, only 1,650 mg/L of Na$^+$ was found; however, aqueous Ca^{2+} concentrations were elevated at 2,290 mg/L suggesting that Na$^+$ had replaced Ca^{2+} on the solid surface of the porous aquifer matrix. Similar Cl$^-$, Na$^+$ and Ca^{2+} aqueous concentration profiles can be found at the other impacted monitoring wells at the site (Table 2.1). Na$^+$ cation exchange at the site will ultimately cause a reduction in aqueous Na$^+$ concentrations and a retardation of the transport of the Na$^+$ plume. Na$^+$ concentrations in the plume will therefore be reduced through dilution with ambient fresh groundwater and will be further reduced by a variable amount according to the CEC of the soil.

4.4.6 Clay Dispersion

Clay particles generally have a net negative charge. This causes cations in solution to be attracted to the negatively charged surface of the clay. This results in cations being preferentially concentrated near the clay surface and gives rise to the double layer structure of clays that consists of the layer of strongly bound cations near the surface of the clay and a layer of weakly bound cations move between the solution and the clay surface. The weakly bound layer of cations is called the diffuse layer. When two clay particles approach each other, the positively charged diffuse layer causes the two particles to be repelled. The thickness of the diffuse layer depends on the ionic strength of the solution, where a higher ionic strength causes the diffuse layer to compress.

The more narrow the diffuse layer, the greater the chance that clay particles will approach each other and clump together, a process known as flocculation. The process of flocculation promotes the formation of soil aggregates and good soil structure.

Diffuse layer cations are most likely to participate in exchange reactions with other cations in solution. When diffuse layer Ca^{2+} cations exchange with Na^+ ions in solution, the larger ionic radius of the Na^+ cation does not enable as many Na^+ ions near the surface of the clay particle and the net negative charge of the clay surface is not neutralised. The net negatively charged clay particles will then repel each other, a process known as dispersion. Hydrated cations are also attracted to the negatively charged clay tetrahedral interlayers, which then causes the clay layers to swell and leads to a breakdown of the soil structure.

The best indicator for determining the potential for breakdown of soil structure is the ratio of the electrical conductivity (EC) of the soil to the sodium-adsorption ratio (SAR) of the soil (Richards, 1954):

$$SAR = \frac{[Na^+]}{\sqrt{\dfrac{[Ca^{2+}]+[Mg^{2+}]}{2}}} \qquad 4.12$$

where [ ] is concentration in milliequivalents/litre. An elevated SAR (greater than 7.0) can cause the structure of medium and fine textured soils to degrade, especially if the EC of the soil is not also correspondingly high. An elevated EC will tend to suppress the negative effects of dispersion in fine grained soils by promoting flocculation (Sumner, 1993).

Soil within the tile drainage area and a background location were sampled on July 29, 2004, after approximately 1 year of operation of the tile drainage system and analysed for saturated paste EC and SAR (WorelyParsons Komex, 2005b). EC and SAR values are plotted in Figure 4.3.

Soils with elevated SAR and lower EC are present at the site. In particular, borehole P04-2 contained very elevated SAR values ranging up to 35.4 but relatively low EC values at less than 12 dS/m (Figure 4.3). Similar patterns can be observed at shallow depths in other boreholes including P04-3 and P04-6. Elevated concentrations of exchangeable Na^+ will ultimately cause the hydraulic conductivity of the soil to be reduced by dispersion and migration of colloid particles that ultimately become logged in the conducting pores, thereby reducing hydraulic conductivity by a reduction in effective porosity, and the swelling of the clay minerals in the soil which usually occurs at large exchangeable sodium percentages and NaCl concentrations exceeding 584 mg/L (10^{-2} M) (Aringhieri and Giachetti, 2001). The reduction in the hydraulic conductivity of the soil that clay dispersion can cause will further hinder soil and groundwater remediation efforts as the capacity for soil flushing is reduced. The tendency will be for plumes to remain relatively stagnant and for contaminant concentrations to remain high over long periods of time.

4.4.7 Vegetation

Plants can affect salt accumulation and distribution patterns by influencing water fluxes across the ecosystem-unsaturated zone-aquifer continuum (Nosetto et al., 2007). Many studies have been conducted worldwide on the use of salt-tolerant plants to increase the productivity of salt-affected soils. Deep-rooted salt-tolerant crops such as safflower have been grown to lower shallow saline water tables resulting from growth of highly irrigated crops such as cotton (Bassil and Kaffka, 2002). Several studies have shown that growing salt-tolerant crops on highly saline sodic soils can significantly decrease soil salinity levels in comparison to unplanted control plots (Akhter et al., 2003). Cultivation of salt-tolerant plants helps to restore soil structure and permeability through plant root penetration and solubilisation of native soil calcium carbonate, which ultimately results in enhanced leaching of salts. The binding of the plant organic matter with soil particles also appears to release Na^+, which subsequently leaches to lower depths (Akhter et al., 2003).

Figure 4.3. 2004 soil salinity and sodicity within the tile drainage field area.
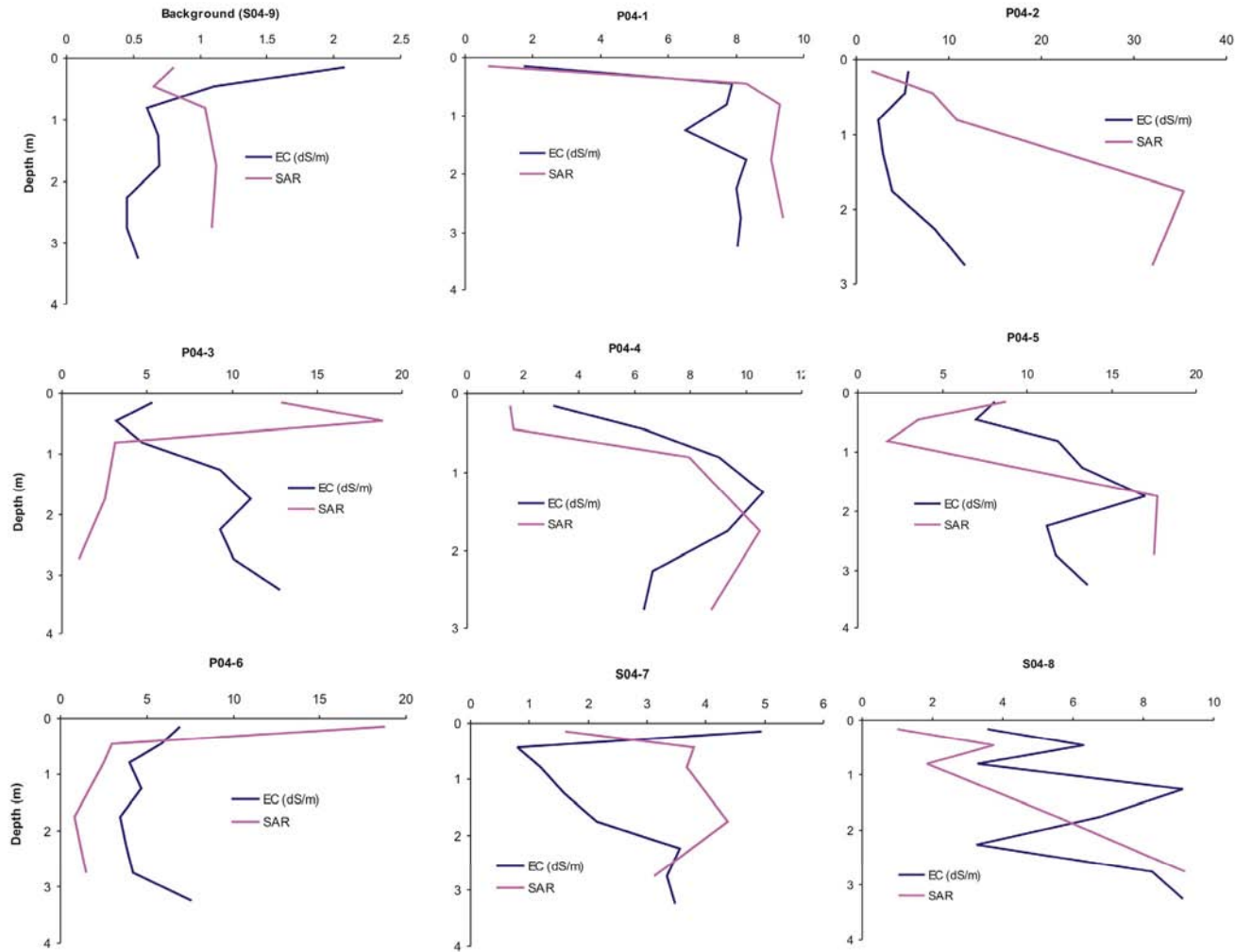
The numerical model built for this study does not account for the presence of vegetation. This may therefore be a source of error in the salt transport simulation results where salt concentrations may be over-predicted in the shallow unsaturated zone at depths less than 2 m and under-predicted at depths just above the water table due to the enhanced leaching of the salts from the rooting zone downward toward the water table.

4.5 Summary

Three hydrostratigraphic units of interest were identified at the site. These consist of the shallow, variably saturated silt loam located between ground surface and a depth of 6.25 m underlain by a fully-saturated fine grained sand lens approximately 1.25 m thick. Lower permeability glacial till was encountered underlying the sand lens. The mean saturated hydraulic conductivity of the silt loam calculated from hydraulic conductivity tests conducted at the site was 4.3×10^{-7} m/s. The hydraulic conductivity of the sand aquifer is estimated to be on the order of 4.4×10^{-5} m/s.

Groundwater flow within the unsaturated silt loam is predominantly downward towards the water table, although during some months of the year, upward flow may also occur. Groundwater flow within the saturated silt loam and the sand aquifer is to the northwest. Evidence for hydraulic separation between the silt loam and the underlying Horseshoe Canyon Formation sandstone can be seen from groundwater chemistry results where chloride concentrations remain well within background concentrations (<22 mg/L) within the Horseshoe Canyon Formation whereas much more elevated concentrations were detected in the silt loam (up to 19,000 mg/L).

Potential important inputs of water into the system include precipitation and potential outputs include surface water run-off, snow blowoff and sublimation, evapotranspiration and water loss due to the tile drainage system. The top infiltration boundary flux was calculated using output from VSMB and the relationship in equation 4.5. The monthly top infiltration boundary fluxes ranged from a minimum of -80.58 mm in July 1998 to a

maximum of +112.85 mm in September 1984. Annual infiltration boundary fluxes between 1984 and 2006 ranged from -33.15 mm/yr in 1987 to +88.20 mm/yr in 1997.

Transport of NaCl at the site is complex with the physical properties of the hydrostratigraphic units, the physical and chemical properties of NaCl and the nature of the produced water release all interacting to produce the currently observed plume. Unfortunately little is known of the produced water release that is responsible for the plume onsite. Due to the relatively elevated TDS observed in onsite monitoring wells ranging up to 32,700 mg/L in 1998, density-dependent groundwater flow is likely a significant process at the site in addition to the normally considered transport processes of diffusion, advection and mechanical dispersion. The CEC of the site silt loam is relatively elevated and cation exchange may be attenuating Na^+ transport as indicated by laboratory analysis of Ca^{2+} and Na^+ concentrations in shallow groundwater monitoring wells at the site. Clay dispersion and swelling is associated with Na^+ cation exchange in fine grained sediments which often results in a decrease in the hydraulic conductivity of the soil. EC and SAR results from soil samples collected at the site indicate that clay dispersion may be a problem on a local scale at the site, in particular in the vicinity of monitoring well P04-2A. This is consistent with the very low hydraulic conductivity (7.1×10^{-9} m/s) measured at monitoring well P04-2A.

The following chapter presents an introduction to the numerical model code chosen for this study in addition to the results of some benchmarking exercises performed for testing the density-dependent flow and transport component of the numerical model.

Chapter Five: Density-Dependent Flow and Transport Benchmarking

5.1 Introduction

Numerical models are typically benchmarked by verifying the code against standard analytical solutions to assess the accuracy of the numerical approximations. This becomes more complicated with density-dependent flow and transport simulations as analytical solutions are generally not available due to the complexities of the problem. Standardised test problems have therefore been proposed in the literature to act as benchmarks for density-dependent groundwater flow and transport models. Two density-dependent problems that are in widespread use for code benchmarking include the (Henry, 1964) salt-water intrusion problem and the (Elder, 1967) salt-convection problem. The following chapter includes an overview of the Henry and Elder density-dependent flow and transport benchmarking problems and a discussion of the simulation results performed in MIN3PD, the numerical model code that was selected for this study.

MIN3PD is a variably-saturated finite volume code capable of simulating density-dependent flow and transport in one, two or three spatial dimensions (Henderson et al., 2007; Mayer et al., 2002). Advective-dispersive transport in the aqueous phase can be considered and the model formulation is based on the global implicit solution approach (Steefel and Lasaga, 1994) which considers reaction and transport processes simultaneously. The model was chosen for this study because it was capable of simulating variably saturated density-dependent solute transport and could be extended to included heterogeneous reactions such as ion exchange, all of which were identified as important elements in the conceptual model of the study area.

5.2 Henry (1964) Problem

5.2.1 Problem Overview

The Henry (1964) salt-water intrusion problem consists of a 2D cross-section through an isotropic, homogeneous, confined aquifer. The problem describes the advance of

a saltwater front into a freshwater aquifer. It is classified as a weakly coupled flow and transport problem because the problem involves a total density variation of only 2.5%.

Henry (1964) developed a semi-analytical solution technique for this problem based on the Boussinesq approximation which consists of analytical expressions for the stream function and the salt concentration in the form of Fourier series. The resulting algebraic equations for determining the coefficients of the Fourier series are then solved by numerical techniques. Although widely used, the Henry (1964) problem remains controversial since no numerical model to date has been able to closely reproduce the original semi-analytical results (Kolditz et al., 1998). It has been suggested that there may have been some inaccuracies in the original analytical solution by Henry and that some subsequent numerical solutions contained inaccuracies due to discretisation and truncation errors (Croucher and O'Sullivan, 1995). The original semi-analytic solution developed by Henry was in fact later re-evaluated and was shown to contain several inaccuracies (Segol, 1994). The revised solution was compared by Segol (1994) to a finite element solution and the results were shown to be in closer agreement. It was suggested that this comparison was flawed; however, because the sea boundary conditions were different between the two solutions (Simpson and Clement, 2004). Inaccuracies, controversies and deficiencies aside, the Henry (1964) problem remains an important and popular problem for benchmarking density-dependent flow and transport models.

5.2.2 Model Domain, Grid, Boundary and Initial Conditions

The model domain consists of a 2D rectangular cross-section 2 m in length and 1 m in depth. A schematic of the problem, including boundary and initial conditions is included in Figure 5.1.

Figure 5.1. Domain, Boundary and Initial Conditions for the Henry Problem.
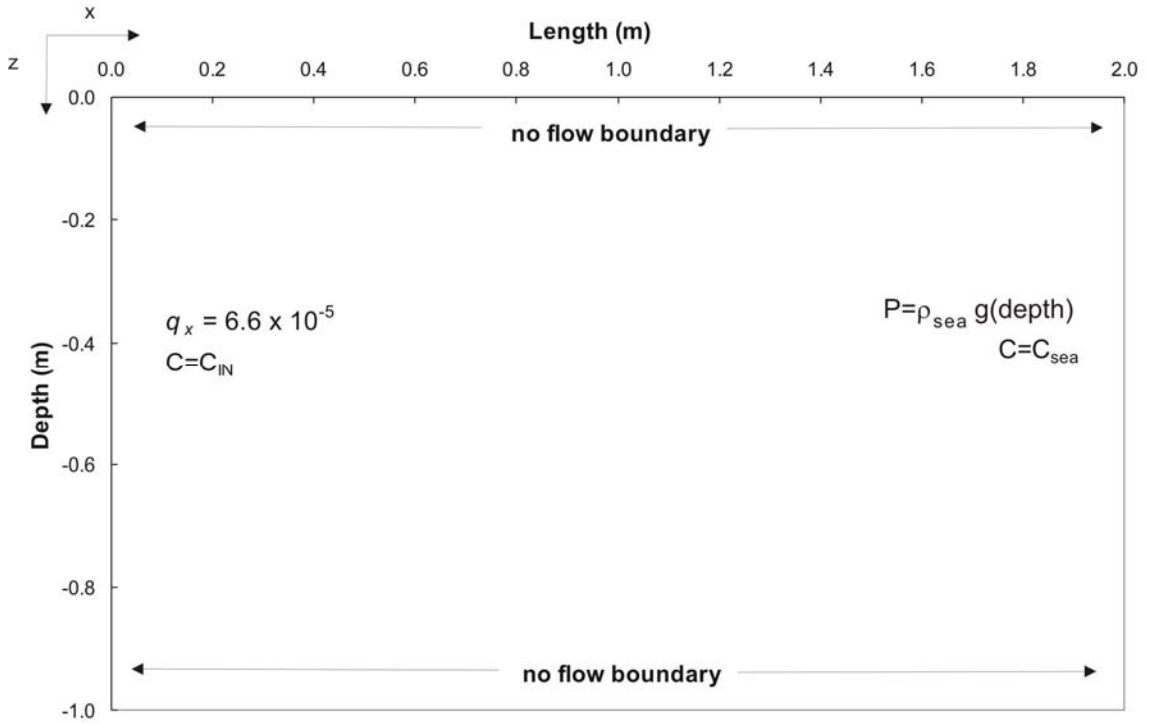
The initial simulation of the Henry problem used the same level of discretisation as the finite element solutions implemented by Voss and Souza (1987) and Oldenburg and Pruess (1994). It consisted of a regularly discretised 2D grid with a total of 231 nodes, where $N_x = 21$ and $N_z = 11$. A constant flux of freshwater recharge was applied to the left-hand side inland boundary (q_x) at a rate of 6.6×10^{-5} m/s while the right-hand side sea boundary consisted of a hydrostatic pressure head boundary calculated using the density of seawater ($P = \rho_{sea} \, g(depth)$). The top and bottom boundaries were no flow boundaries (Figure 5.1).

The sodium and chloride concentrations of the initial water in the aquifer and the freshwater infiltrating on the left boundary (C_{IN}) were set to 0.0005 mg/L, respectively. This was due to numerical difficulties encountered in the code when 0 mg/L concentrations were assigned. The TDS of the seawater (C_{sea}) was set at 36,592 mg/L as specified in Voss and Souza (1987). A summary of model input parameter values are included in Table 5.1. The simulation was performed a total of four times with

successively finer grids by halving the discretisation each time to evaluate the truncation error in the solution. The finest grid used consisted of 168 horizontal nodes and 88 vertical nodes for a total of 14,784 nodes in the grid.

Table 5.1. Summary of model input parameters for Henry Problem.

Symbol	Parameter	Value	Units
D_m	Coefficient of Molecular Diffusion	1.886e-5	m^2/s
α_L and α_T	Longitudinal and Transverse Dispersivity	0.0	m
g	Acceleration due to Gravity	9.8	m/s^2
K	Hydraulic Conductivity	1.0e-2	m/s
q_x	Right Boundary Recharge Flux	6.6e-5	m/s
S_s	Specific Storage	0.0	m^{-1}
ϕ	Porosity	0.35	-
ρ	Freshwater Density	1000	kg/m^3
ρ_s	Saltwater Density	1025	kg/m^3
C_{IN}	Cl and Na concentration on land-side boundary	0.0005	mg/L
C_{sea}	NaCl concentration at sea-side boundary	36,592	mg/L
$\dfrac{\partial \rho}{\partial C}$	Slope of line relating fluid density to TDS concentration (both in g/L)	0.7	-

5.2.3 Time Step and Solver Information

The MIN3PD code contains an adaptive time-stepping scheme which requires the specification of a minimum and maximum time step Δt. After obtaining the solution at time level *L*, the next time step is chosen in the following manner (Therrien and Sudicky, 1996):

$$\Delta t^{L+1} = \frac{S_w^*}{\max\left[S_{w_i}^{L+1} - S_{w_i}^L\right]} \Delta t^L \qquad\qquad 5.1$$

where S_{w_i} is the water saturation at node *i* and S_w^* is the maximum change in water saturation allowed during a time step and was specified as 0.1 in the input file. For each simulation of the Henry problem the minimum time step was set at approximately 1×10^{-7} seconds and the maximum time step was set at 144 minutes. The maximum time step was kept small to minimise numerical dispersion in the solution. The courant

criteria is related to the travel distance across a grid cell of a particle during a time step and was defined as:

$$C_o = \frac{v \Delta t}{\Delta x} \leq 0.9 \qquad\qquad 5.2$$

where v is the groundwater velocity and Δx is the distance between adjacent nodes in the direction of groundwater flow. The courant criteria also controls the size of the maximum time step used during this simulation. The transient flow and solute transport parts of the problem were solved simultaneously using the same time steps.

An upstream spatial weighting scheme was used to model the advective transport. No tortuosity correction was applied to the problem and the tortuosity was set to unity as specified in Oldenburg and Pruess (1994). The solver package WATSOLV (VanderKwaak et al., 1997) is implemented in MIN3PD and the settings for the solution to the transient flow problem were the same as those for the solute transport problem.

5.3 Elder (1967) Problem

5.3.1 Problem Overview

The Elder (1967) salt-convection problem is a free convection problem that was originally designed as pure thermal convection but has subsequently been adapted for pure solute convection. The large maximum density change of 20% makes it a strongly coupled flow and transport problem. The original Elder problem consisted of laminar fluid flow in a closed rectangular box modeled in cross-section. The flow within the box was initiated by a vertical temperature gradient and thermally-induced density gradients caused fingering of the denser water within the box. Elder (1967) studied the problem physically in the laboratory using a Hele-shaw cell and obtained a numerical solution as well. The problem was then modified by Elder with parameters suited to porous media flow where the density-dependence was caused by variations in solute concentration. The modified Elder problem has since become a standard benchmark problem for testing density-dependent numerical models for strongly coupled flow and transport problems

(Boufadel et al., 1999; Kolditz et al., 1998; Oldenburg and Pruess, 1995; Simpson and Clement, 2003; Voss and Souza, 1987).

5.3.2 Model Domain, Grid, Boundary and Initial Conditions

The model domain for the Elder problem consists of a 2D rectangular cross-section 600 m in length (x-direction) and 150 m in depth (z-direction). A schematic of the problem, including boundary and initial conditions is included in Figure 5.2.

Figure 5.2. Domain, boundary and initial conditions for the Elder Problem.
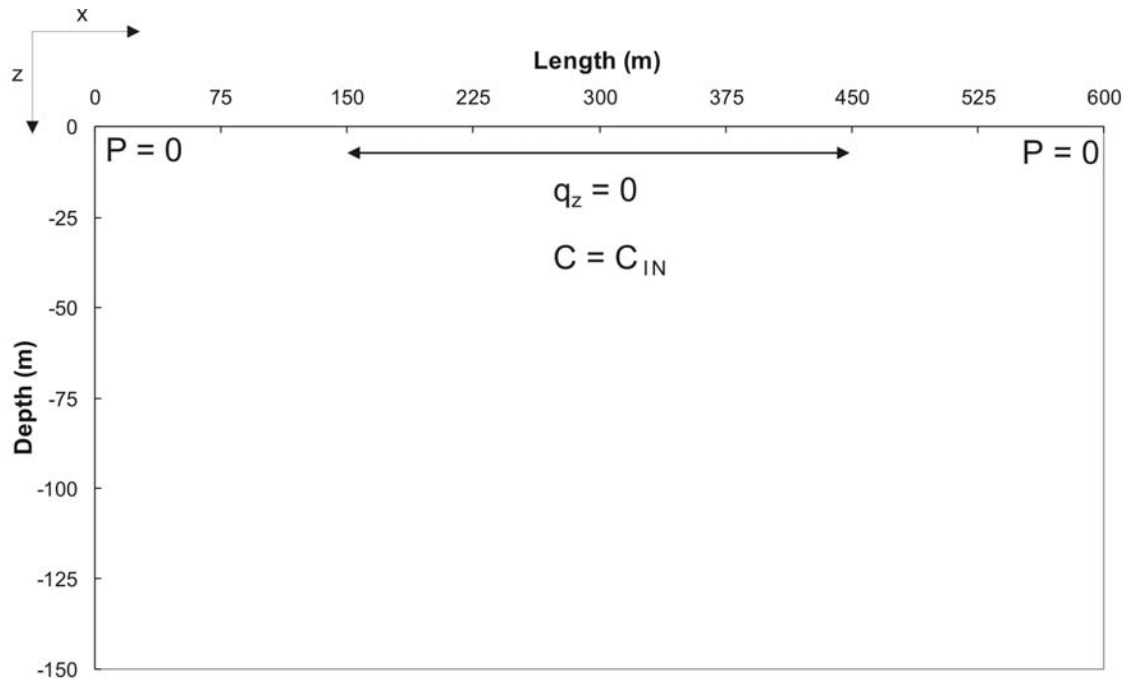
The grid used in the initial simulation of the Elder problem contained the same level of discretisation as the finite element solutions obtained by Voss and Souza (1987) and Oldenburg and Pruess (1995). It consisted of 45 nodes in the x-direction and 26 nodes in the z-direction (coarse grid) for a total of 1,170 nodes. The grid was subsequently refined to 90 nodes in the x-direction and 52 nodes in the z-direction for a total of 4,680 nodes (fine grid) and then refined again to 180 nodes in the x-direction and 104 nodes in the z-direction for a total of 18,720 nodes (very fine grid) to obtain levels of discretisation

similar to those used by other authors (Kolditz et al., 1998; Oldenburg and Pruess, 1995; Simpson and Clement, 2003).

Elder's problem involves transport in a closed rectangular box by diffusion. Each side of the model domain consisted of a no-flow boundary condition (Figure 5.2). At both of the top corners of the model domain a constant pressure head value of 0 was specified and the pressure was initially hydrostatic. At the top of the rectangle along the x-axis between 150 and 450 m was a constant source (C_{in}) with a concentration of 310,000 mg/L of NaCl (188,057 mg/L Cl$^-$ and 121,943 mg/L Na$^+$). Using a salt concentration approximately equal to the maximum solubility of salt in water simulates a high concentration boundary layer that could have been formed by the evaporation of water from a salt lake; however, in this case, evaporation is assumed to have ceased in accordance with the original Elder problem (Boufadel et al., 1999). A summary of model input parameter values are included in Table 5.2.

Table 5.2. Summary of Input Parameters for Elder Problem.

Symbol	Parameter	Value	Units
D_m	Coefficient of Molecular Diffusion	3.565e-6	m^2/s
α_L and α_T	Longitudinal and Transverse Dispersivity	0	m
g	Acceleration due to Gravity	9.81	m/s^2
K	Hydraulic Conductivity	4.75e-6	m/s
μ	Viscosity	1e-3	Pa s
S_s	Specific Storage	0.0	m^{-1}
ϕ	Porosity	0.1	-
ρ	Freshwater Density	1,000	kg/m^3
ρ_s	Brine Density	1,200	kg/m^3
C_{IN}	Salt concentration at source boundary	310,000	mg/L
$\dfrac{\partial \rho}{\partial C}$	Slope of line relating fluid density to TDS concentration (both in g/L)	0.6452	-

5.3.3 Time Step and Solver Information

The MIN3PD code contains an adaptive time stepping scheme as outlined in Section 5.2.3 which requires the specification of a minimum time step and a maximum time step. For each simulation of the Elder Problem the minimum time step was set at approximately 1×10^{-3} seconds and the maximum time step was set at 86.4 seconds. The transient flow and solute transport parts of the problem were solved simultaneously using the same time steps.

Upstream weighting was used to model the advective transport. No tortuosity correction was applied to the problem and the tortuosity was set to unity as specified in Oldenburg and Pruess (1994). The solver package WATSOLV (VanderKwaak et al, 1997) is implemented in MIN3PD.

5.4 RESULTS AND DISCUSSION

5.4.1 Henry Problem

The results of the Henry problem for the coarse, medium, fine and very fine grids at a simulation time of 2 days are included in Figure 5.3. The simulation results show that seawater is intruding into the model domain through the lower right-hand side boundary and that the denser seawater is moving in underneath the freshwater. Seawater also appears to be intruding into the model domain in the upper right hand corner in the top 0.2 m along the boundary. This feature was not observed in the results of other authors, likely because many solutions reviewed for this study (Simpson and Clement, 2004; Voss and Souza, 1987) used the modified boundary condition:

$$\frac{\partial C}{\partial x} = 0 \qquad\qquad 5.3$$

applied to the upper 0.2 m of the sea-side boundary while this study used Henry's original sea-side boundary condition of $C = C_{sea}$. Other authors likely used the modified boundary condition to eliminate seawater intruding in the upper sea-side boundary of the model domain which is the result of a non-physically based boundary condition.

Seawater would not be expected to intrude into the upper corner of the aquifer due to the density-differences between the aquifer groundwater and the intruding seawater. The MIN3PD solutions should therefore not be compared to the other solutions near the upper part of the sea boundary; however, throughout the remainder of the aquifer, comparisons can still be made (Croucher and O'Sullivan, 1995).

Figure 5.3. Positions of the 25, 50 and 75% isochlors for the MIN3PD solution to the Henry Problem at t = 2 days. Results are shown for the coarse grid (a), the medium grid (b), the fine grid (c), and the very fine grid (d).
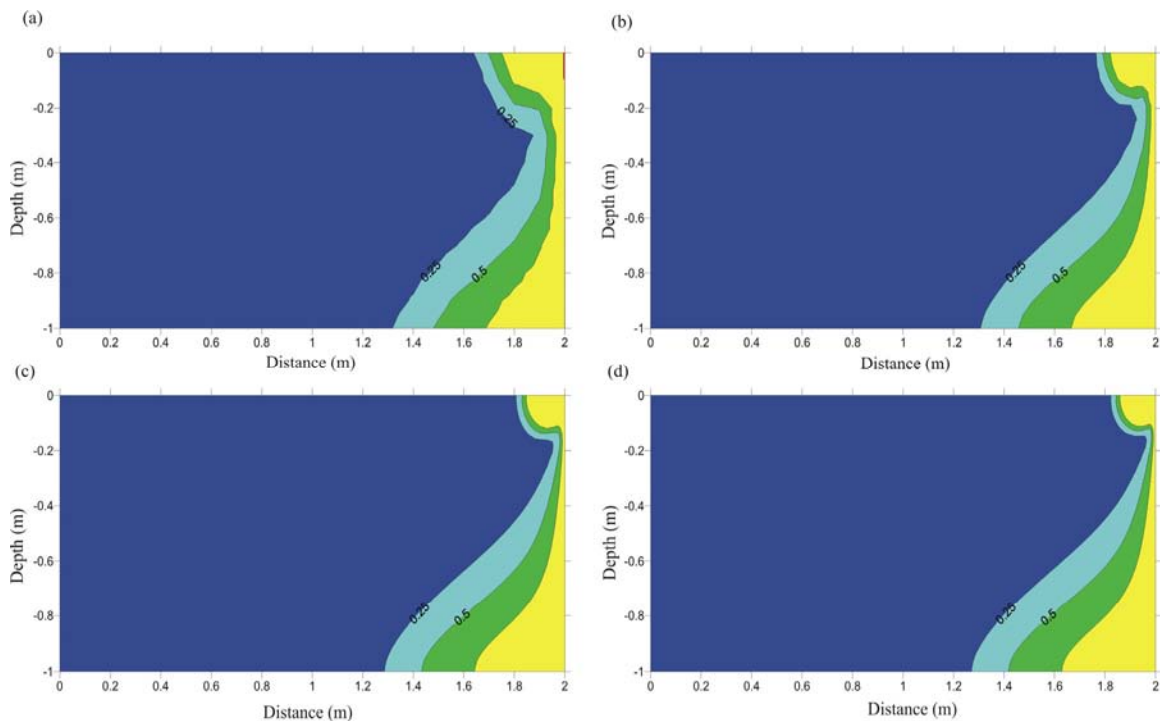
In general, the results of the Henry problem simulation in MIN3PD agree well with the results of other authors (Figure 5.4). The same pattern of seawater intruding into the lower part of the model domain can be seen. The positions of the isochlors also compare well with published results from other models. The 0.50 isochlor in the MIN3PD simulation (Figure 5.3) extends to the 1.42 m mark along the bottom boundary of the model domain. The 0.50 isochlor in the majority of the published results extends between 1.15 m (Croucher and O'Sullivan, 1995) and 1.40 m (Simpson and Clement,

2004; Voss and Souza, 1987) from the edge of the freshwater aquifer along the bottom boundary (Figure 5.4).

Figure 5.4. The steady state Henry Problem results of (a) Simpson and Clement (2004) using a grid with Nx = 41 and Nz = 21 and (b) MIN3PD using the same grid.
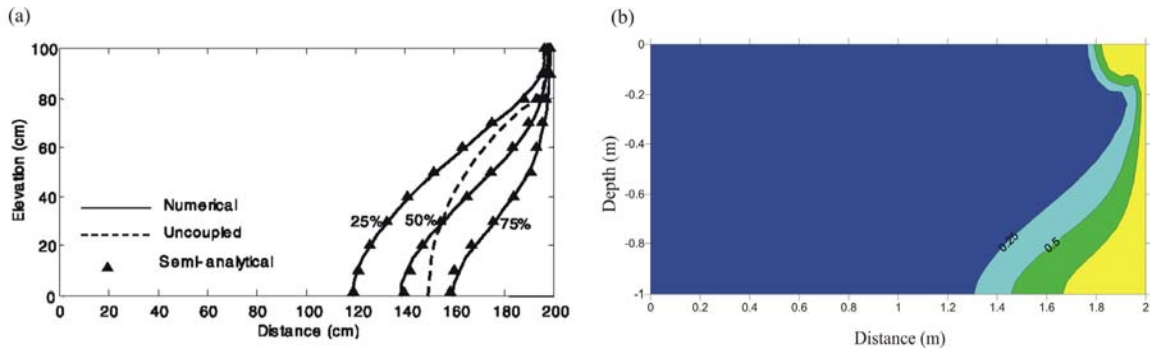
5.4.2 Elder Problem

Given the range of solutions present in the literature, a qualitative comparison was undertaken between MIN3PD results and the results of other authors who published results with similarly discretised grids. The MIN3PD coarse grid results were compared with the results of Oldenburg and Pruess (1994) and Voss and Souza (1987; Figure 5.5), the MIN3PD fine grid results were compared with the results of Simpson and Clement (2003; Figure 5.6) and the MIN3PD very fine grid results were compared with the results of Kolditz et al. (1998; Figure 5.7).

The results of Voss and Souza (1987) and Oldenburg and Pruess (1994) show the 0.6 isochlor forming a single lobe extending beyond 125 m depth while the MIN3PD 0.6 isochlor continued to show three lobes that extended less than 100 m depth (Figure 5.5). The shape of the 0.2 isochlor is different for each of the simulations with the results of Voss and Souza (1987) showing one large lobe with two smaller side lobes, the results of Oldenburg and Pruess (1994) showing a single large lobe and the MIN3PD results showing two large side lobes and a smaller centre lobe. The maximum depths of the 0.2 isochlors; however, were similar in each of the simulations.

Figure 5.5. Positions of the 0.6 and 0.2 isochlors for the Elder Problem with $N_x = 45$ and $N_z = 26$ (coarse grid) at t = 2, 10 and 20 years. Results from (a) Voss and Souza (1987), (b) Oldenburg and Pruess (1994) and (c) MIN3PD.
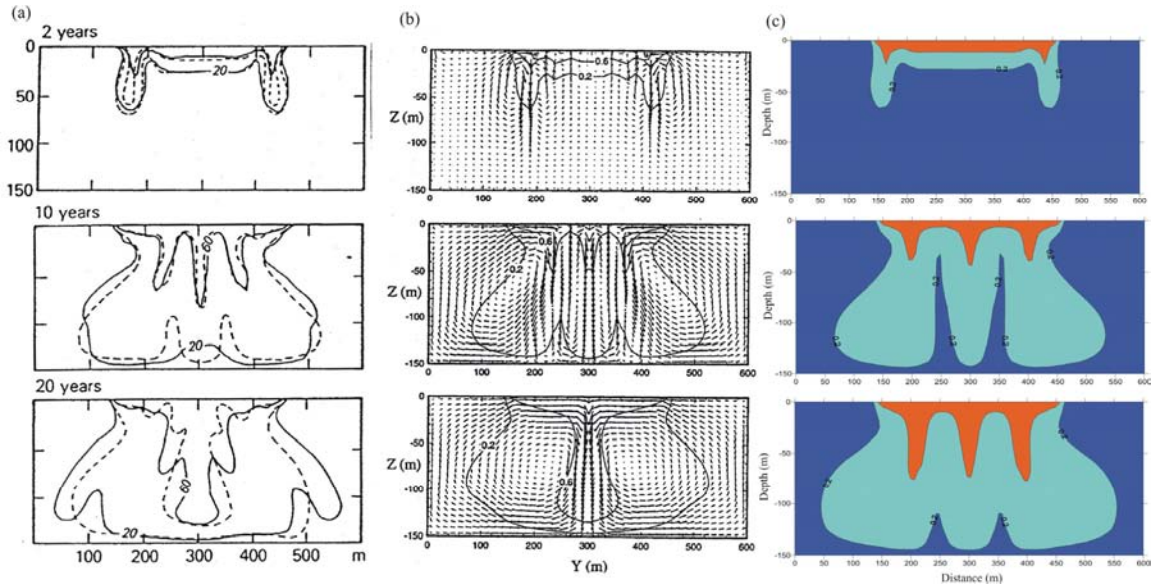
Figure 5.6. Positions of the 0.6 and 0.2 isochlors for the Elder Problem with $N_x = 90$ and $N_z = 52$ (fine grid) at t = 2, 4 and 10 years for (a) the results of Simpson and Clement (2003) and (b) MIN3PD.
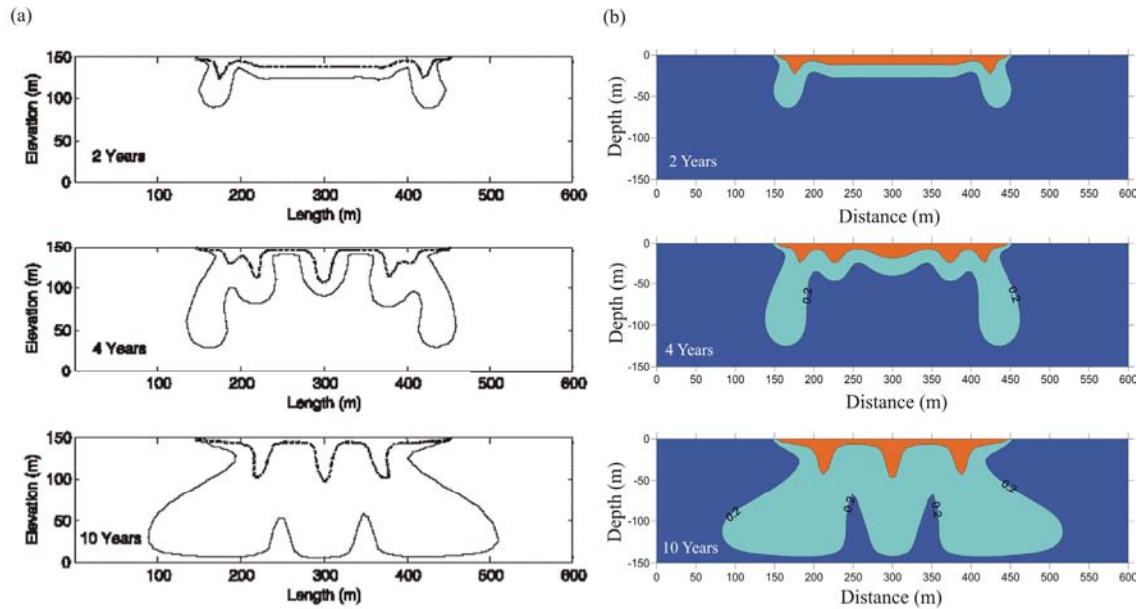
The MIN3PD fine grid results agree quite well with the fine grid results of Simpson and Clement (2003; Figure 5.6). Both the shape and the depth of penetration of the 0.2 and 0.6 isochlors are virtually identical at t = 2 years. At t = 4 years, the number of lobes and the maximum depths of the 0.2 isochlors are virtually the same. The 0.6 isochlors have the same number of lobes; however, the results of Simpson and Clement (2003) show the 0.6 isochlor penetrating to a slightly greater depth. At t = 10 years, the shapes and depths of penetration of both the 0.6 and 0.2 isochlors are virtually the same, with the exception of the central lobe of the 0.2 isochlor in the MIN3PD simulation which was slightly smaller than in the Simpson and Clement (2003) simulation.

The MIN3PD very fine grid results are compared to the very fine mesh results of Kolditz et al. (1998; Figure 5.7). The 0.6 isochlors for the 10, 15 and 20-year simulations of Kolditz et al. (1998) contained two major lobes that extended almost to the base of the model domain after t = 10 years, while the MIN3PD simulation 0.6 isochlors for the same time periods contained three major lobes that remained in the upper half of the model domain beyond t = 20 years (Figure 5.7). The 0.2 isochlors in both simulations extended to the base of the model domain after t = 10 years; however, in the Kolditz et al. (1998) simulation, there were 4 lobes at 10 years and 2 lobes at 15 and 20 years, while in the MIN3PD simulations there were 3 lobes at each of the simulation times (Figure 5.7).

Figure 5.7. Positions of the 0.6 and 0.2 isochlors for the Elder Problem with $N_x = 180$ and $N_z = 104$ (very fine grid) at $t = 4$, 10, 15, and 20 years for (a) the results of Kolditz et al. (1998) and (b) MIN3PD.
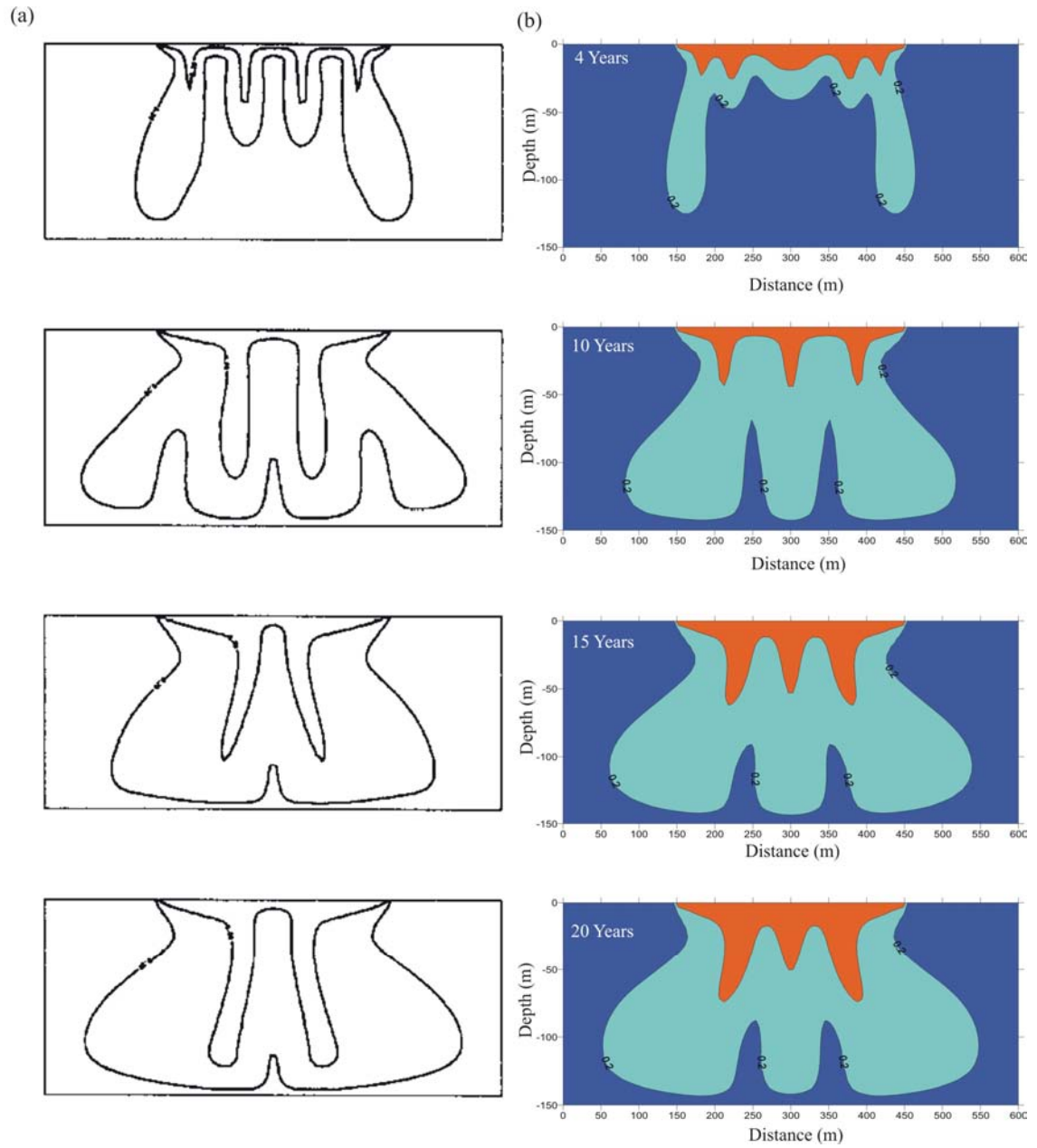
5.5 Summary

The results of this exercise show that although benchmark problems can be a useful check on density-dependent flow and transport codes, the process of achieving an exact match to previously published results can be long and in some cases, may not be possible. Numerical models of strongly coupled groundwater-brine transport and flow regimes are very sensitive to model input parameters and to the numerical solution method itself. Factors such as molecular diffusivity, numerical dispersion, and changes in initial conditions can greatly influence model results (Oldenburg and Pruess, 1995).

The fit between the results of the Henry problem solved using MIN3PD and other numerical models was good taking into account the differences in the sea-side boundary condition. The essential features of the problem, that seawater intrudes approximately 1 m into the lower part of the aquifer, were well captured. However, according to Simpson and Clement (2003), the solution to the Henry problem depends largely on boundary forcing and therefore the Henry salt-water intrusion problem has limited usefulness in benchmarking density-dependent flow models. The flow patterns in the Elder salt-convection problem are completely determined by the internal balance of pressure and gravity forces and therefore it is more suited to the testing of density-dependent flow and transport problems (Simpson and Clement, 2003).

The fit between the results of the Elder problem simulated using MIN3PD and those of Simpson and Clement (2003) using a refined grid was quite good; however, the fit between MIN3PD results and those of other authors was variable. At early times up to and including 10 years, the fit between the number of salt lobes and the general depths to which the isochlors extended was generally good. At later times, however, the salt lobes in the other numerical models tended to coalesce into larger blobs and the number of fingers was generally reduced whereas in MIN3PD, the salt lobes tended to remain distinct and the same number of salt fingers was seen at 15 and 20 years as was observed at 10 years. At the field scale, the salt-fingering phenomenon develops due to heterogeneities in the aquifer. According to Mazzia et al. (2001) salt fingers develop in

a numerical model because of perturbations due to the local truncation error inherent in the spatial and temporal discretisation. The size of the truncation error goes to zero as the grid spacing and the time step go to zero. It is therefore impossible to completely eliminate truncation error from a simulation as there will always be a certain grid spacing and time step interval, no matter how small these both become. The tendency for there to be a large number of small fingers at early simulation times that coalesce into larger fingers at later times is due to hydrodynamic and/or numerical dispersion. This phenomenon was more evident with the Elder problem simulation results of other authors than with the MIN3PD results, where salt fingers tended to remain more distinct.
In a simulation of a real problem, it would be difficult to distinguish between numerical dispersion in the simulation and actual physical dispersion. The solution to the Elder problem also depends heavily on numerical discretisation and the level of modeling sophistication used to generate the results (Simpson and Clement, 2003).

Benchmarking the MIN3PD code validated that the code can accurately represent the physical process of density-dependent flow and transport. If this process is a factor at the site, the benchmarking process increased the confidence that these effects would be accounted for in the flow and transport model simulation results for the site.

The following chapter presents a preliminary, large scale numerical model for the study area. The preliminary numerical model was calibrated and a sensitivity analysis was performed to determine the most important features that must be included in the tile drainage simulations.
.

Chapter Six: Numerical Model

6.1 Introduction

6.1.1 Governing Equations

The computer program MIN3PD was used to simulate variably-saturated flow and transport of NaCl brine. MIN3PD represents a generalization of MIN3P (Mayer et al., 2002) that simulates the movement of variable density fluids in variably-saturated media under isothermal conditions and reactive chemical transport. Physical properties of the fluids, including density and viscosity, are computed as a function of dissolved solute concentrations. The statement of fluid mass conservation implemented in MIN3PD for variable density fluids in variably-saturated media is given by (Henderson et al., 2007):

$$\frac{\partial}{\partial t}(S_a \phi \rho) - \nabla \cdot \left[\rho \frac{k_r \mathbf{k}}{\mu}(\nabla P_a + \rho g \nabla z) \right] = \rho Q_a \qquad 6.1$$

where t is time, S_a is the saturation of the aqueous phase, ϕ is the porosity, ρ is the density of the fluid, k_r is the relative permeability of the porous medium, $\mathbf{k}$ is the intrinsic permeability tensor, μ is the dynamic viscosity, P_a is the fluid pressure, g is the acceleration due to gravity, z is the height above the datum, and Q_a is a source/sink term for the aqueous phase. The fluid mass accumulation term in equation 6.1 includes temporal changes in fluid pressure, saturation and the total solute concentration:

$$\frac{\partial}{\partial t}(S_a \phi \rho) = S_a \rho S_p \frac{\partial P_a}{\partial t} + \rho \phi \frac{\partial S_a}{\partial P_a}\frac{\partial P_a}{\partial t} + S_a \phi \frac{\partial \rho}{\partial c_t}\frac{\partial c_t}{\partial t} \qquad 6.2$$

where S_p is the specific storage coefficient defined with respect to changes in fluid pressure and c_t is the total dissolved solute concentration. The S_p coefficient is related to the specific storage coefficient S_s by the following relationship:

$$S_p = \frac{S_s}{\rho_f g} \qquad 6.3$$

where ρ_f is the reference freshwater density. Multi-component reactive transport is implemented in MIN3PD with the following mass conservation equation for component A_j written in terms of total component concentration T_j (Mayer et al., 2002):

$$\frac{\partial}{\partial t}\left[S_a\phi T_j^a\right]+\frac{\partial}{\partial t}\left[S_g\phi T_j^g\right]+\nabla\cdot\left[\mathbf{q}_a T_j^a\right]-\nabla\cdot\left[S_a\phi\mathbf{D}_a\nabla T_j^a\right]$$
$$-\nabla\cdot\left[S_g\phi\mathbf{D}_g\nabla T_j^g\right]-Q_j^{a,a}-Q_j^{a,s}-Q_j^{a,ext}-Q_j^{g,ext}=0\qquad j=1,N_c$$

6.4

where S_g is the saturation of the gaseous phase, T_j^a is the total aqueous component

concentration for component A_j^c, $\mathbf{q}_a$ is the Darcy Flux vector, $\mathbf{D}_a$ and $\mathbf{D}_g$ are the

dispersion tensors for the aqueous and gaseous phases, respectively, $Q_j^{a,a}$ and $Q_j^{a,s}$

are internal source and sink terms for the total aqueous component concentrations due to

intra-aqueous kinetic reactions and kinetically controlled dissolution-precipitation

reactions, respectively, and $Q_j^{a,ext}$ and $Q_j^{g,ext}$ are external source and sink terms for the

aqueous and gaseous phases, respectively.

6.1.2 Numerical Methods

The numerical model MIN3PD employs the fully-implicit method to handle time

discretisation and the spatial discretisation is based on a control volume block centred

finite difference method. The finite volume method is an extension of the finite

difference method that can handle unstructured grids in an easier fashion (Rausch et al.,

2005). Discretisation with the finite volume method within MIN3PD is based on mass

balance for a cell (or volume) within a regular grid. The discretisation error for the finite

volume approximation of the transport equation is proportional to the square of the

maximum distance between two nodes (Rausch et al., 2005). Reducing the grid size by

half leads therefore leads to a reduction of the spatial truncation error by a factor of 4.

6.2 Numerical Model Construction

6.2.1 Model Domain and Grid

A simplified 2D approach was taken based on the conceptual model of groundwater flow

within the unsaturated silt loam deposits being primarily vertically downward and

groundwater flow within the saturated silt loam and sand aquifer being primarily laterally

to the north. The 2D model domain consists of a sub-section of the site that covers the

southern portion of the tile drainage system where the core samples were taken. A sub-section of the site was chosen because the processes being investigated by this study; salt plume migration in the unsaturated zone and the effectiveness of tile drainage systems as a method of salt remediation, could be adequately represented by the smaller domain. Figure 6.1 shows the model domain cross-section line A-A'.

Figure 6.2 shows a schematic cross-section of the numerical model domain. The north-south cross-section was taken parallel to the direction of saturated groundwater flow in order to capture the main features of both the saturated and unsaturated flow systems. Also, because the tile drain lines run east-west across the site, a north-south cross-section perpendicular to the locations of the tile drain lines will enable the effect of the drain on the water table position to be easily seen. The numerical model domain consists of an area 1,125 m^2 from an elevation of 718.0 to 725.5 m in the vertical (z) direction and 150 m extending north-south in the horizontal (x) direction.

The model domain was discretised using a constant 1.0 m grid spacing (Δx) in the x-direction for a total of 150 nodes (N_x) and an irregular grid spacing (Δz) in the z-direction consisting of 7 different discretisation intervals. The irregular grid spacing in the z-direction was necessary due to the very small nodal spacing required in the unsaturated zone to ensure model convergence. The finite difference model rule of thumb was used to expand the nodal spacing downward into the saturated zone by increasing the nodal spacing by no more than 1.5 times the previous nodal spacing (Anderson and Woessner, 2002). There was a total of 172 nodes (N_z) in the z-direction for a total of 25,800 nodes in the model domain. Table 6.1 provides a summary of the numerical model spatial discretisation.

Figure 6.1. Site plan with model domain cross-section line.
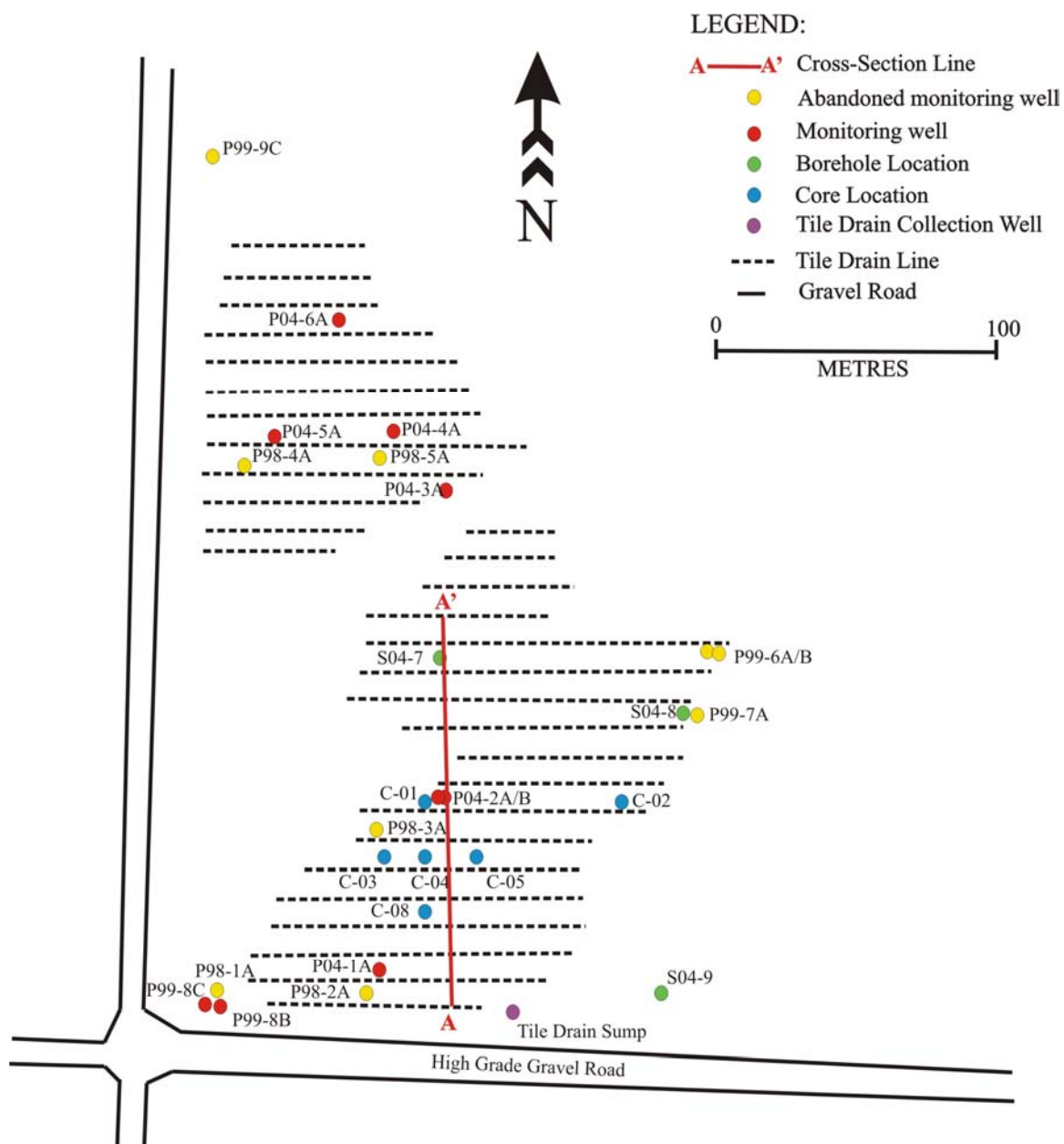
Figure 6.2. Numerical model domain, initial and boundary conditions.
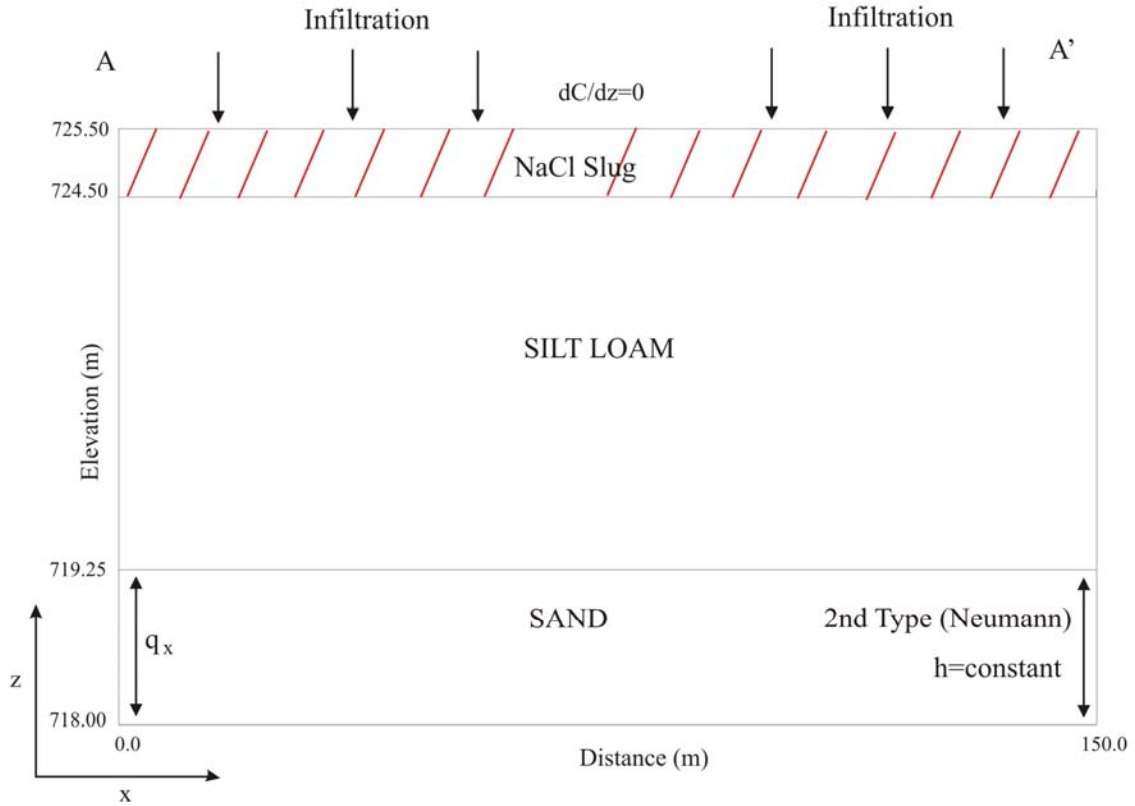
6.2.2 Aquifer Parameters

The hydrostratigraphic units represented in the numerical model consist of the silt loam and the underlying sand aquifer. The aquifer parameters specified for both units are summarised in Table 6.2. The soil unsaturated and hydraulic parameters, with the exception of van Genuchten parameter α, assigned to both the silt loam and the sand aquifer were derived experimentally in the laboratory and through analysis of field tests as described in Sections 3.4.2 and 4.2.2. The value of α used in the variably-saturated numerical model for silt loam was 0.48 m^{-1} which is very similar to the average value of α (0.50 m^{-1}) obtained from analysis of 332 silt loam soil samples (Schaap and Leij, 1998). The specific storage (S_s) for the silt loam and the sand aquifer was calculated using the following relationship:

$$S_s = \rho_w g \left(\beta_p + \phi \beta_w \right) \qquad 6.5$$

where ρ_w is the density of freshwater, g is the acceleration due to gravity, β_p is the

coefficient of vertical compressibility of the soil type and was taken as 2.6 x 10^{-7} m^2/N

for the silt loam and 1 x 10^{-7} m^2/N for the sand (Domenico and Schwartz, 1998), ϕ is the

porosity and β_w is the fluid compressibility.

In natural soils, a less-compacted, higher hydraulic conductivity layer would be expected

to be present near the ground surface due to tilling and the presence of roots and worm

holes that create macroporosity and soil structure. In order to simulate this higher

permeability layer, the top 0.5 m of the model domain was assigned a different hydraulic

conductivity every 0.1 m that varied linearly from a hydraulic conductivity of

4.25 x 10^{-7} m/s at en elevation of 725.0 m to an upper limit of 4.25 x 10^{-6} m/s at the

ground surface elevation of 725.5 m. This resulted in a total of six different hydraulic

conductivities within the silt loam hydrostratigraphic unit. The higher permeability

layers act to allow more rapid infiltration of precipitation in the top 50 cm of the soil

profile, similar to what would be observed in the presence of a natural tilled soil with

roots and worm holes, and was required for the solution to converge. A summary of the

hydraulic conductivities assigned within the numerical model is included in Table 6.3.

Table 6.1. Numerical model spatial discretisation.

x-direction discretisation interval	x min (m)	x max (m)	Dx (m)	Nx
1	0.0	150.0	1.00	150

z-direction discretisation interval	z min (m)	z max (m)	Dz (m)	Nz
1	718.00	724.00	0.10	60
2	724.00	724.21	0.07	3
3	724.21	724.36	0.05	3
4	724.36	724.45	0.03	3
5	724.45	724.47	0.02	1
6	724.47	724.50	0.015	2
7	724.50	725.50	0.01	100
			Total Grid Nodes	25,800

Table 6.2. Summary of aquifer and transport parameters assigned in the numerical model.

Aquifer Parameter	Silt Loam	Sand	Units
Porosity	0.51	0.38	-
Hydraulic Conductivity	4.25E-07*	4.44E-05	m/s
Specific Storage Coefficient	2.50E-03	1.00E-03	m^{-1}
Residual Saturation	0.137	0.125	-
van Genuchten Parameter alpha	0.480	3.65	m^{-1}
van Genuchten Parameter n	1.09	2.7	-
Transport Parameters			
Longitudinal Dispersivity	3.0		m
Transverse Dispersivity	0.03		m
Gaseous Phase Diffusion	1.50E-05		m^2/s
Aqueous Phase Diffusion	1.00E-09		m^2/s
Initial Souce NaCl Concentration	100,000		mg/L
Background NaCl Concentration	10		mg/L
Fluid Density/TDS (both in g/L)	0.6410		-

Notes:
* - increases linearly between 725.0 and 725.5 m elevation from 4.25E-07 to 4.25E-06 m/s

Table 6.3. Summary of hydraulic conductivities assigned in the numerical model.

Zone Name	Elevation Range (m)	Hydraulic Conductivity (m/s)
Silt Loam Zone 1	725.40 - 725.50	4.25E-06
Silt Loam Zone 2	725.30 - 725.40	3.52E-06
Silt Loam Zone 3	725.20 - 725.30	2.75E-06
Silt Loam Zone 4	725.10 - 725.20	1.99E-06
Silt Loam Zone 5	725.00 - 725.10	1.22E-06
Silt Loam	719.25 - 725.00	4.25E-07
Sand	718.00 - 719.25	4.44E-05

6.2.3 Flow Boundary and Initial Conditions

The boundary conditions used for the flow simulations are illustrated in Figure 6.2.
The top boundary condition is represented by the infiltration across the ground surface
and was calculated using VSMB according to the methodology outlined in Section 4.3.1.
The top boundary infiltration fluxes had to be modified, however, as the model could not
handle very large positive or negative fluxes across the top boundary. The infiltration
values were therefore smoothed by limiting the maximum infiltration to values of
± 50 mm/month. Half of the excess infiltration was then added to the previous month
and half was added to the following month. In this way extreme values were eliminated
but the total annual infiltration remained the same. The original and modified infiltration
values are plotted in Figure 6.3.

The north and south boundaries across the silt loam were represented by no-flow
boundaries. This is justified on the basis that the hydraulic conductivity of the silt loam
unit was relatively low and therefore the lateral flow across the unit could reasonably be
neglected for the purposes of this study. The sand aquifer underlying the silt loam was
assigned a constant flux boundary condition (q_x) across the south side which represented
lateral flow through the aquifer and into the model domain. The south side sand flux
boundary was assigned a constant value of 4.20 m/yr given the average hydraulic
gradient across the site calculate in June 1999 was 0.003 m/m to the north and the
hydraulic conductivity of the sand was 4.44×10^{-5} m/s. A constant-head boundary across
the north side of the sand aquifer was assigned the value of 724.0 m and allows water to
exit the aquifer. The base of the numerical model was assigned a no-flow boundary that
is represented by the glacial till unit underlying the sand aquifer. The steady state flow
model with average annual infiltration across the top boundary (16.08 mm/yr) was used
as the initial condition for the transient model.

Figure 6.3. Original and modified infiltration boundary condition values.
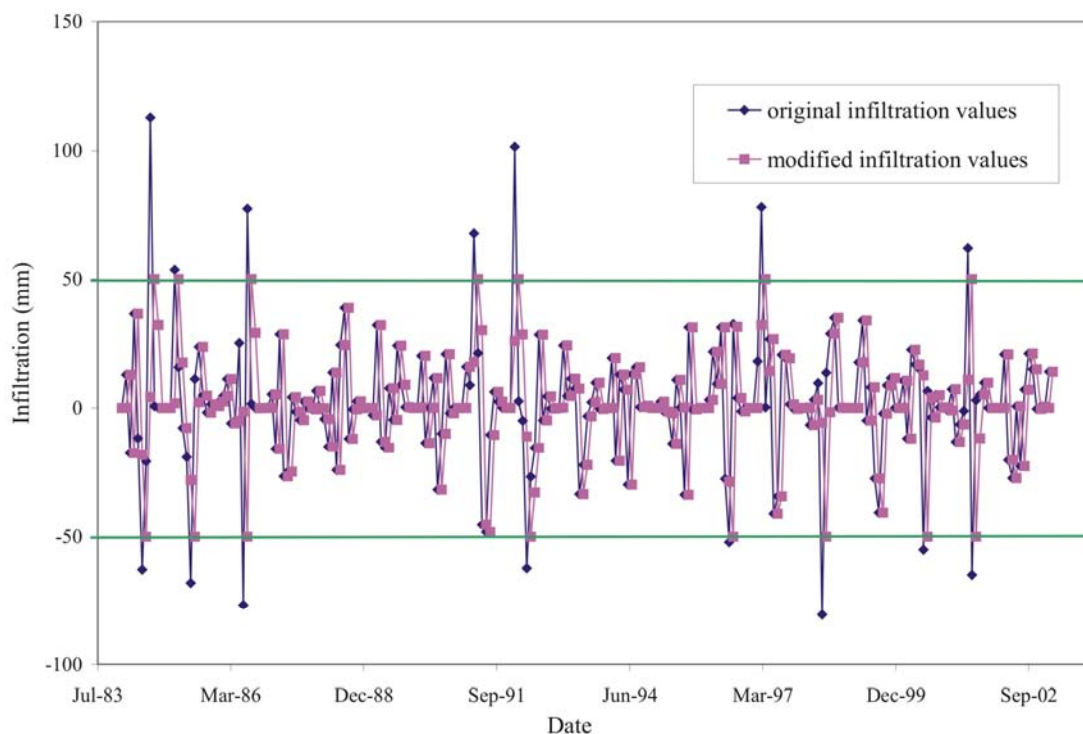
6.2.4 Transport Parameters

Transport parameters used in the numerical model are summarised in Table 6.2. Standard values for the aqueous and gaseous phase diffusion coefficients were specified at 1.0×10^{-9} and 1.5×10^{-5} m^2/s, respectively (Fetter, 2001). Initially, the longitudinal and transverse dispersivities were specified as 3.0 and 0.03 m as dispersion is not believed to be a dominant process at the site.

6.2.5 Transport Boundary and Initial Conditions

The boundary and initial conditions for the transport simulations of sodium chloride were selected based on the assumption of a one-time spill resulting in a slug of sodium chloride being released on to the ground surface and penetrating instantaneously to a depth of 1 m. The initial condition of the transport simulation therefore consisted of a slug of NaCl brine that extended across the entire length of the model domain to a depth of 1 m. The initial concentration of the NaCl brine slug was an important model

calibration parameter since chloride can be used as an indicator of groundwater flow patterns and advective transport rates. The background NaCl concentration in the remaining model domain was chosen to be 10 mg/L based on background concentrations sampled from monitoring wells completed within the base of the glacial till at depths of approximately 20 m.

The boundary condition across the top of the model domain was a specified mass flux boundary that was set to 0 so that chloride mass does not enter or exit out of the top of the model domain. There is a strong physical basis for this boundary condition since any chloride moving upward in the unsaturated soil would remain in the soil and would not be lost at the ground surface through evaporation or other means. The boundary conditions across the sand aquifer consisted of freshwater entering the aquifer on the south side and a second-type Neumann boundary condition that allows mass to exit the model domain in the sand aquifer. In reality, NaCl brine may be entering the sand aquifer on the south side; however, as this concentration was unknown and the processes of interest in this study are operating within the upper part of the silt loam, a simplified freshwater input boundary was deemed acceptable. The remaining transport boundaries along the north and south no-flow boundaries of the silt loam consisted of zero advective and dispersive mass flux boundaries, that is solute does not exit or enter the model domain along those boundaries. The transport simulation initial and boundary conditions are illustrated in Figure 6.2.

6.3 Calibration

The concentrations of both sodium and chloride in the NaCl brine were taken into account when calculating the maximum TDS of the aqueous solution for the density-dependent simulations. Transport simulation results are only presented for chloride; however, since the process of cation exchange was not simulated and, therefore, the simulated sodium distribution is not expected to be representative of the actual distribution of sodium. NaCl and chloride concentrations are discussed in the text in concentration units of mg/L since these units are generally more intuitive. Chloride

concentration maps, however, present chloride concentrations in units of mol/L or molarity (M) as this was the output format from MIN3PD. Table 6.4 list the conversion between M chloride and mg/L chloride.

Table 6.4. Chloride concentration conversion.

1 mg/L Cl⁻ = 2.8 x 10⁻⁵ M Cl⁻
1 M Cl⁻ = 35,453 mg/L Cl⁻

6.3.1 Calibration Targets

Flow model calibration targets consisted of groundwater elevation data taken at the site on June 29, 1999, the last date available prior to the construction of the tile drainage system. The average water table elevation across the site on June 29, 1999 was 724.52 m and the water table elevation at monitoring well P98-3, the closest well to the area of interest was 724.62 m. The November 1998 and the November 2004 chloride distributions within the silt loam in the vicinity of monitoring wells P98-3A and P04-2A were used as calibration targets for the transport model.

6.3.2 Calibration Results

The initial flow simulation was run using a constant top infiltration boundary condition represented by the average infiltration value calculated using VSMB from January 1984 to March 2003 (16.08 mm/yr). The constant head boundary on the north side of the model domain was adjusted until the water table elevation at the mid-point of the model domain was approximately 724.5 m which was achieved with a constant head boundary value of 724.0 m. This simulation was run until flow into the system was equal to flow out of the system, achieved after approximately one year. This steady state hydraulic head distribution was then used as the initial condition for the time-variable infiltration flow model.

The time-variable infiltration flow model was run for a period of 7,030 days (19.26 years) corresponding to the period from January 1, 1984 until March 31, 2003, just prior to installation of the tile drainage system. The simulated water table elevation of 724.67 m at 5,659 days is within 0.05 m of the measured water table elevation of 724.62 m at monitoring well P98-3 on June 29, 1999.

Once the flow model was calibrated, the chloride transport simulation was run with the one-time brine slug scenario for 7,030 days, or approximately 20 years using the modified time-variable infiltration top boundary. The initial slug NaCl concentrations were then adjusted until a reasonable match was obtained between 1.5 and 4 m depth with chloride concentrations measured at shallow monitoring wells P98-3A (8,110 mg/L; Table 2.1) and P04-2A (8,930 mg/L; Table 2.2) in November 1998 and 2004, respectively. This was achieved with an initial NaCl brine concentration of 100,000 mg/L which was judged to be reasonable based on the NaCl concentrations measured in produced water in Alberta (Hitchon et al., 1998). The simulated chloride distributions at 5,397 days (November 10, 1998) and 7,030 days (March 31, 2003) are included in Figure 6.4.

Figure 6.4. Simulated chloride distribution (M) at (a) 5,397 days (November 10, 1998) and (b) 7,030 days (March 31, 2003).
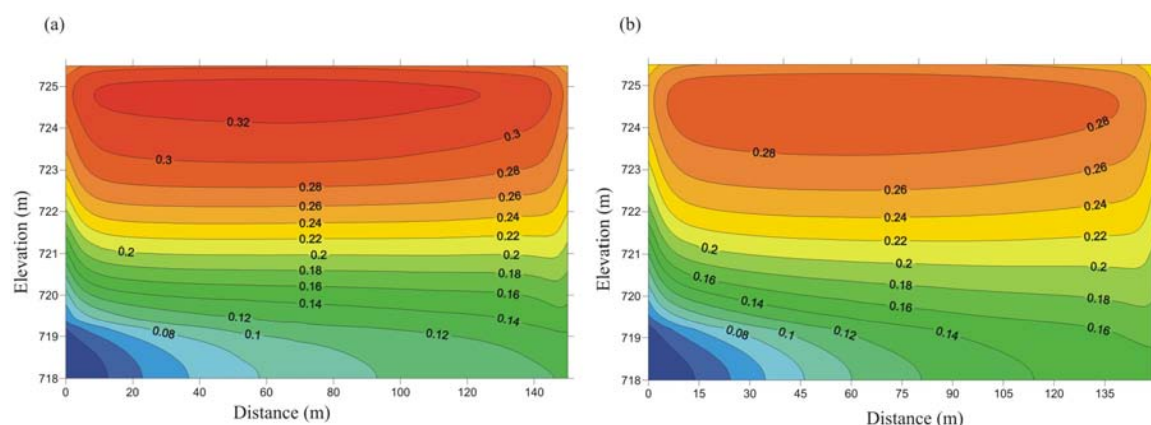
6.4 Sensitivity Analysis

The purpose of a sensitivity analysis is to quantify uncertainty in the calibrated model caused by uncertainty in the estimates of aquifer parameters, stresses, and boundary conditions implemented within the numerical model (Anderson and Woessner, 2002). Typically sensitivity analyses are performed by changing one parameter value at a time. The magnitude of change in the sensitivity analysis solution from the calibrated model is a measure of the sensitivity of the solution to that particular parameter. In this sensitivity analysis, the hydraulic conductivity of the silt loam, the top infiltration boundary condition, the magnitude of the dispersivity parameter and the effect of implementing density-dependent flow on the simulated chloride distribution will be examined to quantify the sensitivity of the transport model to these parameters.

6.4.1 Silt Loam Hydraulic Conductivity

The hydraulic conductivity of the silt loam affects the rate at which salt can be flushed vertically downward through the unsaturated zone and also laterally toward the tile drain within the saturated zone. The sensitivity of the model results due to the uncertainty in the hydraulic conductivity of the silt loam was estimated by running the numerical model twice, once with one half-order of magnitude higher hydraulic conductivity and once with one half-order lower hydraulic conductivity than the original hydraulic conductivity assigned to the silt loam (4.25×10^{-7} m/s). The hydraulic conductivities used in the sensitivity analysis are summarised in Table 6.5. The simulated chloride distributions at $t = 7,030$ days have been plotted for the upper and lower limits of the hydraulic conductivity in Figure 6.5. The simulated chloride distribution with the original hydraulic conductivity has also been included for comparison purposes.

The maximum simulated chloride concentration after 7,030 days is highest in the simulation with the upper limit hydraulic conductivity while simulations run with the original hydraulic conductivity and the lower limit hydraulic conductivity have lower maximum chloride concentrations. This is likely because the contrast in hydraulic conductivity between the silt loam and the sand aquifer is lower in the simulation with

the highest hydraulic conductivity which results in a different hydraulic head distribution within the model domain. This in turn causes a change in solute mixing within the simulation domain. Increasing the hydraulic conductivity of the silt loam by one half-order of magnitude in the simulation resulted in maximum chloride concentrations after 7,030 days that were 7% higher (0.321 M or 11,380 mg/L) than the maximum chloride concentrations in the original simulation (0.299 M or 10,600 mg/L). Decreasing the hydraulic conductivity of the silt loam by one half-order of magnitude resulted in maximum chloride concentration that were 2% higher (0.305 M or 10,813 mg/L) than the maximum chloride concentrations in the original simulation. The simulated chloride distribution is therefore judged to be relatively insensitive to changes in the hydraulic conductivity of the silt loam within one order of magnitude.

Table 6.5. Summary of hydraulic conductivity sensitivity analysis values.

Zone Name	Elevation Range (m)	Hydraulic Conductivity (m/s)
Upper Limit Hydraulic Conductivity		
Silt Loam Zone 1	725.40 - 725.50	2.34E-05
Silt Loam Zone 2	725.30 - 725.40	1.94E-05
Silt Loam Zone 3	725.20 - 725.30	1.52E-05
Silt Loam Zone 4	725.10 - 725.20	1.10E-05
Silt Loam Zone 5	725.00 - 725.10	6.74E-06
Silt Loam	719.25 - 725.00	2.34E-06
Sand	718.00 - 719.25	4.44E-05
Lower Limit Hydraulic Conductivity		
Silt Loam Zone 1	725.40 - 725.50	2.34E-06
Silt Loam Zone 2	725.30 - 725.40	1.94E-06
Silt Loam Zone 3	725.20 - 725.30	1.52E-06
Silt Loam Zone 4	725.10 - 725.20	1.10E-06
Silt Loam Zone 5	725.00 - 725.10	6.74E-07
Silt Loam	719.25 - 725.00	2.34E-07
Sand	718.00 - 719.25	4.44E-05

Figure 6.5. Silt loam hydraulic conductivity sensitivity analysis chloride distributions (M) at t = 7,030 days for (a) K = 2.34 x 10^{-6} m/s (b) K = 4.25 x 10^{-7} m/s and (c) K = 2.34 x 10^{-7} m/s.
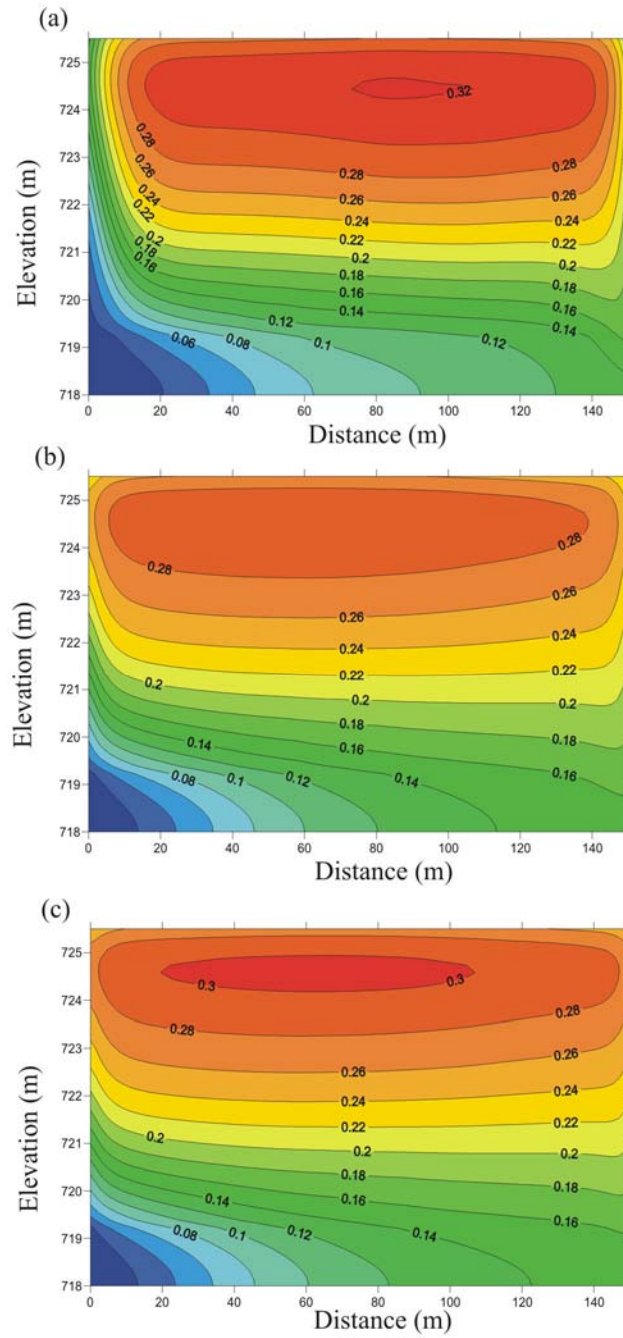
6.4.2 Infiltration Boundary Condition

The magnitude of the infiltration boundary condition has been found to be one of the more important parameters in unsaturated flow and transport numerical models for prediction of advective transport rates (Nichols and Freshley, 1993; Tiedeman et al., 2003). A near-surface unsaturated flow and transport model may therefore also be sensitive not only to the magnitude of the infiltration parameter, but also to seasonal variations in the infiltration parameter, which can be substantial in semi-arid northern Canadian climates.

The time-variable boundary condition was difficult to implement in the numerical model. Hydraulic conductivity profiles had to be modified and extreme infiltration values had to be eliminated to avoid numerical difficulties associated with ponded water in the model. In addition, implementing the time-variable infiltration boundary added considerably to transport model run-times (120 minutes for time-variable infiltration versus 4 minutes for constant infiltration). In this section, the results of the sensitivity analysis of the model to a constant infiltration parameter averaged over a 20-year period versus a monthly time-variable infiltration parameter over the same time-period are presented.

The mean annual infiltration calculated using VSMB between January 1984 and March 2003 was 16.08 mm/year (Appendix D). This value was used as a constant top infiltration boundary in the transport model and was run for a period of 7,030 days. The remaining model parameters and boundaries were the same as in the original model. The results of the constant infiltration boundary simulation at a time of 7,030 days are included in Figure 6.6. The time-variable infiltration results are included in Figure 6.6 for comparison purposes. Note that the colour scale was changed between Figures 6.4 and 6.5 to more clearly show the range in chloride concentrations.

A comparison of the constant infiltration and time-variable infiltration results shows that the constant infiltration model maximum chloride concentrations in the upper 1 m of the model domain are approximately double (or 10,000 mg/L greater) those of the time-

variable infiltration model. This is the case even though the initial source NaCl concentration and the dispersivity values were the exactly the same in both simulations. In the constant infiltration model, the chloride plume migrated vertically approximately 5.0 m bgs to an elevation of approximately 720.5 m after 7,030 days (Figure 6.6). In the time-variable infiltration model, the chloride plume migrated to the base of the model domain, 7.5 m bgs, after 7,030 days. This suggests that the shallow-unsaturated flow and transport model is very sensitive to the time-variable infiltration boundary and that higher precipitation months play an important role at the site by acting to dilute the near-surface chloride concentrations and promote greater vertical downward migration of the chloride plume over time.

Figure 6.6. Infiltration parameter sensitivity analysis chloride distributions (M) at t = 7,030 days for (a) constant infiltration and (b) time-variable infiltration.
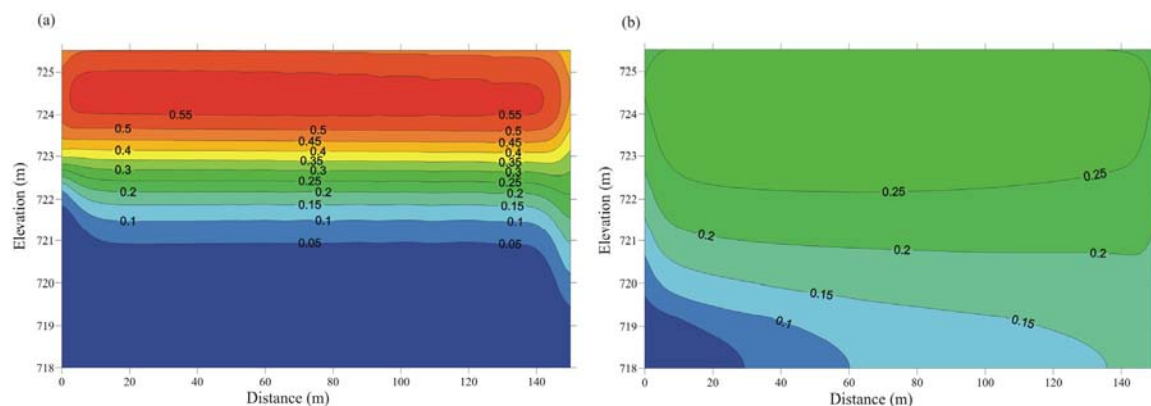
6.4.3 Density-Dependent Flow

When the concentration of solutes in groundwater reaches large values, the density of the groundwater solute plume can have a higher density than the ambient groundwater, which contains lower solute concentrations. The resulting density gradients may affect the migration of the contaminants due to density-dependent flow. To find out how density-dependent flow affects the concentration and distribution of the chloride plume in the variably-saturated flow and transport model over a period of 20 years, the original flow and transport model was re-run with the density-dependent flow module of

MIN3PD enabled. Running the variably-saturated simulation in density-dependent mode increased the simulation run-times considerably from 2 hours for the non-density-dependent time-variable infiltration simulations to an average of 228 hours (9.5 days) for the same simulation in density-dependent mode. The results of the density-dependent flow and transport simulation at 7,030 days are included in Figure 6.7.

Figure 6.7. Density-dependent flow sensitivity analysis simulated chloride distributions (M) at t = 7,030 days for (a) density-dependent flow and (b) non-density-dependent flow.
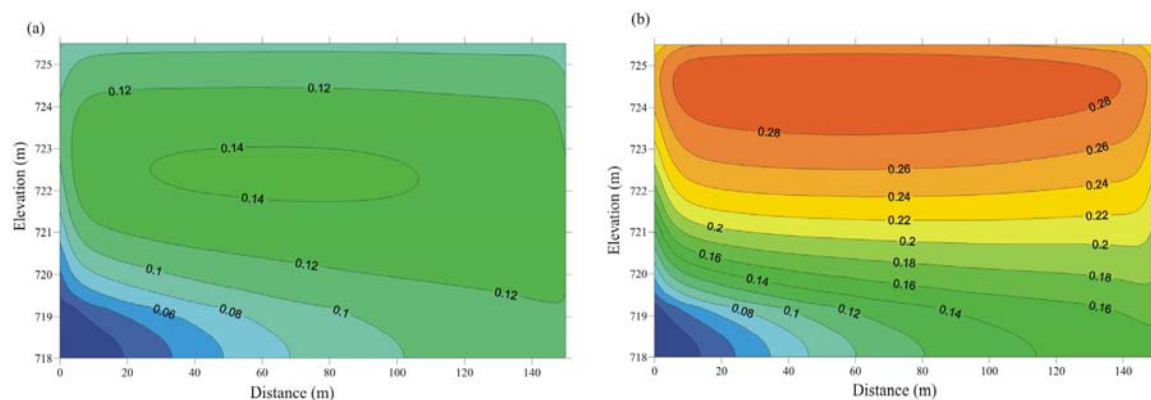
A comparison of the density-dependent simulation and the non-density-dependent simulation shows that the maximum chloride plume concentrations in the density-dependent flow simulation (0.14 M or 4,963 mg/L) are approximately half the maximum chloride concentrations of the non-density driven flow simulation (0.29 M or 10,281 mg/L). In addition, the maximum chloride concentration within the plume migrated to a depth of 3.5 m bgs in the density-dependent flow simulation while the maximum chloride concentration in the non-density-dependent flow simulation remained relatively close to the ground surface at a depth of approximately 1.5 m bgs. This suggests that density effects cause the chloride plume to become more dilute over time as the centre of the plume sinks more rapidly in the vertical direction.

The density-dependent simulation was re-run with the NaCl concentration of the initial slug increased to 150,000 mg/L from 100,000 mg/L. The results of this simulation at 7,030 days are included in Figure 6.8. When the higher initial NaCl concentration of the

source slug is used, the resulting maximum chloride concentration in the plume after 20 years increased to approximately 0.21 M (7,445 mg/L), which is more representative of chloride concentrations measured in shallow monitoring wells at the site in 2004.

Figure 6.8. Sensitivity analysis chloride distribution (M) at t = 7,030 days for (a) density-dependent flow with initial NaCl = 150,000 mg/L and (b) non-density-dependent flow with initial NaCl = 100,000 mg/L.
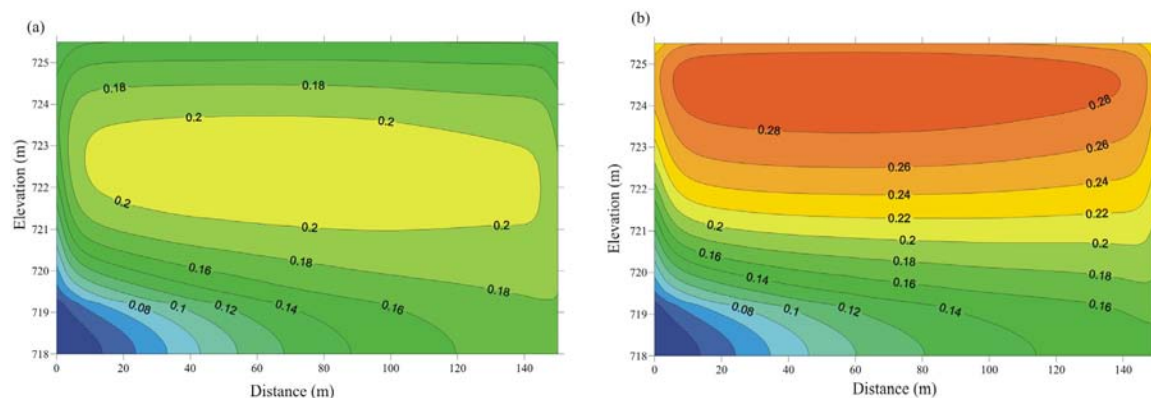
These results show that the variably-saturated flow and transport model is sensitive to density-dependent flow. To achieve a chloride plume with similar maximum concentrations to those measured at onsite groundwater monitoring wells after 7,030 days, the concentration of the initial NaCl slug had to be increased by 50,000 m/L, a large difference in the initial concentration of the chloride slug.

6.4.4 Dispersivity

Dispersivity is an intrinsic aquifer property which can be regarding as a solute mixing length within the aquifer (Rausch et al., 2005). When doing predictive simulations to determine impact to downgradient receptors, a dispersivity value that is too high could result in a plume that is too spread out and an under-prediction of maximum chloride concentrations while a dispersivity value that is too low could result in a plume that is too compact and an over-prediction of maximum chloride concentrations. Because of the relatively large degree of uncertainty associated with the dispersivity parameter and its

importance in the predictive simulations, dispersivity has therefore been included in the sensitivity analysis.

The salt plume is not believed to have evolved in a dispersion-dominated system due to the low-level of solute spreading observed in concentration profiles taken onsite with geophysical methods approximately 20 years after the spill (WorelyParsons Komex, 2005a). Relatively low dispersivity values (a longitudinal dispersivity of 3.0 m and a transverse dispersivity of 0.03 m) were therefore used in the preliminary flow and transport model. The dispersivity in both the longitudinal and transverse directions were then modified by $\pm 50\%$, respectively, in an attempt to quantify the uncertainty in this parameter in the numerical model.

In the first sensitivity analysis simulation, a longitudinal dispersivity of 4.5 m and a transverse dispersivity of 0.045 m was used. The remaining model parameters and boundary conditions were the same as in the calibrated flow and transport model. The results of this simulation at a time of 7,030 days are included in Figure 6.9. In the second simulation, a longitudinal dispersivity of 1.5 m and a transverse dispersivity of 0.015 m was used. The remaining model parameters and boundary conditions were the same as in the calibrated flow and transport model. The results of this simulation at a time of 7,030 days are also included in Figure 6.9. For comparison purposes, the results of the preliminary transport model with a longitudinal dispersivity of 3.0 m and a transverse dispersivity of 0.03 m at a time of 7,030 days have also been included in Figure 6.9. In each of the simulations, the grid Peclet number was much less than 2.0, ensuring that physical dispersion dominated potential numerical dispersion in the solutions.

Figure 6.9. Dispersivity sensitivity analysis chloride distributions (M) at t = 7,030 days for (a) α_L of 4.5 m and α_T of 0.045 m (b) α_L of 3.0 m and α_T of 0.03 m and (c) α_L 1.5 m and α_T of 0.015 m.
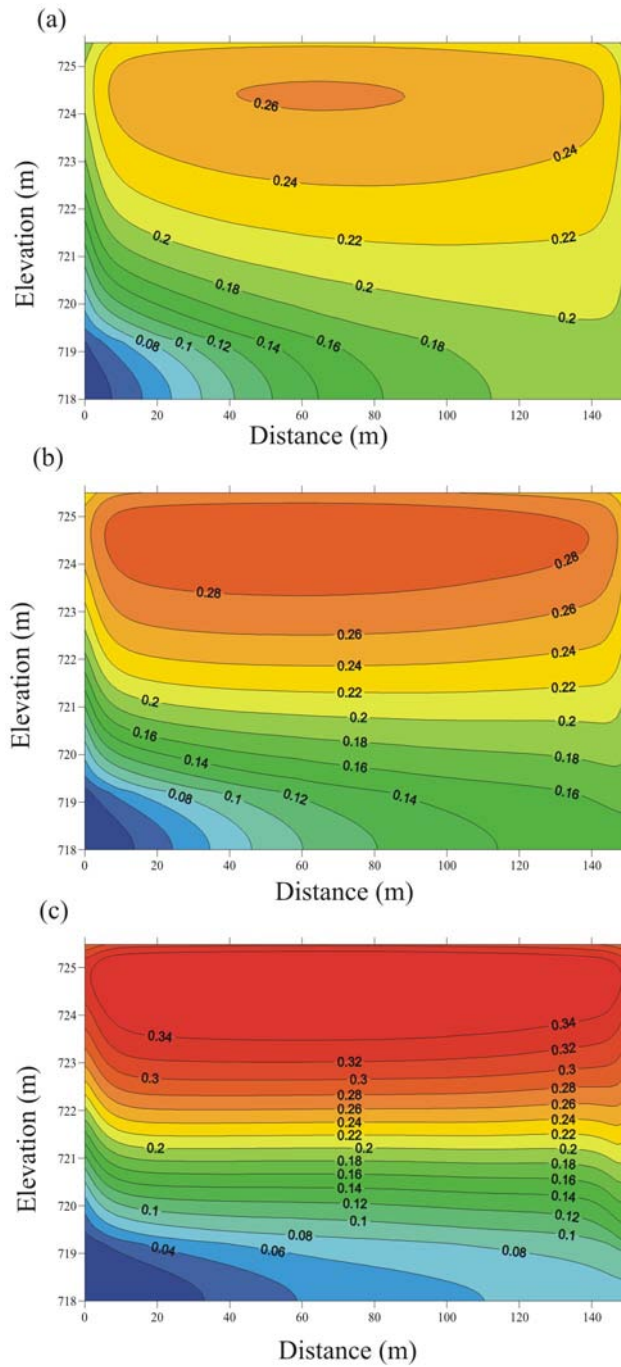
Increasing the simulation dispersivity by 50% had the effect of decreasing the maximum chloride concentration in the plume by approximately 10% while decreasing the simulation dispersivity by 50% had the effect of increasing the maximum chloride concentration in the plume by approximately 28% (Figure 6.9). The difference in maximum chloride concentrations between the dispersivity end-members in the sensitivity analysis simulations is 0.11 M (3,900 mg/L; Figure 6.9).

The chloride plume in the lower dispersivity simulation exhibited a sharper concentration front and less dilution and the chloride plume in the higher dispersivity simulation exhibited a more diffuse concentration front, in particular along the north no-flow boundary within the silt loam unit, and more dilution. However, at an elevation of 721 m and a distance of 75 m, the average chloride concentrations in each of the simulations were more similar and ranged from 0.18 M Cl$^-$ (6,382 mg/L) in the lowest dispersivity simulation to 0.21 M Cl$^-$ (7,445 mg/L) in the medium and highest dispersivity simulations.

The variably-saturated flow and transport model appears to be most sensitive to the dispersivity parameter along the north no-flow boundary and in the near-subsurface. At depth and along the south no-flow boundary the model does not appear to be as sensitive to the value of the dispersivity parameter due to the effects of the influx of freshwater flowing through the sand aquifer.

6.5 Summary

The code MIN3PD was used to develop a preliminary 2D variably-saturated groundwater flow and transport model for the salt plume based on site-collected data and the conceptual model developed in Chapter 4. The model domain was 150 m in the horizontal direction by 7.5 m in the vertical direction. A 2D approach was used in the numerical modeling based on the conceptual model of groundwater flow within the unsaturated silt loam being primarily vertically downward and saturated groundwater flow being primarily laterally to the north in both the silt loam and the underlying sand

aquifer. The soil unsaturated and hydraulic parameters assigned to both hydrostratigraphic units were derived experimentally and through analysis of field tests.

The initial condition for the transport simulations was based on the assumption of a one-time spill resulting in a slug of NaCl being released at the ground surface and penetrating instantaneously to a depth of 1 m. The initial concentration of the NaCl brine was an important model calibration parameter since the original volume and chloride concentration of the spill was unknown. The simulations incorporated time-variable infiltration in order to investigate the effect of precipitation variations on contaminant transport. Flow model calibration targets included groundwater elevation data measured at the site prior to the construction of the tile drainage system while the November 1998 and 2004 chloride distributions were used as calibration targets for the transport model. An initial NaCl slug concentration of 100,000 mg/L was used in the non-density-dependent flow and transport model.

A sensitivity analysis was conducted on the preliminary numerical model to determine the sensitivity of the chloride transport model to parameters that were time-consuming to implement, such as time-variable infiltration and density-dependent flow or uncertain, such as the hydraulic conductivity and dispersivity of the silt loam. The simulated chloride distribution was found to be very sensitive to both the time-variable infiltration boundary and density-dependent flow with chloride concentrations considerably higher in simulations run with constant infiltration and non-density-dependent flow. It is hypothesised that heavier precipitation months may act at the site to dilute the near-surface chloride concentrations and promote greater vertical downward migration of the chloride plume over time. In the density-dependent simulations, maximum chloride concentrations were approximately one half the concentrations in the non-density-dependent simulations and the centre of the plume migrated to a much greater depth. This suggests that density effects cause the chloride plume to become more dilute over time as the centre of the plume sinks more rapidly in the vertical direction.

The simulated chloride distribution was found to be relatively insensitive to the value of the hydraulic conductivity of the silt loam. Increasing the hydraulic conductivity of the silt loam by one half-order of magnitude to 2.34×10^{-6} m/s resulted in maximum chloride concentrations after 7,030 days that were 7% higher (0.321 M or 11,380 mg/L) than the maximum chloride concentrations in the original simulation (0.299 M or 10,600 mg/L). Decreasing the hydraulic conductivity of the silt loam by one half-order of magnitude to 2.34×10^{-7} m/s resulted in maximum chloride concentration that were 2% higher (0.305 M or 10,813 mg/L) than the maximum chloride concentrations in the original simulation.

The dispersivity sensitivity analysis results were more ambiguous given the uncertainty in the initial concentration of the NaCl plume source. Increasing the simulation dispersivity by 50% had the effect of decreasing the maximum chloride concentration of the plume by 10% while decreasing the simulation dispersivity by 50% had the effect of increasing the maximum chloride concentration in the plume by approximately 28%. As expected, the chloride plume in the lower dispersivity simulation exhibited a sharper concentration front and less dilution than the simulation in the higher dispersivity simulation. The numerical model appears to be most sensitive to the dispersivity parameter along the north no-flow boundary and in the shallow subsurface. At depth the model does not appear to be as sensitive to the dispersivity parameter.

Important lessons were learned during the development of the preliminary numerical model and through the sensitivity analysis. First, the simulations demonstrated that MIN3PD could reproduce pre-tile drain salt concentrations using hydraulic parameters measured at the site and reasonable estimates for other parameters and initial conditions. It was determined that the sand aquifer was not a significant hydrostratigraphic unit in terms of simulating the shallow chloride distribution at the site and that it need not be incorporated in subsequent simulations. It was found that the current distribution of chloride at the site could be reasonably well simulated assuming a single NaCl brine spill occurred approximately 20 years ago. It was also determined that time-variable

infiltration and density-dependent flow should be incorporated in subsequent simulations even though both these elements add considerably to model run-times.

The following chapter describes the numerical model that was developed for the tile drain simulations based on the preliminary numerical model. Tile drain simulation results are also presented.

Chapter Seven: Tile Drainage Simulations

7.1 Introduction

The objective of the tile drain simulations was to assess the effectiveness of tile drainage systems as a method of salt remediation in Alberta. Soils at the study site consist of glacially-derived surficial deposits with interbedded sand layers, a common soil type in many areas across Alberta. The continental climate at the site is also typical of many areas in Alberta with four distinct temperature seasons and annual precipitation levels that are relatively low. It is hoped that lessons learned at this site may be applicable to a range of salt-impacted sites across Alberta.

Simulations were run for a four-year time period from 2003 to 2006 to evaluate chloride mass removal by the tile drainage system and results were compared to field data collected over the same time period at the site. Lessons learned in the preliminary numerical modeling were applied in the tile drainage simulations. Additional short-term simulations focussed on evaluating tile drainage system design parameters were also conducted. These included the spacing between the drainage lines and the effect of irrigating the drainage area with fresh water to promote salt flushing. Longer-term predictive simulations were also run to estimate the time it would take for chloride concentrations in the pore-water within the shallow subsurface to meet generic regulatory criteria and to evaluate whether the tile drainage system provides an advantage in terms of shortening salt remediation times at the site as opposed to natural attenuation.

7.2 Model Domain and Grid

The model domain for the base-case tile drain simulation was 5 m in the x-direction (horizontal), 6 m in the z-direction (vertical). For a 2D simulation in MIN3PD the y-direction must be assigned a thickness of 1 m by default. Due to the symmetry of tile drainage flow fields, it was only necessary to make the x-direction spacing equivalent to half the actual spacing between the drains at the site to simulate chloride transport in the vicinity of the tile drain. A total of 6,902 nodes, 17 in the x-direction and 406 in the

z-direction, were used to discretise the domain. A very fine z-discretisation of $\Delta z = 0.01$ m was used in the top 3.8 m of the domain to allow for the higher pressure gradients caused by the introduction of a tile drain. A summary of the grid discretisation used in the tile drain simulations is included in Table 7.1

Table 7.1. Grid discretisation used in the tile drain simulations.

x-direction discretisation interval	x min (m)	x max (m)	Dx (m)	Nx
1	0.000	0.600	0.1	6
2	0.600	1.200	0.15	4
3	1.200	1.400	0.2	1
4	1.400	2.000	0.3	2
5	2.000	2.450	0.45	1
6	2.450	3.100	0.65	1
7	3.100	5.000	0.95	2
z-direction discretisation interval	z min (m)	z max (m)	Dz (m)	Nz
1	719.50	721.50	0.10	20
2	721.50	721.57	0.07	1
3	721.57	721.62	0.05	1
4	721.62	721.65	0.03	1
5	721.65	721.67	0.02	1
6	721.67	721.70	0.015	2
7	721.70	725.50	0.01	380
			Total Grid Nodes	6,902

7.3 Boundary Conditions

Flow boundary conditions for the tile drain simulations are illustrated in Figure 7.1 and summarised in Table 7.2. No-flow boundaries were assigned to the sides of the domain and a time-variable specified flux infiltration boundary was assigned to the top of the domain. The infiltration boundary was implemented as outlined in Section 6.2.3, except that the magnitude of the infiltration values were further constrained to no more than +/- 25 mm/month for the tile drain simulations to avoid numerical difficulties associated with water ponding in the MIN3PD code. A seepage face boundary condition was assigned to the tile drain.

Figure 7.1. Flow and transport boundary conditions used in the tile drain simulations.
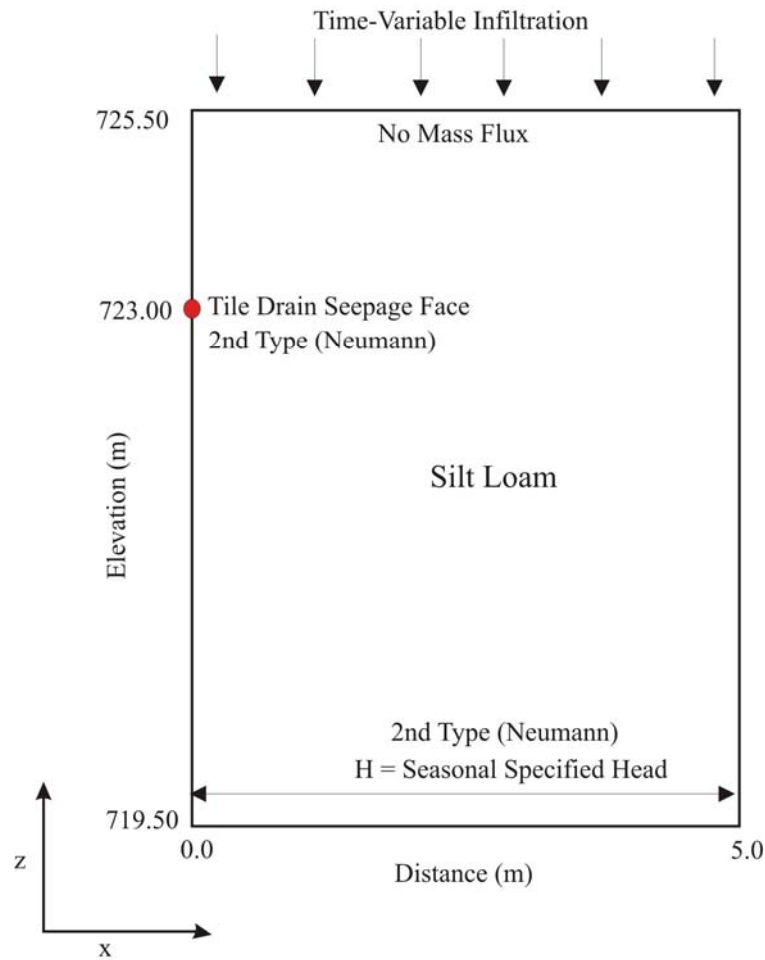
A seepage face boundary node is assigned a pressure head equal to atmospheric pressure when the node is saturated and becomes a no-flux boundary when the node is unsaturated. This is similar to the behaviour of a tile drain line which collects water when water levels are above the elevation of the drain and the surrounding soil is saturated and remains dry when the water level falls below the drain and the surrounding soil is unsaturated. The seepage face boundary condition was assigned to one node on the left edge of the model domain at an elevation of 723.00 to 723.01 m and was assigned a reference hydraulic head of 723.0 m. This is similar to the elevation of tile drain line S-7 located adjacent to monitoring well nest P04-2A/B (Figure 2.1).

Table 7.2. Tile drain simulation flow and transport boundary conditions.

| Boundary Conditions		
Model Boundary	**Flow**	**Transport**
Top Boundary	time-variable recharge	3rd Type (specified mass flux = 0)
Side Boundaries	no-flow	3rd Type (specified mass flux = 0)
Bottom Boundary	specified head	2nd type (Neumann)
Tile Drain Node	seepage face	2nd type (Neumann)

The bottom boundary consisted of specified hydraulic head boundary that was implemented based on analysis of site-collected groundwater elevation data at monitoring wells P04-2A/B. Groundwater elevations at these monitoring wells showed distinct variation between winter (January to March) when the groundwater elevation was below the elevation of the tile drain, and summer-late fall (April to December) when the groundwater elevation was above the level of the tile drain (Figure 7.2). The bottom specified head boundary was therefore assigned to be below the tile drain elevation between January and March and above the tile drain elevation between April and December. Due to the numerical difficulties encountered in the code when the groundwater elevation is more than a few centimetres above the elevation of the tile drain, the difference between the winter and summer-late fall specified head values was intentionally kept small. The specified hydraulic head values of the bottom boundary were 722.97 m from January to March and 723.03 m from April to December of each year.

Transport boundary conditions included a third-type specified mass flux boundary = 0 at the top of the model domain and along both sides. Second type boundaries (Neumann) were specified along the bottom of the model domain and at the tile drain node.

Figure 7.2. Seasonal variation in groundwater elevations between 2004 and 2006 at selected monitoring wells at the site.
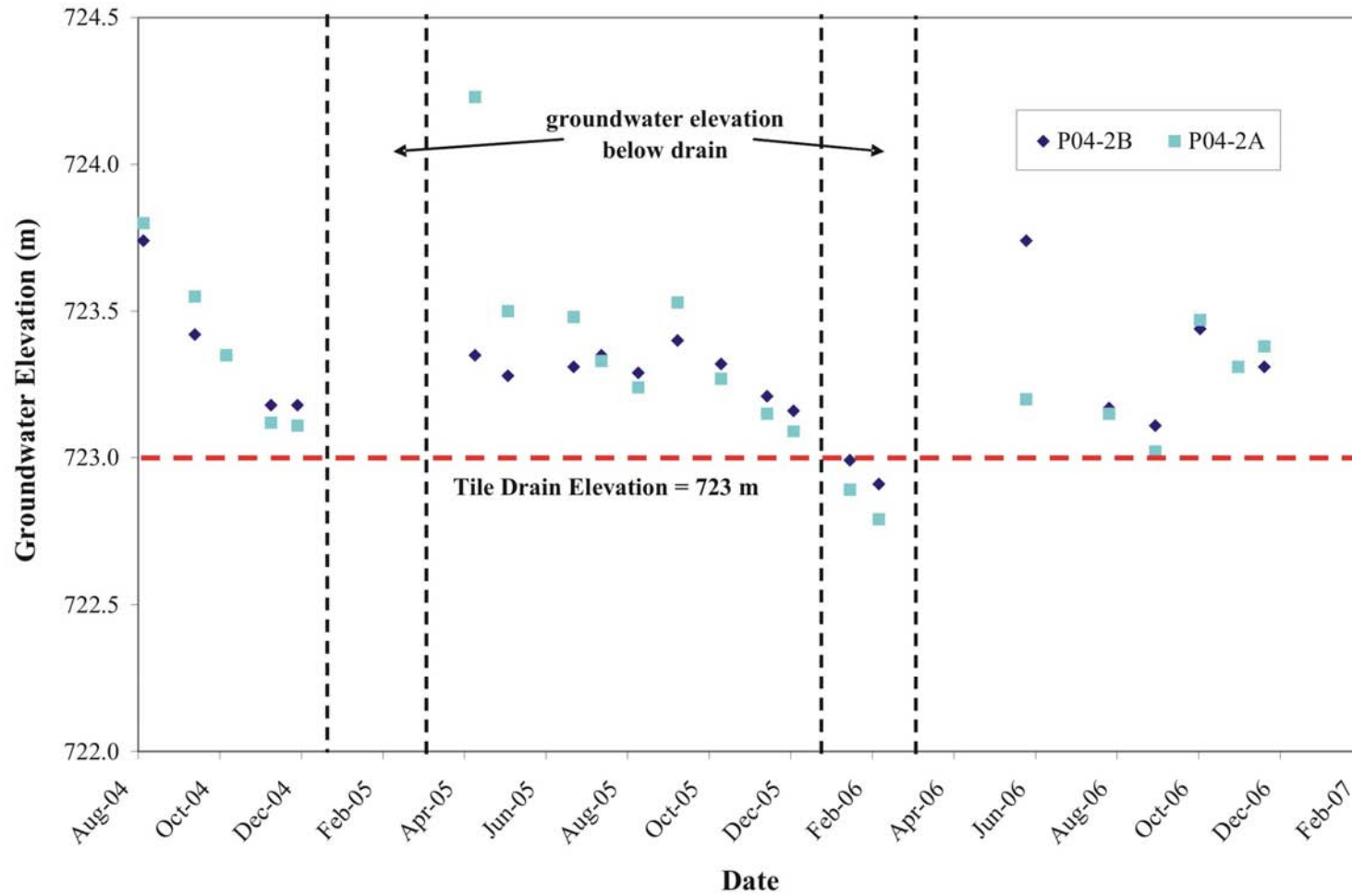
7.4 Aquifer and Transport Parameters

Aquifer parameters used in the tile drain simulations were the same as those used in the
preliminary numerical model and are summarised in Table 7.3. The only exception is
that the sand aquifer was not included in the tile drain model as it is present at a depth not
considered important for the prediction of shallow salt concentrations at the site.
The lithology in the tile drain simulations therefore consisted only of silt loam. Transport
parameters used in the tile drain simulations are also summarised in Table 7.3 and were
the same as in the preliminary numerical model, with the exception of the longitudinal
dispersivity and transverse dispersivities which were assigned to be 1.5 and 0.15 m,
respectively, as it was found that these dispersivities adequately accounted for the solute
spreading observed at the site.

Table 7.3. Summary of aquifer and transport parameters used in the tile drain numerical
model.

Aquifer Parameter	Silt Loam	Units
Porosity	0.51	-
Hydraulic Conductivity	4.25E-07*	m/s
Specific Storage Coefficient	2.50E-03	m^{-1}
Residual Saturation	0.137	-
van Genuchten Parameter alpha	0.480	m^{-1}
van Genuchten Parameter n	1.09	-
Transport Parameters		
Longitudinal Dispersivity	1.5	m
Transverse Dispersivity	0.15	m
Gaseous Phase Diffusion	1.50E-05	m^2/s
Aqueous Phase Diffusion	1.00E-09	m^2/s
Initial NaCl Distribution	20-year simulated NaCl distribution**	-
Background NaCl Concentration	10	mg/L

Notes:

* - increases linearly between 725.0 and 725.5 m elevation from 4.25E-07 to 4.25E-06 m/s

** - see section 7.5.2 for details

7.5 Initial Conditions

7.5.1 Flow

The steady state solution to the tile drain flow simulation was used as the initial condition for the transient flow simulations. The steady state hydraulic head and pressure head profiles are included in Figure 7.3. The steady state flow simulation was assigned a constant infiltration boundary that was the average of the monthly infiltration at the site between 2003-2006 (22.24 mm/yr) and a constant head bottom boundary that was the average of the two seasonal specified head values (722.97 m in the winter and 723.03 m in the summer) which was 723.0 m. The aquifer parameters were as outlined in Section 7.4.

7.5.2 Transport

A 20-year density-dependent flow and transport simulation was run in the tile drain domain to obtain the initial chloride distribution for the transport tile drain simulations. The aquifer and transport parameters used in this simulation are summarised in Table 7.4.

Table 7.4. Summary of aquifer and transport parameters used in the density-dependent flow simulation to obtain the initial NaCl distribution for the tile drain simulations.

Aquifer Parameter	Silt Loam	Units
Porosity	0.51	-
Hydraulic Conductivity	4.25E-07*	m/s
Specific Storage Coefficient	2.50E-03	m^{-1}
Residual Saturation	0.137	-
van Genuchten Parameter alpha	0.480	m^{-1}
van Genuchten Parameter n	1.09	-
Transport Parameters		
Longitudinal Dispersivity	1.5	m
Transverse Dispersivity	0.15	m
Gaseous Phase Diffusion	1.50E-05	m^2/s
Aqueous Phase Diffusion	1.00E-09	m^2/s
Initial Souce NaCl Concentration	200,000	mg/L
Background NaCl Concentration	10	mg/L
Fluid Density/TDS (both in g/L)	0.6205	-

Notes:

* - increases linearly between 725.0 and 725.5 m elevation from 4.25E-07 to 4.25E-06 m/s

The initial TDS of the NaCl slug was set at 200,000 mg/L which gives a maximum initial chloride concentration of approximately 121,327 mg/L. This chloride concentration is within range of the estimated mean produced water chloride concentration of 112,000 mg/L in the production field during the time when the site was in operation (AMEC Earth and Environmental, 2007). The boundary conditions used in the 20-year density-dependent flow and transport simulation are summarised in Table 7.5. The time-variable top infiltration boundary was constrained to no more than +/-50 mm/month as outlined in the preliminary numerical model (Section 6.2.3). The remaining flow boundary conditions consisted of a specified hydraulic head boundary set at 724.50 m across the bottom of the model domain and no flow boundaries across both side boundaries. The bottom hydraulic head boundary value of 724.50 m was chosen as it is approximately equal to the mean value of groundwater elevations measured at site shallow monitoring wells in June 1999 (724.53 m), prior to the installation of the tile drainage system (Appendix C). Transport boundary conditions are also summarised in Table 7.5 and were the same as those outlined in Section 7.3, with the exception of the tile drain node, which was not present in the 20-year density-dependent flow simulation.

Table 7.5. Boundary conditions used in the density-dependent flow simulation used to obtain the initial NaCl distribution for the tile drain simulations.

Boundary Conditions		
Model Boundary	Flow	Transport
Top Boundary	time-variable recharge	3rd Type (specified mass flux = 0)
Side Boundaries	no-flow	3rd Type (specified mass flux = 0)
Bottom Boundary	specified head (724.50 m)	2nd type (Neumann)

The 20-year density-dependent flow and transport simulated NaCl distribution was used as the initial condition for all of the tile drain transport simulations and is included in Figure 7.3. Because cation exchange was not included as part of the simulated transport processes, the simulated sodium profiles are not representative of the actual distribution of sodium at the site and therefore only the simulated chloride profiles are shown.

Figure 7.3. Tile drain steady state flow simulation (a) hydraulic head (m) and (b) pressure head (m) contours.
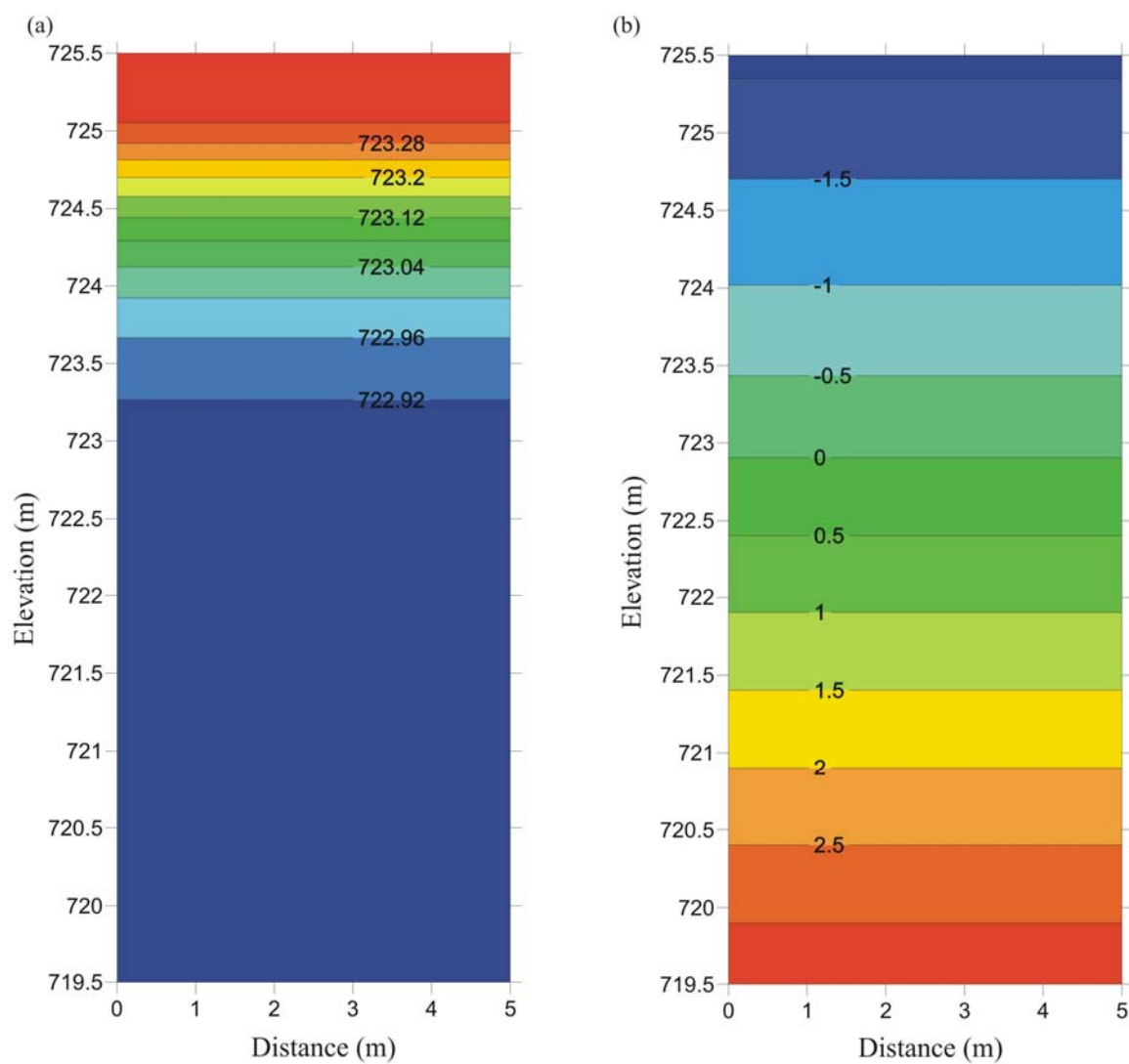
Figure 7.4. Simulated 20-year density-dependent flow and transport chloride distribution (M).
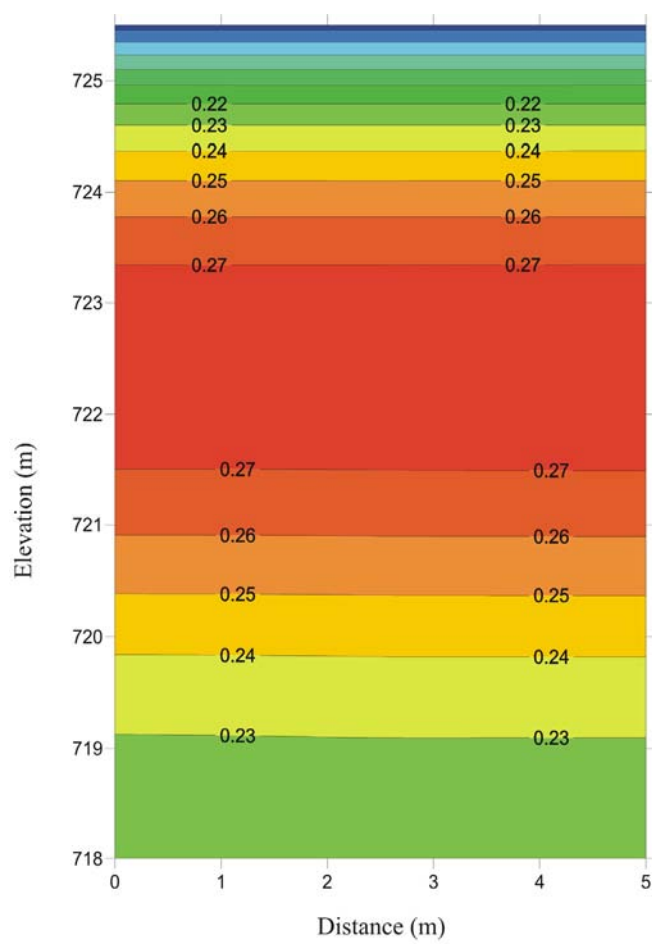
7.6 Tile Drainage Model Calibration

7.6.1 Flow Model

The objective of flow model calibration was to achieve seasonal variations in water levels that roughly matched the seasonal variation of measured water levels at the site. Specifically, the simulated water levels should be either above or below the elevation of the tile drain at various times of the year where the groundwater elevation was measured as such onsite. This would have the effect of having the simulated tile drain either active or inactive during the months that it would have been so at the site. An exact match for water levels was not sought as the MIN3PD code encounters numerical difficulties with hydraulic head levels greater than a few centimetres above the tile drain.

The calibration approach for the tile drainage flow model was based on specifying values for reasonably well constrained parameters, such as aquifer properties and the top infiltration boundary, and varying the values for the less well constrained lower boundary condition. The simulated results were then compared to site-measured water levels in order to select the lower boundary condition that provided the best fit to the observed data. Specified flux and constant specified head boundary conditions were both evaluated for the lower model boundary; however, only a seasonally-variable specified head boundary was able to produce the desired changes in water levels. Other types of boundary conditions consistently resulted in water levels that were too low and below the elevation of the tile drain, especially during the summer months when most of the drainage was actually occurring onsite. The physical basis for this may be that there is surrounding aquifer support from the area outside of the tile drainage field that keeps the groundwater elevation within the tile drainage field area high in the summer, even though there is little groundwater infiltration during that time.

7.6.2 Transport Model

The transport model calibration approach was similar to that of the flow model, except there were more unconstrained parameters including the initial TDS of the salt spill,

the aquifer dispersivity and the date of the salt spill. It is recognized this combination of unknown parameters can give rise to a non-unique solution. For example, increasing the aquifer dispersivity and decreasing the time since the spill would give a similar result to decreasing the aquifer dispersivity and increasing the time since the spill. However, from the known mean chloride concentrations in the production field at the time the site was in operation and anecdotal reports from onsite operators, reasonable estimates were made for the initial TDS of the spill water and the time of the salt spill. Model calibration was then achieved by adjusting the aquifer dispersivity and comparing the 20-year results with the 1998, 1999 and 2004 chloride concentrations at the site since there is no site groundwater quality data available between 1999 and 2004.

The simulated chloride concentrations are compared to actual chloride concentrations measured in 1998 at shallow monitoring wells P98-2A and P98-3A, in 1999 at shallow well P99-7A, and in 2004-2006 at nested monitoring wells P04-2A and P04-2B in Figure 7.5. For comparison purposes, the simulated chloride concentrations at the midpoint depth of the screened intervals of P04-2A (2.34 m bgs) and P04-2B (7.32 m bgs) are plotted in Figure 7.5. The simulated 1998 concentrations are within the range of concentrations measured at onsite monitoring wells between 1998 and 1999 (Figure 7.5). The simulated 2003 chloride concentrations at 7.32 m bgs and 2.34 m bgs fall between the chloride concentrations measured in 1998/99 and in 2004. The simulated distribution is therefore judged to be a reasonable approximation of chloride concentrations at the site just prior to the installation of the tile drainage system in 2003.

Due to numerical instabilities, it was impossible to run the tile drain simulations with density-dependent flow. To determine the effect of density-dependent flow on chloride concentrations, two simulations were run without a tile drain for the period 2003 to 2006, one simulation with and one simulation without density-dependent flow. The simulated chloride distribution for November 2006 has been plotted in Figure 7.6.

Figure 7.5. Comparison of chloride concentrations measured between 1998 and 2006 and simulated chloride concentrations.
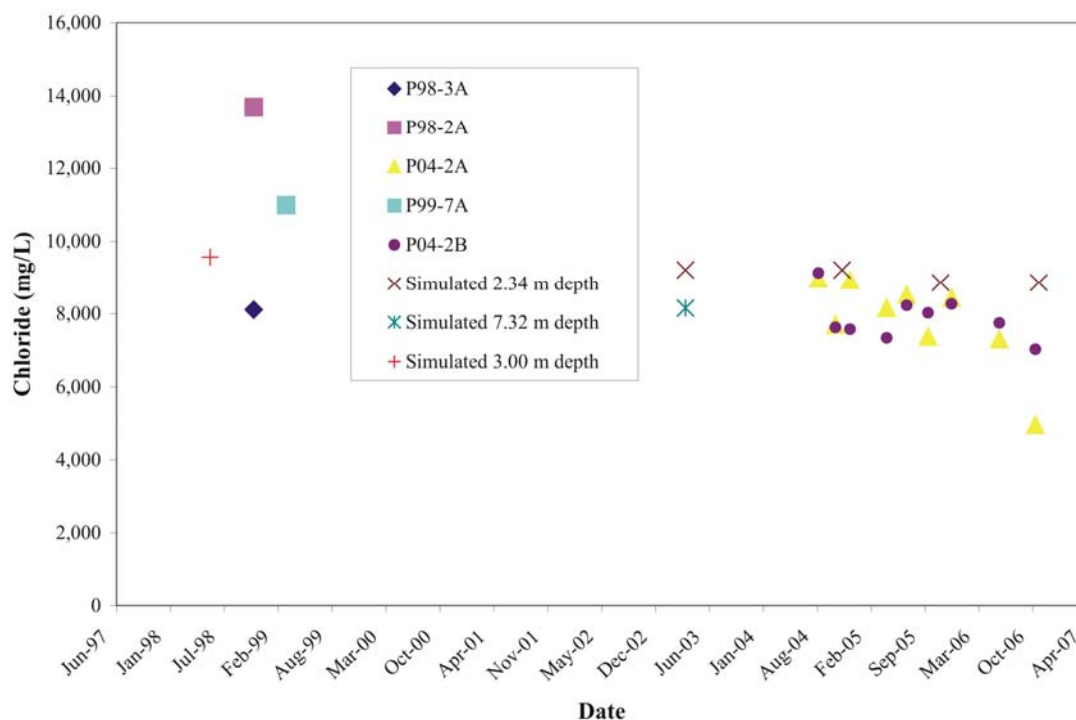
Density-dependent flow appears to have the effect of increasing chloride flushing in the unsaturated zone in comparison to the simulations without density-dependent flow, similar to the results of the sensitivity analysis of the preliminary numerical model. This may be due to greater sinking of the salt in the density-dependent simulations which thereby limits upward movement of the salt. The largest difference in the predicted chloride concentrations in the two simulations occurs in the upper 1.5 m of the model domain (Figure 7.6). The minimum chloride concentration in the density-dependent flow simulation in 2006 was 0.11 M (3,900 mg/L) while the minimum chloride concentration in the non-density dependent flow simulation in 2006 was 0.17 M (5,850 mg/L). The minimum chloride concentration in the non-density dependent simulation is approximately 1.5 times greater than the minimum chloride concentration in the density-dependent simulation. Maximum chloride concentrations in both simulations were more similar and were 0.25 M in the density-dependent simulation and 0.26 M (9,218 mg/L) in the non-density dependent simulation. Running tile drain simulations without density-

dependent flow will tend to under-predict the amount of chloride flushing in the unsaturated zone and over-predict the minimum chloride concentrations in the simulation domain. As salt concentrations decrease over time in the model domain, ignoring the effects of density-dependent flow will have less of an effect on the predicted chloride concentrations.

Figure 7.6. November 2006 simulated chloride concentrations (M) without a tile drain (a) density-dependent flow and (b) without density-dependent flow.
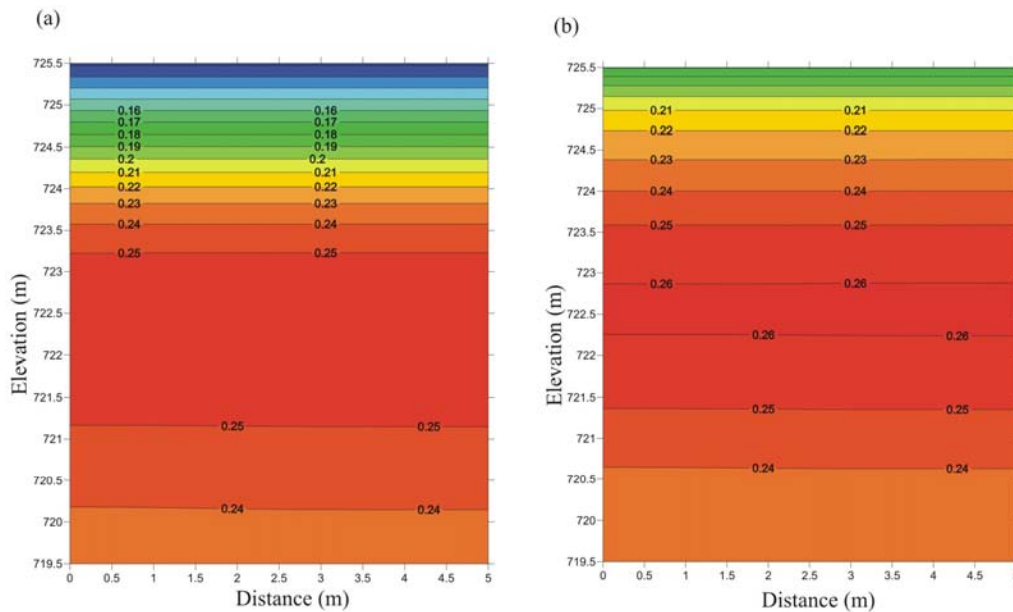
7.7 Tile Drainage System Evaluation Scenarios

7.7.1 Tile Drain System Performance 2003-2006

The initial tile drain simulation was run from the beginning of 2003, the year the tile drainage system was commissioned, up to the end of December 2006, the last year that weather data was available for the study area. The simulated chloride distribution has been plotted for November 2003, 2004, 2005 and 2006 and is included in Figure 7.7.

Figure 7.7. Simulated chloride distribution (M) with a tile drain for November (a) 2003, (b) 2004, (c) 2005 and (d) 2006.
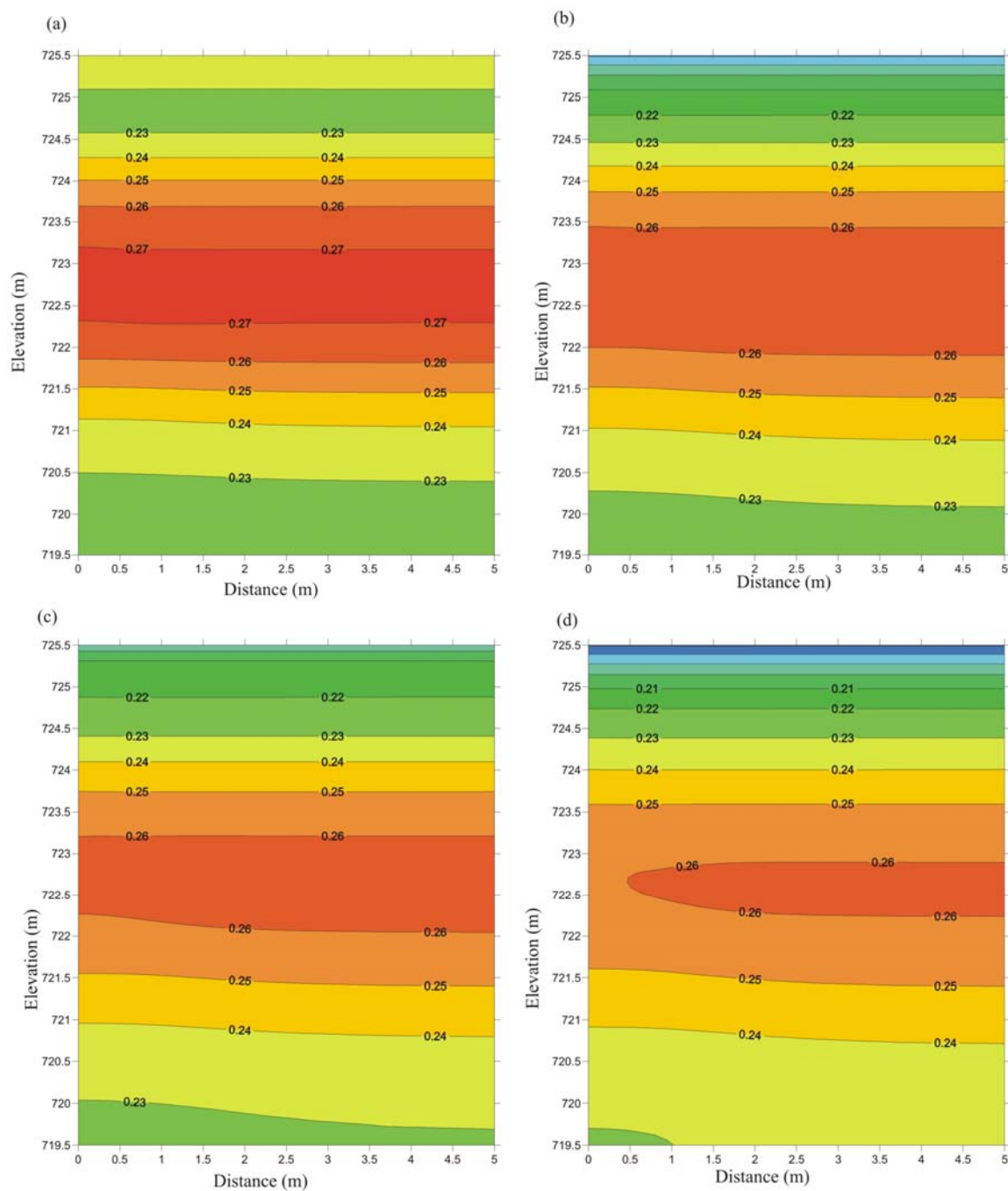
To estimate the change in chloride mass balance due to the presence of a tile drain, the simulation was run twice; once with a tile drain and once without a tile drain since the mass balance could only be calculated for the entire simulation domain. The chloride and water mass balance files from the tile drain and no drain simulations were compared to assess differences in chloride transport in the simulated flow systems due to the tile drain. The simulated chloride mass influx and outflux from both the tile drain and no drain simulations are included in Figure 7.8 and the simulated water inflow and outflow from both the tile drain and no drain simulations are included in Figure 7.9.

Differences in mass balance between the tile drain and no drain simulations are due to a combination of mass exiting the domain at the bottom boundary, mass entering the domain at the bottom boundary and/or mass exiting the domain at the tile drain node (for the tile drain simulation). For both simulations, mass exiting the model domain at the bottom boundary cannot be distinguished from mass exiting the model domain though the tile drain because the mass balance could only be calculated for the entire simulation domain. Differences between mass influxes are due to chloride or water entering the model domain across the bottom boundary as mass is not permitted to enter the model domain through the tile drain node.

A comparison of the simulated chloride mass influx for the tile drain and the no drain simulation shows that more chloride mass enters the simulation domain in the tile drain simulation than in the no drain simulation (Figure 7.8). This additional mass enters the simulation domain across the bottom boundary due to changes in the flow system caused by the tile drain. A comparison of the simulated chloride mass outflux with the tile drain and without the tile drain shows that a significant amount of chloride is removed from the system even without the tile drain due to chloride exiting along the Neumann type boundary at the base of the model. However, the overall chloride mass outflux is higher in the tile drain simulation, where chloride can also exit through the tile drain in addition to across the bottom boundary (Figure 7.8). In both simulations, chloride mass outflux is higher than chloride mass influx, with a change in storage of -3,115 g of chloride in the

no drain simulation and a change in storage of -3,595 g of chloride in the tile drain simulation at the end of the simulation period. Between 2003 and the end of 2006, approximately 480 g more chloride is removed from the tile drain simulation domain than from the no drain simulation domain. The chloride mass influxes and outfluxes are variable and during some periods of the year, the chloride fluxes are the same in both the tile drain and no drain simulations.

Figure 7.8. 2003-2006 simulated chloride mass influx and outflux from tile drain and no drain simulations over the simulated drainage area of 5 m^2.
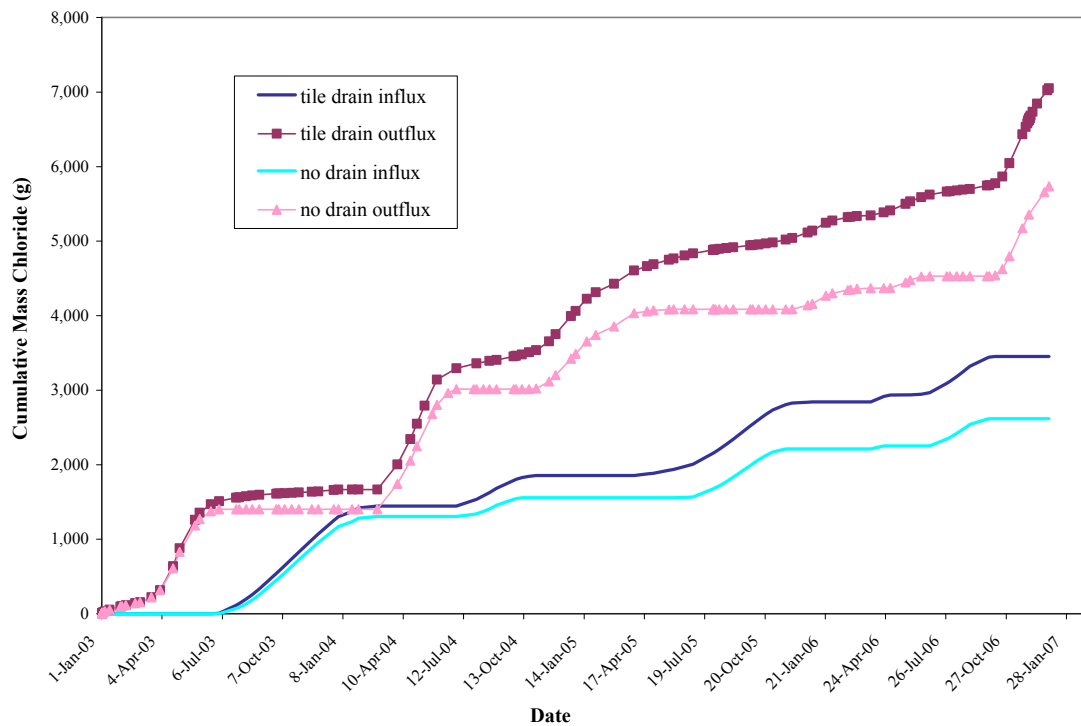

During the periods listed below, a higher rate of chloride mass outflux was present in the simulation with the tile drain as compared to the simulation with no drain:

- June 18, 2003 to December 24, 2003
- July 1, 2004 to November 21, 2004
- May 24, 2005 to December 24, 2005
- June 18, 2006 to October 10, 2006

During the other times of the year, the winter and spring months, the rate of chloride mass outflux from both the tile drain and no drain simulations appears to be about the same. This makes sense as during the winter months (January to March) groundwater elevations are set below the elevation of the tile drain and therefore the tile drain is inactive and no chloride would be expected to be removed via the tile drain. Seasonal variations in the mass influx and outflux therefore appear to be the result of a combination of the effects of the groundwater elevation, controlled by the specified head boundary at the base of the model domain, and the hydraulic gradient, which is affected by the presence of the drain, and the magnitude of the time-variable top infiltration boundary flux.

Figure 7.9. 2003-2006 simulated cumulative water inflow and outflow for tile drain and no drain simulations over the simulated drainage area of 5 m^2.
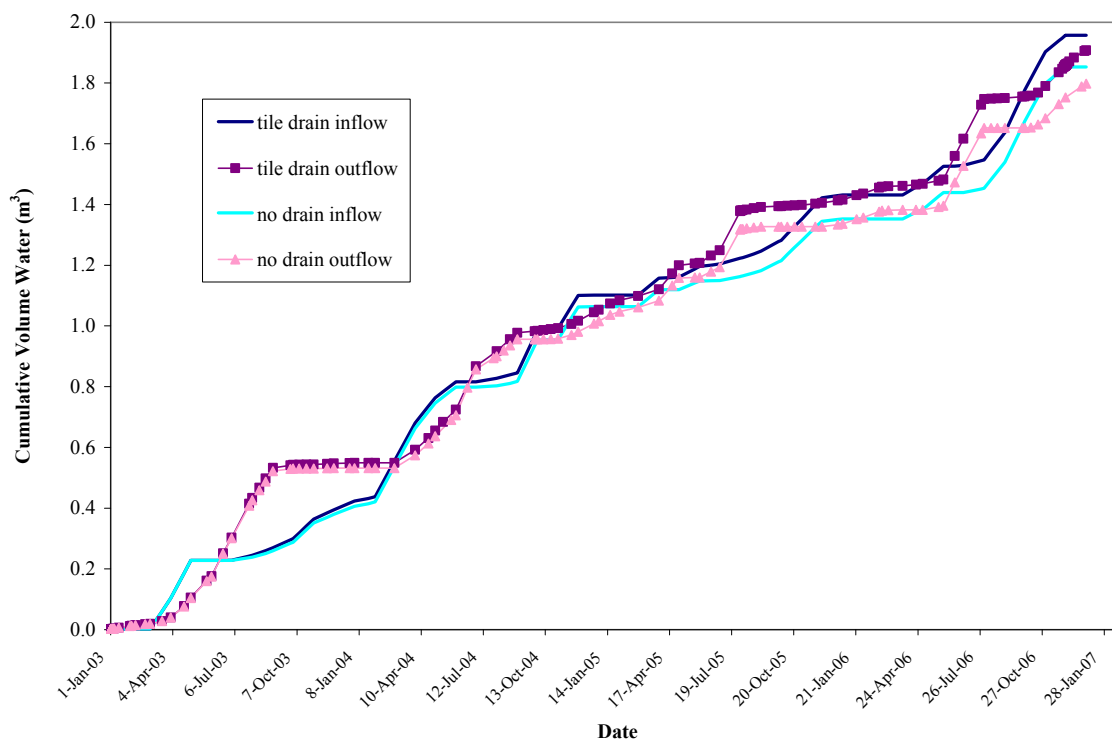
A comparison of water mass balance shows that the tile drain simulation water inflow follow the same basic pattern as the no drain water inflow except the magnitude of the tile drain inflow is slightly higher (Figure 7.9). The tile drain simulation water outflow

also follows the same basic pattern as the no drain water outflow except again, the magnitude of the tile drain simulation water outflow is slightly higher. The water mass balance plots also exhibit seasonal variation where inflows are sometimes greater and sometimes less than outflows. For example, from June 2003 to March 2004 the outflux of water was significantly greater than the influx of water in both the tile drain and no drain simulations (Figure 7.9). Because the mass balance results from both the tile drain and no drain simulations were similar, this difference is likely due to the influence of the top infiltration boundary, which was the same in both simulations and during the last half of 2003, infiltration was strongly negative at -61.67 mm (Appendix D). Similarly, between March and June 2004, the influx of water in both simulations was greater than the outflux of water. The net infiltration during this time was +41.65 mm (Figure 7.9; Appendix D).

It should be noted that these simulation results only apply in the specific case where there is water support from an underlying aquifer, as at the study site. The tile drain simulation was re-run with the bottom boundary assigned to be a no flow boundary to compare the results to a case where underlying aquifer support is not present. The mass balance results for both simulations are plotted in Figure 7.10 and Figure 7.11. The simulated chloride distribution has been plotted for November 2003, 2004, 2005 and 2006 and is included in Figure 7.12.

There are no entry points for chloride in the no-flow bottom boundary simulation and therefore the chloride mass influx is 0 (Figure 7.10). The only exit point for chloride in the simulation with the no-flow bottom boundary is the tile drain. In the no-flow bottom boundary simulation, much less chloride and water was produced than in the specified head bottom boundary simulation indicating that the bottom boundary condition greatly influences the mass of chloride that can be produced at the tile drain.

Figure 7.10. Effect of lower boundary condition on simulated system cumulative chloride mass influx and outflux 2003-2006.
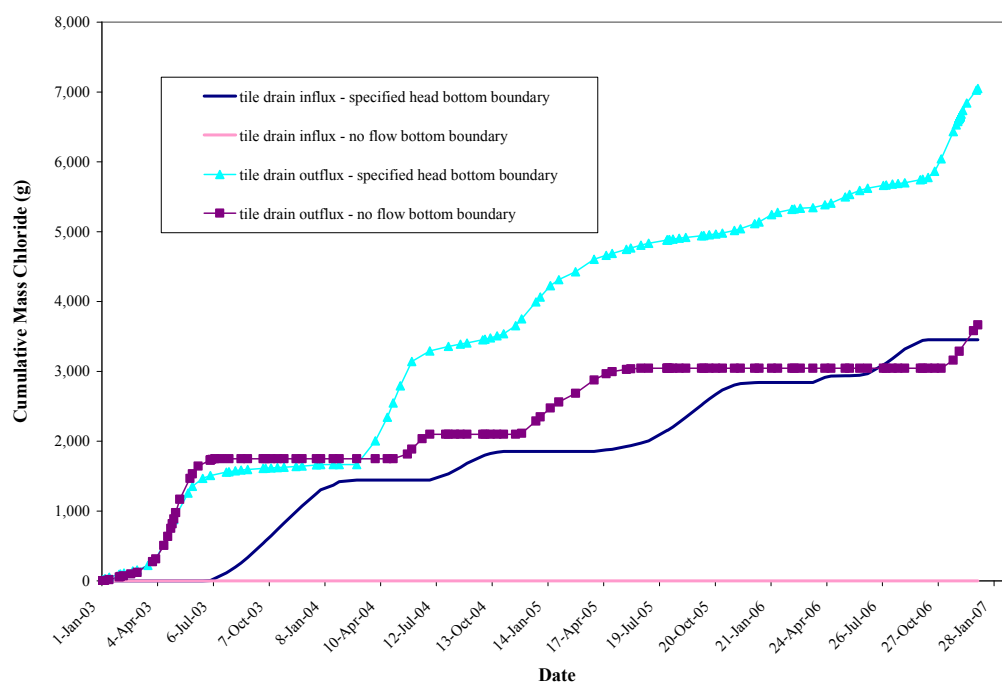

Figure 7.11. Effect of lower boundary condition on simulated system cumulative water volume inflow and outflow 2003-2006.
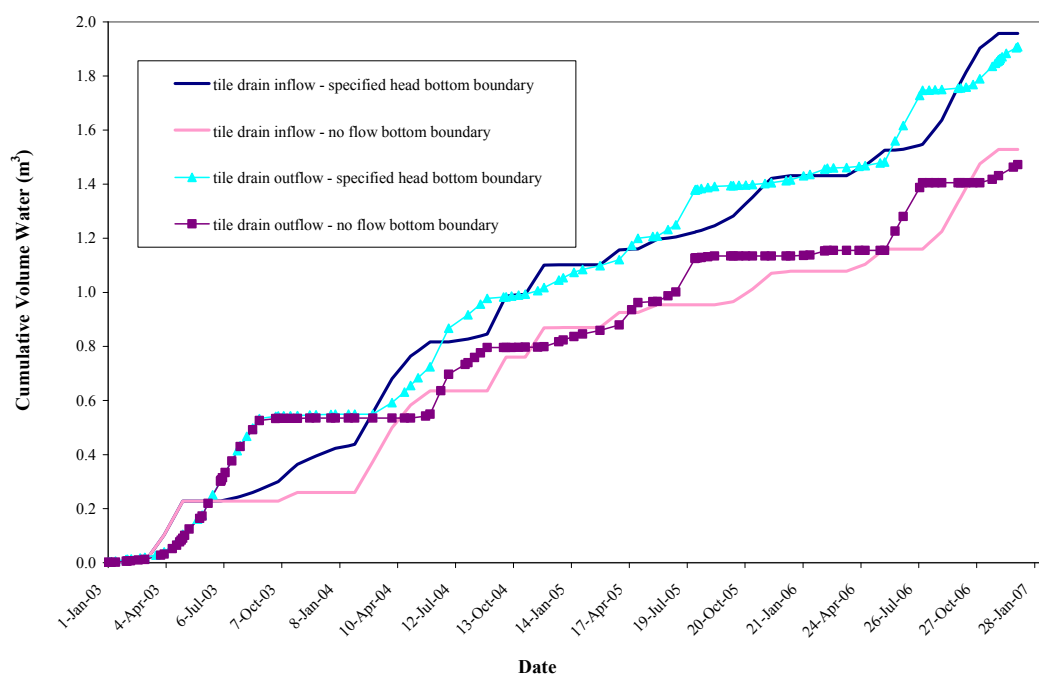
Figure 7.12. Simulated chloride distribution (M) for tile drain with no flow bottom boundary for November (a) 2003, (b) 2004, (c) 2005 and (d) 2006.
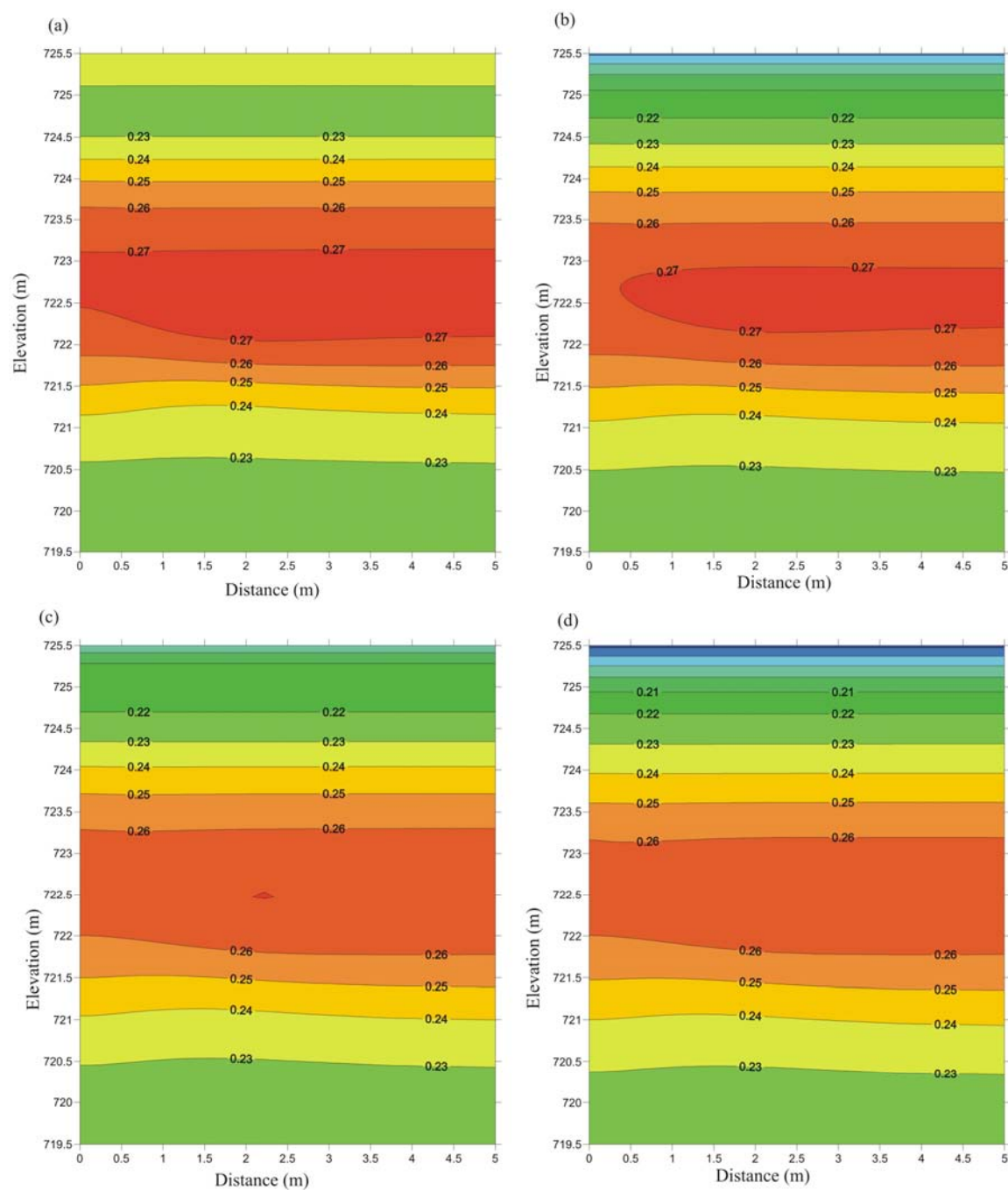
A comparison of Figure 7.7 and Figure 7.12 shows that chloride concentrations are higher in the middle of the simulation domain with the no-flow lower boundary. This is because the water table is below the level of the tile drain and therefore the drain is inactive during a greater proportion of the time due to the no-flow lower boundary condition. By 2006, chloride concentrations at the bottom of the simulation domain are lower in the simulation with the no-flow lower boundary (compare Figure 7.7(d) and Figure 7.12(d)). This is because the lower transport boundary condition of the specified head simulation is a Neumann boundary condition that, depending on the direction of groundwater flow, allows chloride to either exit the simulation domain along the bottom boundary or re-enter it at a concentration equal to the chloride concentration of the lower boundary nodes. The no-flow boundary simulation does not allow chloride to enter or exit the simulation domain along the bottom boundary.

7.7.2 Tile Drain Spacing

The tile drain lines at the site are installed at a spacing of 10 m apart. The objective of this evaluation scenario was to determine the optimal spacing between the tile drains to maximise chloride mass removal at the site. The effect of the spacing of the tile drain lines on chloride mass removal was evaluated by running three simulations with different tile drain spacing, each with the tile drain and without. In this way the chloride mass removed due to changes in the flow system caused by the tile drain was calculated over the simulation period. The chloride mass outflux was compared for each simulated tile drain spacing was then compared to determine which spacing optimises chloride removal at the site.

The simulations were run in three different size model domains that simulated three different tile drain spacing configurations. The elevation (z-direction) of each model domain was kept constant; however, the horizontal distance (x-direction) was adjusted to simulate different spacing between tile drain lines. The tile drain line spacing scenarios evaluated included 5 m, 10 m and 20 m apart. These were simulated in model domains that had horizontal (x-direction) distances of 2.5 m, 5 m and 10 m, respectively. The

model domain and grid discretisation for the 10 m tile drain spacing scenario (base-case) was described in Section 7.2. Table 7.6 contains a summary of the model domain dimensions and the grid discretisations used in the tile drain simulations for the 5 m and 20 m drain spacings, respectively. Initial and boundary conditions were identical in each of the simulations and were implemented as outlined in Sections 7.3 to 7.5. The simulations were run for the period from 2003 to 2006.

The tile drain spacing simulations were evaluated by comparing the change in mass removed due to the drain because the difference in the simulated domain sizes made a direct comparison of the simulation results impossible. Figure 7.14 shows the results for the tile drain and no drain simulations for the 5 m, 10 m and 20 m simulated tile drain spacings, respectively. The difference between the chloride mass outflux in each of the tile drain and no drain spacing simulations has been summarised in Table 7.7. The closest tile drain spacing (5 m) has the greatest chloride mass outflux due to the tile drain (1,335 g) while the widest tile drain spacing (20 m) had the lowest chloride mass outflux due to the tile drain (1,279 g; Table 7.7). Because the simulation domain represents one half of the flow field to a tile drain, a 20 m cross-section across the site with drains spaced 20 m apart would contain two simulation domains and the mass balance results would need to be multiplied by 2. Similarly, a 20 m cross-section across the site with drains spaced 10 m apart would contain four simulation domains and the mass balance results would need to be multiplied by 4, and a 20 m cross-section across the site with drains spaced 5 m apart would contain eight simulation domains and the mass balance results would need to be multiplied by 8.

Multiplying the mass of chloride produced due to the drain by the number of drains in a 20 m cross-section, the mass of chloride produced using 5 m tile drain spacing (10,678 g) is just over four times the mass produced using 20 m tile drain spacing (2,558 g; Table 7.7). The mass of chloride produced per tile drain is also highest for more closely spaced tile drain lines (Table 7.7).

Table 7.6. Summary of model domain and grid discretisation for tile drain spacing simulations.

Tile Drain Spacing: 5 m				
z-direction discretisation interval	z min (m)	z max (m)	Dz (m)	Nz
1	719.500	721.500	0.1	20
2	721.500	721.570	0.07	1
3	721.570	721.620	0.05	1
4	721.620	721.650	0.03	1
5	721.650	721.670	0.02	1
6	721.670	721.700	0.015	2
7	721.700	725.500	0.01	380
x-direction discretisation interval	x min (m)	x max (m)	Dx (m)	Nx
1	0.000	0.600	0.1	6
2	0.600	1.500	0.15	6
3	1.500	1.900	0.2	2
4	1.900	2.500	0.3	2
			Total Grid Nodes	6,496

| Tile Drain Spacing: 20 m				
z-direction discretisation interval	z min (m)	z max (m)	Dz (m)	Nz
1	719.500	721.500	0.1	20
2	721.500	721.570	0.07	1
3	721.570	721.620	0.05	1
4	721.620	721.650	0.03	1
5	721.650	721.670	0.02	1
6	721.670	721.700	0.015	2
7	721.700	725.500	0.01	380
x-direction discretisation interval	x min (m)	x max (m)	Dx (m)	Nx
1	0.000	2.000	0.1	20
2	2.000	4.250	0.15	15
3	4.250	6.250	0.2	10
4	6.250	6.850	0.3	2
5	6.850	7.750	0.45	2
6	7.750	9.050	0.65	2
7	9.050	10.000	0.95	1
			Total Grid Nodes	21,112

Figure 7.13. Effect of tile drain spacing on system chloride outflux 2003 to 2006.
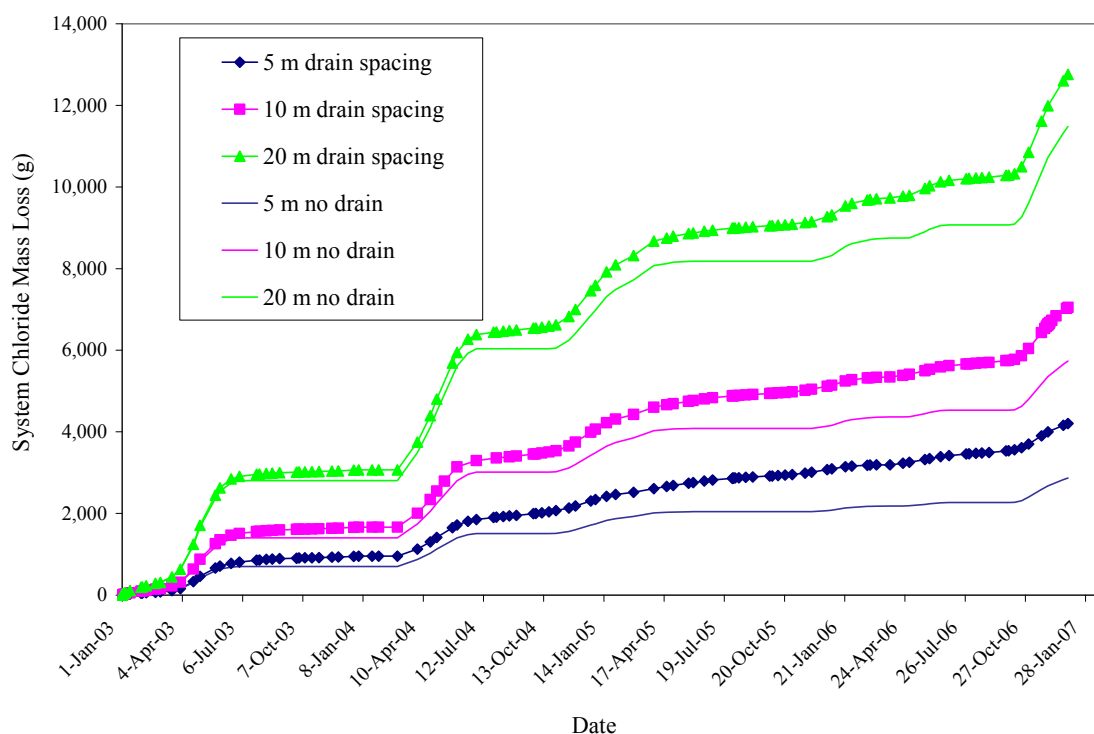
These simulation results suggest that closely spaced tile drain lines produce more chloride than tile drain lines spaced further apart and are consistent with the findings of studies on nitrate-nitrogen leaching where closely spaced tile drain lines produced more leaching than drains spaced further apart (Davis et al., 2000).

Table 7.7. Comparison of total system chloride mass outflux between 2003 and 2006 with different tile drain spacing.

Simulation	Tile Drain Spacing Chloride Mass Outflux (g)		
	5 m	10 m	20 m
Tile Drain	4,203	7,050	12,759
No Drain	2,868	5,733	11,480
Difference due to Drain	1,335	1,317	1,279
Simulation domain multiplier over 20 m	8	4	2
Difference produced over 20 m	10,678	5,267	2,558
g chloride produced per tile drain	2,136	1,756	1,279

7.7.3 Enhanced Infiltration

Along with the hydraulic conductivity of the soil, a major limiting factor in the use of tile drainage systems to flush salts out of the unsaturated zone is the amount of precipitation that is available to infiltrate the unsaturated soils and flush the salts downward towards the tile drains. The average annual precipitation at the site is relatively low with a 15-year climate normal value of 521 mm/year (Environment Canada, 2007a). The site tile drainage system produced 3,484 m^3 of water in 2003, 1,658 m^3 of water in 2004, 2,912 m^3 of water in 2005, and 1,320 m^3 of water in 2006 and covers an area approximately 24,500 m^2 (AMEC Earth and Environmental, 2007). The average TDS of the produced water between 2003 and 2006 was 9,964 mg/L (Table 2.3). In theory, this saline produced water could be treated onsite to remove virtually all of the salt and re-used as irrigation water to promote salt flushing at the site. The objective of this tile drain evaluation scenario was to simulate irrigation of the tile drained areas with treated produced water to determine the effect of enhanced infiltration on unsaturated zone salt remediation times.

The effect of enhanced infiltration on salt remediation with the tile drainage system was investigated by using the base case tile drain model described in Sections 7.2 to 7.5 and increasing the top boundary flux during months of the year where the tile drain is active (April to December) to simulate irrigation events. The flux due to irrigation was chosen to be approximately equal to the volume of water produced in 2004 (1,627.29 m^3) spread over the tile drain area of 24,500 m^2 which is equivalent to an additional flux of +7.38 mm/month of freshwater infiltration passing through the top model boundary. The simulation was run from 2003 to 2006 and the chloride distribution from the enhanced infiltration simulations have been contoured for November of each year in Figure 7.14.

Comparing Figure 7.7 and Figure 7.14, additional flushing of chloride from the unsaturated zone (between 723.03 and 725.5 m elevation) and further dilution of the chloride in the saturated zone can be seen in the enhanced infiltration simulation. By November 2006, the lowest chloride concentration in the unsaturated zone is 0.11 M

(3,900 mg/L) in the enhanced infiltration simulation (Figure 7.14) while the lowest chloride concentration in the unsaturated zone in the base case simulation is 0.18 M (6,382 mg/L; Figure 7.7).

These results may be somewhat misleading; however, since the +7.38 mm/month was added to the infiltration boundary value calculated using the output from VSMB rather than being added as additional precipitation and re-run though VSMB. Because the infiltration boundary calculated using the output from VSMB shows a water deficit (net negative infiltration) during many years (Appendix D) it is unsure how much of the irrigation water would actually cross the top boundary of the soil as infiltration and how much would simply be lost as evapotranspiration.

To quantify the percentage of the irrigation water that would become infiltration at the site, the VSMB model was re-run using weather data from the Calmar weather station from 1969 to 2006 with an additional +7.38 mm/month of precipitation added to the months of April through December for each year from 2003 to 2006. The infiltration values with site irrigation were then calculated with the new output from VSMB using the methodology described in Section 4.3.1. The 2003-2006 infiltration values with site irrigation are included in Table 7.8 and are included with the infiltration values calculated for the site without irrigation for comparison purposes.

In each case there is more infiltration with site irrigation. If all of the water added as irrigation infiltrated into the subsurface, it would result in an additional +66.42 mm/year of infiltration for each year. Comparing the annual net infiltration values in Table 7.8, it is apparent that not all of the irrigation water becomes infiltration. In 2003, 76% of the water added through irrigation was lost, while 33% was lost in 2004, 57% was lost in 2005, and 70% was lost in 2006.

Figure 7.14. Simulated chloride distribution (M) for enhanced infiltration simulation for November (a) 2003, (b) 2004, (c) 2005 and (d) 2006.
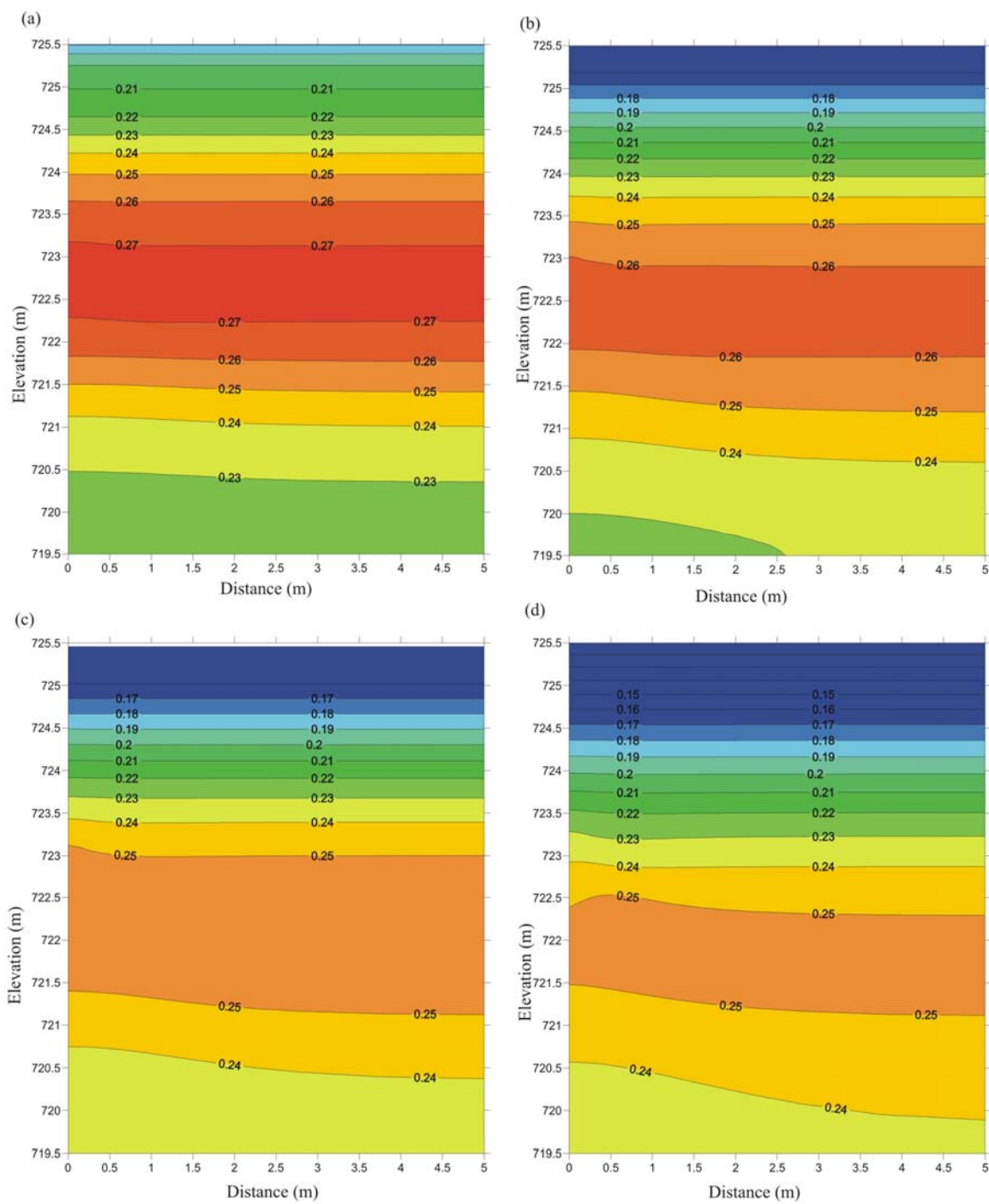
The simulation results suggest that irrigating the tile drainage area with 1,627 m^3/year of freshwater significantly increases the rate at which chloride is flushed out of the unsaturated zone. In reality, however, the irrigation amount would have to be greater to overcome the water deficit at the site and ensure that more of the irrigation water ends up as infiltration and is not lost through evapotranspiration.

7.7.4 Estimated Remediation Time

Although tile drainage systems are a common method of remediating surface salt spills in Alberta, it is still unknown whether these systems are indeed effective and over what time-scales. This is partly due to the fact that environmental reporting requirements were not as stringent in the past as they are today and that very little good-quality long-term monitoring data is available for these systems. The objective of this evaluation scenario was to predict how chloride concentrations would change in the shallow unsaturated zone if the tile drainage system was left in place for a period of 100 years. The simulation was re-run without a tile drain to assess the potential advantage provided by the tile drainage system over natural attenuation in terms of total remediation time.

In the preliminary numerical model sensitivity analysis (Section 6.4), time-variable infiltration was identified as a sensitive parameter when looking at the evolution of salt plumes over time in the unsaturated and shallow saturated zones. In order to predict the change in chloride concentrations over time in the unsaturated zone pore-water, it was essential that the simulations incorporate time-variable infiltration. Because it is impossible to predict what precipitation levels may be in the future, the predictive simulation was conducted with the groundwater infiltration data calculated in VSMB using weather data recorded between 1984 and 2006. It was assumed that the next 22 years groundwater infiltration would be identical to the previous 22 years and so on with the infiltration data repeating every 22 years.

Table 7.8. 2003-2006 infiltration calculated using VSMB without site irrigation and with +7.38 mm/month site irrigation from April to December of each year.

Without Irrigation		With Irrigation	
Date	Infiltration (mm)	Date	Infiltration (mm)
Jan-03	0.53	Jan-03	0.53
Feb-03	0.00	Feb-03	0.00
Mar-03	13.98	Mar-03	13.98
Apr-03	37.19	Apr-03	41.86
May-03	-9.08	May-03	-3.88
Jun-03	-8.68	Jun-03	-0.53
Jul-03	-51.61	Jul-03	-49.89
Aug-03	-5.92	Aug-03	-18.90
Sep-03	-1.65	Sep-03	3.21
Oct-03	6.45	Oct-03	10.84
Nov-03	-0.25	Nov-03	-0.17
Dec-03	0.00	Dec-03	0.00
Total (mm/yr)	-19.05	Total (mm/yr)	-2.95
Jan-04	0.00	Jan-04	0.00
Feb-04	0.00	Feb-04	0.00
Mar-04	70.66	Mar-04	75.20
Apr-04	-6.12	Apr-04	-0.80
May-04	18.87	May-04	20.60
Jun-04	-41.76	Jun-04	-28.85
Jul-04	-0.21	Jul-04	3.28
Aug-04	-16.77	Aug-04	-13.78
Sep-04	36.14	Sep-04	38.54
Oct-04	-5.89	Oct-04	-3.10
Nov-04	21.64	Nov-04	29.38
Dec-04	0.20	Dec-04	0.79
Total (mm/yr)	76.77	Total (mm/yr)	121.26
Jan-05	0.00	Jan-05	0.00
Feb-05	0.00	Feb-05	0.00
Mar-05	11.16	Mar-05	7.64
Apr-05	-14.02	Apr-05	-11.13
May-05	5.75	May-05	8.94
Jun-05	0.98	Jun-05	7.23
Jul-05	-40.69	Jul-05	-37.33
Aug-05	6.19	Aug-05	8.61
Sep-05	2.24	Sep-05	8.03
Oct-05	9.24	Oct-05	15.37
Nov-05	11.67	Nov-05	14.09
Dec-05	1.61	Dec-05	1.12
Total (mm/yr)	-5.86	Total (mm/yr)	22.57
Jan-06	-0.65	Jan-06	-0.88
Feb-06	-3.47	Feb-06	-3.85
Mar-06	0.00	Mar-06	0.00
Apr-06	5.12	Apr-06	5.70
May-06	24.20	May-06	30.08
Jun-06	-37.92	Jun-06	-32.54
Jul-06	-34.13	Jul-06	-36.37
Aug-06	-9.38	Aug-06	-9.28
Sep-06	62.94	Sep-06	68.18
Oct-06	29.29	Oct-06	34.65
Nov-06	0.00	Nov-06	0.00
Dec-06	0.00	Dec-06	0.00
Total (mm/yr)	35.99	Total (mm/yr)	55.70

It is recognised that this is highly unlikely; however, the objective of this evaluation scenario was only to give a rough idea of the time-scales involved for unsaturated zone salt remediation with tile drainage systems. The remaining boundary conditions were the same as outlined in Sections 7.2 to 7.4. The output from the base-case simulations (with and without a tile drain) at the end of 2006 was used as the initial conditions for the predictive simulations. The simulations were run for a total of 100 years from 2007 to 2107. The chloride distributions at 25 years and at 100 years have been plotted for both the tile drain simulation and the natural attenuation simulation in Figure 7.15. Note that the colour scale has been changed from the one used in previous figures to highlight the decrease in chloride concentrations over time.

Chloride distributions are very similar between the tile drain and natural attenuation simulations (Figure 7.15). After 25 years, the chloride concentration in the unsaturated zone, between 723.03 and 725.50 m elevation, was predicted to be approximately 0.17 M (6,027 mg/L). At a simulation time of 100 years, chloride concentrations are predicted to be reduced by a further 2,127 mg/L to 3,900 mg/L (0.11 M), but are still substantially above the generic regulatory guideline of 250 mg/L (Health Canada, 2006) and the site background concentration of 20 mg/L.

A comparison of the tile drain and natural attenuation simulations shows that the tile drain does not appear to offer an advantage in terms of a quicker decrease in chloride concentrations over time as concentrations are very similar in both simulations at the same output times. This is likely due to the fact that there are upward hydraulic gradients in the model domain at times of the year when the top flux boundary is negative which allows additional chloride mass to cross into the model domain at the bottom boundary. The steeper hydraulic gradient induced by the tile drain allows more chloride to enter the bottom corner of the model domain on the side of the tile drain than in the no drain, natural attenuation simulation (Figure 7.16). For long simulation times, this effect can become quite pronounced.

Figure 7.15. Chloride distribution (M) for predictive simulations at 25 years (a) with tile drain and (b) natural attenuation and at 100 years (c) with tile drain and (d) natural attenuation.
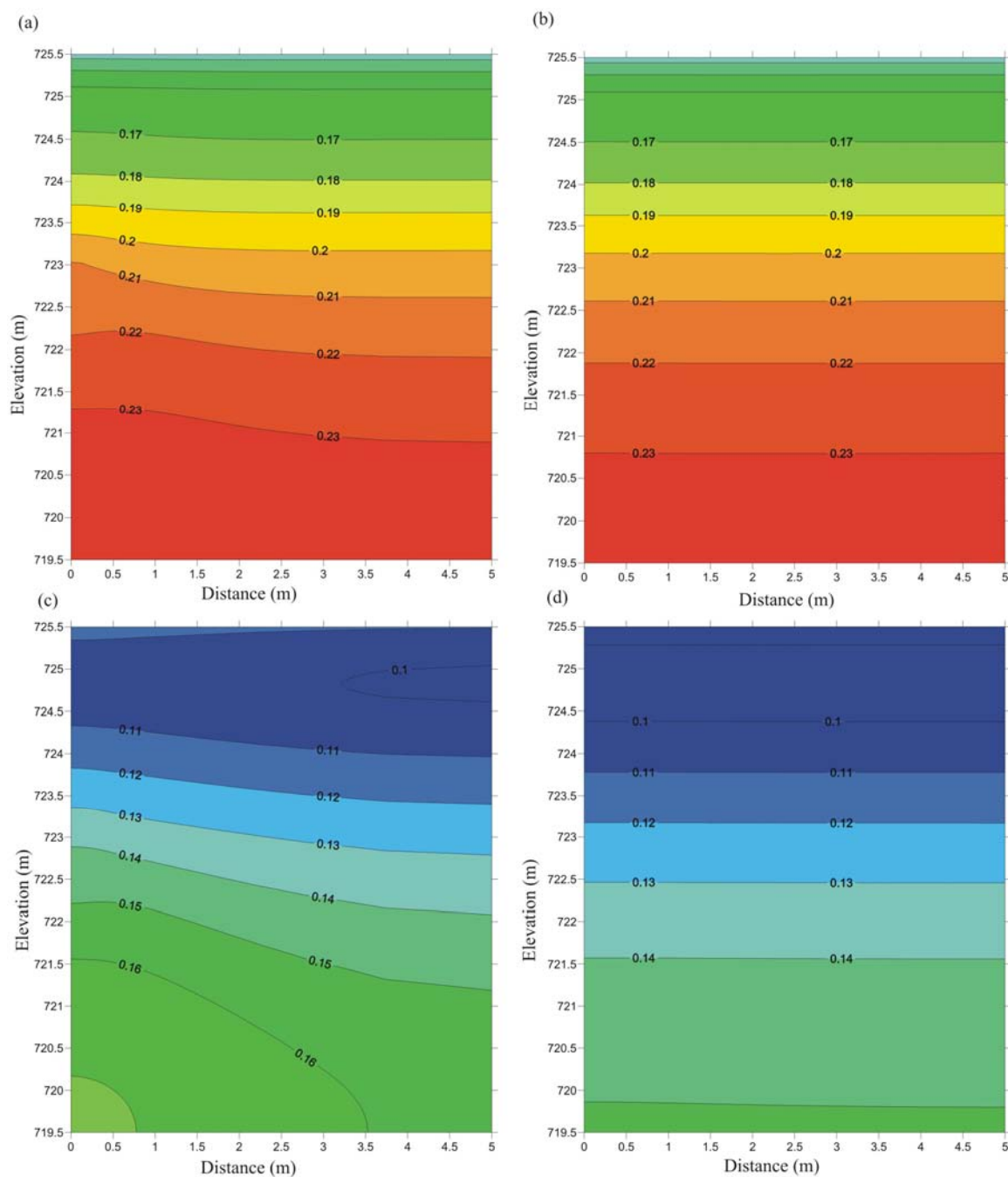
This resulted in similar chloride concentration profiles, even though the chloride outflux in the tile drain simulation was actually greater and more chloride mass was removed by the tile drain simulation over time (Figure 7.16).

Figure 7.16. 2007-2107 simulated chloride mass influx and outflux for tile drain and natural attenuation simulations.
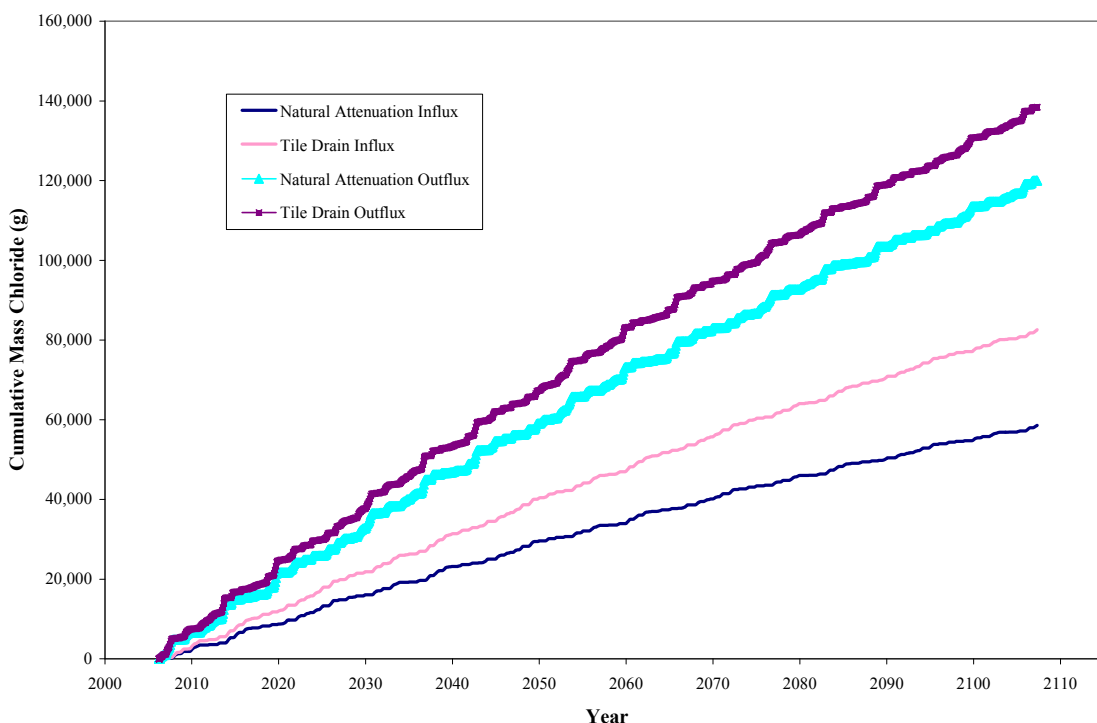
The upward flux of chloride below 719.5 m elevation is a plausible scenario at the study site because the tile drain system was installed well after the salt spill had occurred and the saturated zone below the bottom of the model domain does in fact contain elevated chloride concentrations. For example, the mean chloride concentration at P04-2B, completed between 717.4 and 719.0 m elevation, and below the base of the tile drain simulation model domain at 719.5 m, was 7,889 mg/L (0.22 M) between 2004 and 2006 (Table 2.2). This tile drain simulation therefore represents a site with an underlying contaminated aquifer. These simulations do not take into account, however, the north lateral groundwater flow gradient at the site. This would act as a source of freshwater coming in from the south which is not represented in the model as both the north and

south boundaries are no-flow boundaries. This lateral influx of freshwater would likely serve to further dilute the chloride concentrations in the saturated zone over time and so these simulations likely over-predict remediation times.

Two additional simulations were run to investigate the role of the bottom boundary conditions in the estimated remediation time tile drain simulations. The first scenario consisted of a flow system with aquifer support and a tile drain, similar to the original simulation; however, the bottom transport boundary was changed to a first type, specified concentration set to 10 mg/L NaCl to simulate an underlying uncontaminated aquifer. The second scenario consisted of a flow system without aquifer support with a no-flow lower boundary condition to simulate an underlying aquitard. The only exit for chloride from the aquitard system is the tile drain node. The remaining boundary and initial conditions for these simulations were as described in the scenarios with aquifer support and an underlying contaminated aquifer. The simulated chloride concentration profiles for the underlying uncontaminated aquifer and the underlying aquitard scenarios at 25 and 100 years simulation time are included in Figure 7.17. Note that the colour scales are not the same for scenario with aquifer support from an uncontaminated aquifer the scenario without aquifer support to highlight differences in chloride concentrations between 25 and 100 years.

The 25-year chloride distribution in the simulation with water support from an uncontaminated underlying aquifer (Figure 7.17a) is very different from the 25-year chloride distribution in the original tile drain simulation with the underlying contaminated aquifer (Figure 7.15a).

Figure 7.17. Chloride distribution (M) for tile drain simulations with water support from an uncontaminated underlying aquifer at (a) 25 years and (b) 100 years simulation time and with an underlying aquitard at (c) 25 years and (d) 100 years.
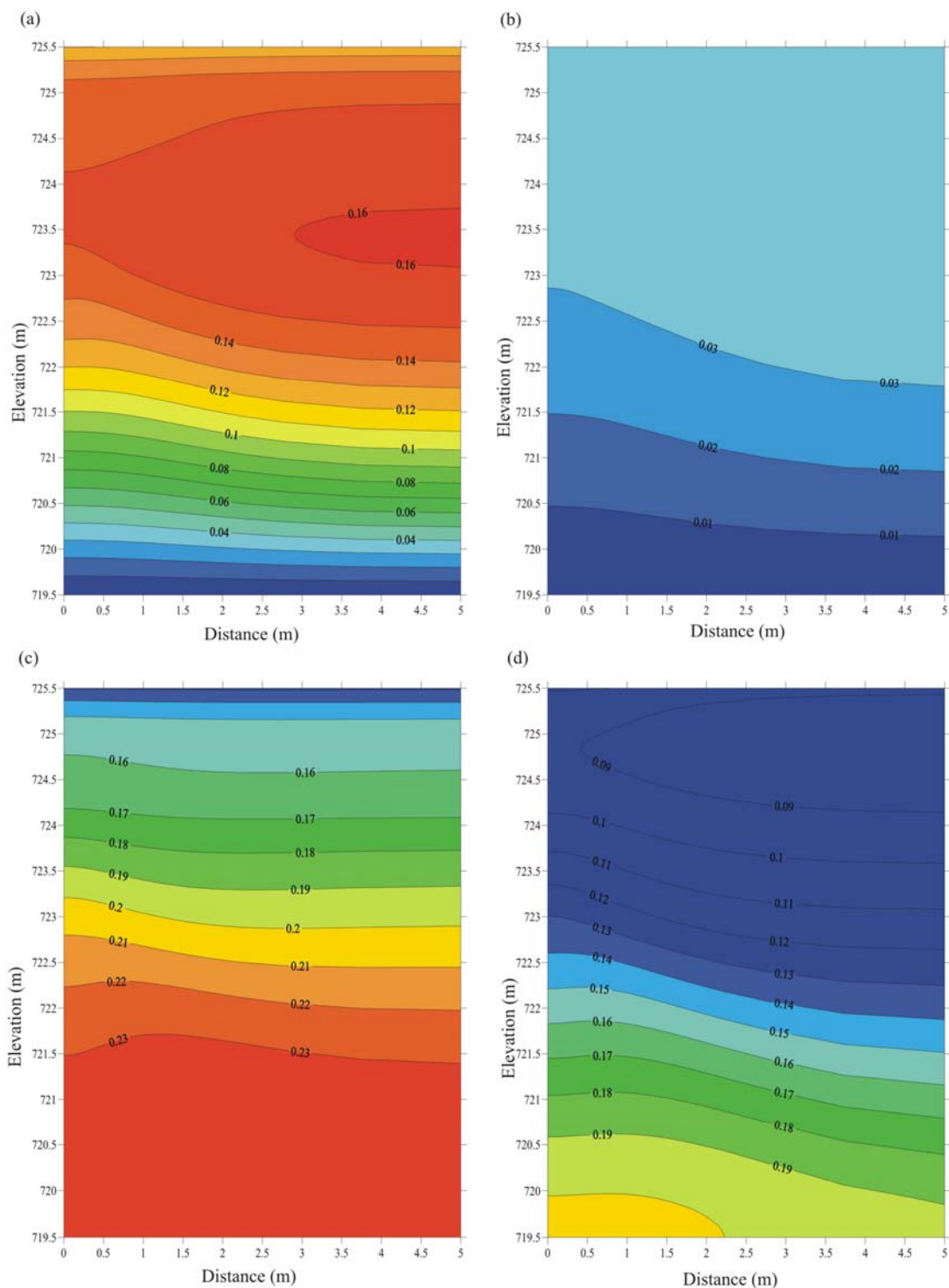
The maximum chloride concentration after 25 years is 5,672 mg/L (0.16 M) with an uncontaminated underlying aquifer while the maximum concentration with a contaminated underlying aquifer is 8,154 mg/L (0.23 M). In addition, the chloride concentration depth profile is very different between the two scenarios, with maximum concentrations occurring in the middle of the model domain at the elevation of the tile drain in the underlying uncontaminated aquifer scenario and at the base of the model in the underlying contaminated aquifer scenario. At 100 years simulation time, maximum chloride concentrations decreased more quickly to 1,064 mg/L (0.03 M) in the top half of the underlying uncontaminated aquifer model domain while maximum chloride concentrations remained more elevated at 5,672 mg/L (0.16 M) in the underlying contaminated aquifer scenario (Figure 7.15c and Figure 7.17b).

In the simulation scenario with an underlying aquitard, the chloride concentration profile at 25 years is very similar to the original tile drain simulation (Figure 7.15a and Figure 7.17c). By 100 years, the maximum chloride concentration in the simulation with an underlying aquitard (no-flow lower boundary) is 7,091 mg/L (0.20 M) at the base of the model domain and only slightly higher than the maximum chloride concentration in the tile drain simulation with an underlying contaminated aquifer at the same simulation time 6,027 mg/L (0.17 M). It would therefore be hard to distinguish between these types of hydrogeological conditions based on chloride concentration profiles alone and in this study, comparison of site-measured water levels with the simulated water table elevation were used to make that distinction.

The 2007-2107 mass balance results for each lower boundary condition tile drain scenario simulation are included in Figure 7.18 and Figure 7.19. Chloride mass balance results show that the rate of chloride outflux for the tile drain simulation with an uncontaminated underlying aquifer, is initially very high and greater than the rate of chloride outflux in both the contaminated underlying aquifer and the underlying aquitard simulations for the first 30 years.

Figure 7.18. 2007-2107 simulated chloride mass influx and outflux for tile drain simulations with underlying contaminated aquifer support, underlying uncontaminated aquifer support, and an underlying aquitard.
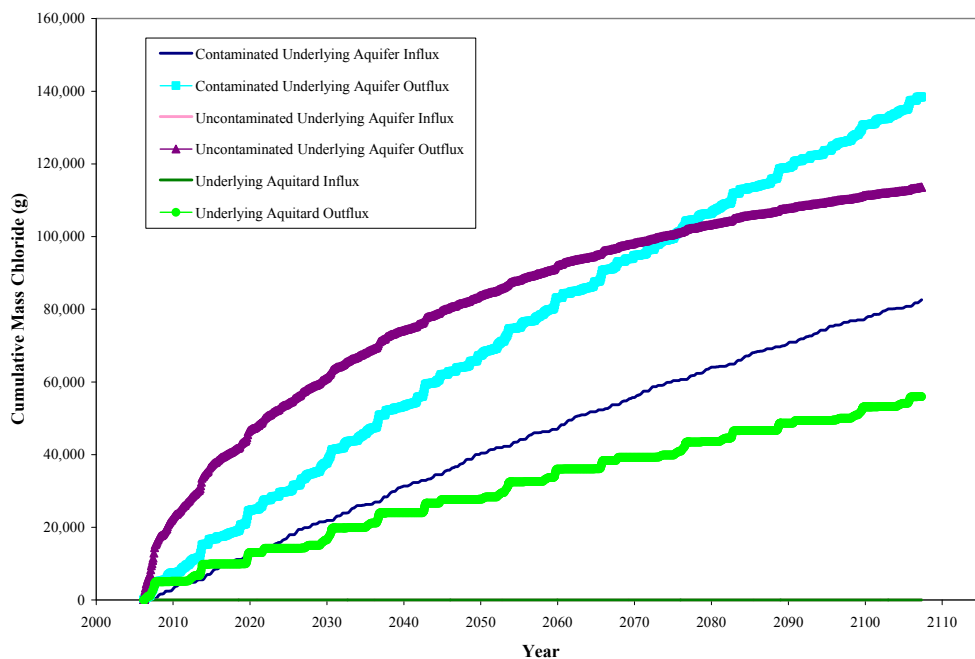

Figure 7.19. 2007-2107 water inflow and outflow for tile drain simulations with underlying contaminated aquifer support, underlying uncontaminated aquifer support, and an underlying aquitard.
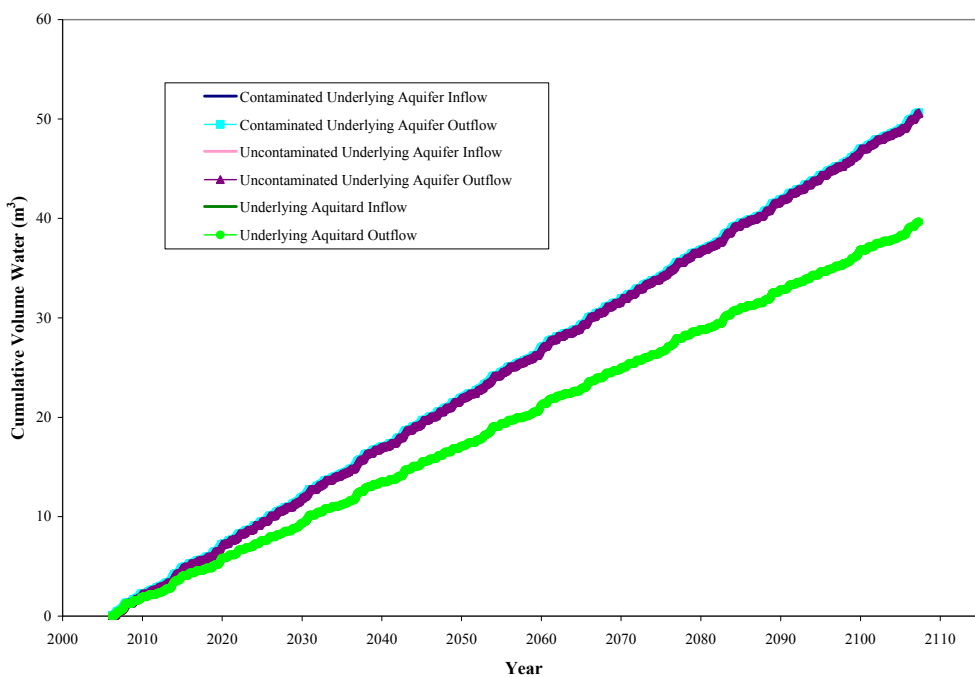
After 2030, however, this rate begins to slow and by 2060, the rate of chloride mass outflux in the uncontaminated underlying aquifer tile drain simulation is approximately equal to the rate of chloride mass outflux for the underlying aquitard tile drain simulation (Figure 7.18). The rates of chloride mass outflux in both the contaminated underlying aquifer and underlying aquitard tile drain simulations remain approximately constant during the 100 year simulation period. The underlying uncontaminated aquifer and the underlying aquitard tile drain simulations have chloride mass influx rates that are approximately equal to zero (Figure 7.18).

The water mass balance results for all three tile drain simulations show that the water inflow is equal to water outflow and that all three systems reached steady state during the 100-year simulation period (Figure 7.19). The water mass balance is the same for both aquifer support simulations, as would be expected given that these simulations contained identical flow boundary conditions. The water inflows and outflow for the underlying aquitard simulation are less than these two simulations, as would be expected since water cannot enter or exit across the bottom boundary in this simulation.

7.8 Summary

Tile drain simulations were run over a four-year time period from 2003 to 2006 to evaluate chloride mass removal by the tile drainage system at the site. Simulation results were compared to field data collected at the site over the same time-period. The simulated chloride mass outflux calculated in MIN3PD indicates that more chloride mass was removed from the system with a tile drain than without a tile drain (natural attenuation).

Additional short-term simulations were run that focussed on evaluating tile drainage system design parameters including the spacing between the drainage lines and the effect of irrigating the drainage area with fresh water to promote salt flushing. The results of the short-term simulations indicate that more closely spaced drainage lines remove more chloride mass per drain than drainage lines that are spaced further apart, however, this

advantage must be balanced with the additional cost to install drainage lines more closely together. Results also showed that freshwater irrigation of the tile drainage area can result in enhanced infiltration through the unsaturated zone and speed up the rate of chloride flushing in the unsaturated zone. The irrigation volume must be sufficient to overcome any net water deficits at the site, however, otherwise most of the water may be lost through evapotranspiration.

Longer-term predictive simulations were also run to estimate the time it would take for chloride remediation in the unsaturated zone with a tile drainage system and by natural attenuation. Predictive simulations incorporated time-variable infiltration, which was identified as a sensitive parameter in the preliminary numerical modeling. The results of the predictive simulations indicate that remediation times for chloride in the unsaturated zone in the case of water support from a contaminated underlying aquifer are long and likely greater than 100 years, both with a tile drain and by natural attenuation. Chloride concentrations in both the tile drainage simulation and the natural attenuation simulation were similar, likely because periodic upward hydraulic gradients allow chloride to enter the simulation domain at the bottom boundary. The greater hydraulic gradient induced by the tile drain caused a greater amount of chloride to enter upward across the bottom boundary into the tile drain domain than in the natural attenuation simulation which resulted in similar chloride concentration profiles, even though the chloride outflux in the tile drain simulation was greater. This situation is not unlike the study area, where elevated chloride concentrations are present at depth and have the potential to move upward due to upward hydraulic gradients.

The best case tile drain remediation scenario was one with water support from an underlying uncontaminated aquifer. The chloride concentrations in this scenario remained lower at depth than the other scenarios and decreased much more quickly over time in the unsaturated zone. This underlines the importance of quick response time for salt releases. The tile drain simulation results indicate that tile drain systems are more effective at removing chloride from the shallow subsurface than natural attenuation

alone; however, they are not necessarily a one-size-fits-all approach. Depending on the unique combination of meteorological and hydrogeological conditions at each site, tile drainage systems may not always offer significant advantages in terms of salt remediation times over natural attenuation.

Chapter Eight: Discussion and Conclusions

8.1 Introduction

The purpose of this study was to evaluate tile drainage systems as a method of salt remediation in Alberta. Data from a well-characterised produced water spill at a former upstream oil and gas site located in central Alberta was used to build a numerical model. The goal of the numerical modeling was to gain an improved understanding of salt transport to tile drains in the shallow subsurface which may ultimately lead to more effective management of salt-impacted sites.

A major produced water release is believed to have occurred at the study site some time in the mid 1980s, although the exact data is unknown. Environmental assessment was initiated at the site in 1998 and EM surveys identified several salt-impacted areas across the site. Groundwater samples taken from monitoring wells installed within the salt-impacted areas in 1998 contained chloride and sodium concentrations ranging up to 19,000 mg/L and 4,170 mg/L, respectively. A tile drainage system was installed across an area 24,500 m^2 in 2003 to remediate the shallow salts at the site. The code MIN3PD (Henderson et al., 2007) was used to simulate variably-saturated density-dependent groundwater flow and transport of salt at the site.

8.2 Discussion

8.2.1 Site Data

Climatic data for the region indicates that the study area is located in a continental climate area with cold winters and cool summers. The average annual precipitation in the area is relatively low at 521 mm/year, of which 25% occurs as snow. Monitoring wells were first installed at the site in 1998. The 1998-1999 chloride concentrations ranged from 7,050 m/L at P98-5A to 19,000 mg/L at P99-6A. A tile drainage system was installed at the site in March 2003 to address the salt impacts. Monitoring of the tile drainage system, including collection of groundwater samples and measurement of water

levels at shallow monitoring wells, was conducted at the site in 2003, 2004, 2005 and 2006. In 2004, the mean chloride concentration at indicator shallow monitoring well P04-2A was 8,533 mg/L while the mean chloride concentration at the adjacent nested deep well P04-2B was 8,117 mg/L. By 2006, after 3 years of operation of the tile drain system, the mean chloride concentration measured at P04-2A was 6,140 mg/L and the mean chloride concentration at P04-2B was 7,390 mg/L. It should be noted that the October 2006 chloride concentration measured at P04-2A was 2,340 mg/L lower than the concentration measured in June 2006 and that the overall decrease in chloride concentrations at P04-2A is likely somewhat lower due to this large seasonal variation in concentrations. The mean chloride concentration in the tile drain collection sump effluent in 2004 was 5,204 mg/L, while the mean chloride concentration in the tile drain sump effluent in 2006 was 5,350 mg/L. The elevated concentrations of sodium and chloride in the collection sump water indicate the tile drainage system is removing sodium and chloride from the subsurface.

Soil water retention curves were measured for eight core samples from C05-02 and C05-03, each of which was later identified as a silt loam through soil textural analysis. The values for the saturated moisture content (θ_s) for three of the samples were consistent with published experimental values for silt loam and ranged from 0.42 to 0.47 m^3/m^3. The remaining θ_s ranged from 0.52 to 0.58 m^3/m^3, which is slightly higher than the published range for silt loam soil. The elevated saturated moisture content of some of the samples may be related to salt concentrations in the soil core samples given the known elevated salinity at the site. Significant soil swelling was observed for both samples 1 and 1d, both of which had elevated θ_s, when they were initially saturated during the experiment, which may support this hypothesis. Additionally, macropores or fractures within the natural cores may have also contributed additional water storage capability. The values obtained for van Genuchten parameter α were generally elevated and not within range of published experimental values. The α values also varied substantially from sample to sample as evidenced by the high values of the variance and standard deviation. It is hypothesised that the soil samples likely contain internal macrostructure

that is dominating the flow parameters. This is plausible since very shallow, natural core samples were analysed and the samples were not re-packed. Other studies have also reported that internal structure can dominate the flow parameters when natural core samples are used for SWRC analysis. The experimentally determined values of α were therefore judged to be not representative of the silt loam at the scale of interest for the numerical model. The value of α used in the numerical model for the silt loam was 0.48 m^{-1} which is similar to the mean value of α obtained from analysis of 332 soil samples (Schaap and Leij, 1998). The values of van Genuchten parameter n obtained experimentally were relatively consistent between the samples and were within range of previously published results. The mean value of n for the silt loam was 1.09.

Three hydrostratigraphic units of interest were identified at the site. These consisted of shallow, variably saturated silt loam located between ground surface and a depth of 6.25 m underlain by a fully-saturated fine grained sand layer approximately 1.25 m thick. Lower permeability glacial till was encountered underlying the sand. The saturated hydraulic conductivity of the silt loam was estimated to be 4.25 x 10^{-7} m/s based on the results of hydraulic conductivity tests conducted at the site. The hydraulic conductivity of the sand aquifer is estimated to be on the order of 4.44 x 10^{-5} m/s based on grain size analysis data from sand samples collected onsite. Groundwater flow within the unsaturated silt loam is predominantly downward towards the water table, although during some months of the year, upward flow may also occur. Evidence for upward hydraulic gradients is seen in the November 30, 2004 groundwater elevations measured at nested monitoring wells P04-2A/B where deep well P04-2B contained a groundwater elevation of 723.18 m and shallow well P04-2A contained a groundwater elevation of 723.11 m. Upward hydraulic gradients can hamper salt flushing out of the shallow subsurface as salt is continuously re-introduced by the upward gradients after it is flushed downward. The salt tends to move vertically up and down in the soil profile rather than being permanently flushed downward.

8.2.2 Numerical Modeling

The preliminary numerical model constructed for this study was a larger scale model that was used to obtain the 2003 chloride distribution at the site. The 2003 chloride distribution was later used as the initial condition for the tile drain simulations. The uncertainty in both the initial salt concentration and the time of the produced water release presented a challenge to model calibration. For the purposes of this study, and based on anecdotal evidence from onsite operators, it was assumed that the produced water release occurred in 1984. The preliminary model also served to identify sensitive parameters that needed to be taken into account in the tile drain simulations. Results of the preliminary model sensitivity analysis showed that the model was quite sensitive to the time-variable infiltration boundary. When the 20-year simulation was run using a constant average infiltration boundary, maximum chloride concentrations in the upper 1 m of the model domain were approximately double the concentrations of the simulation run using a monthly time-variable infiltration boundary. Also, the toe of the chloride plume migrated to a much greater depth in the time-variable infiltration simulation, even though the initial source NaCl concentration and the dispersivity values were the same in both cases. Based on a comparison of site-measured chloride concentrations with the simulated time-variable infiltration chloride concentrations, seasonal variations in precipitation appear to be an important mechanism acting at the site to dilute the near-surface chloride concentrations over time and promote greater depth of migration of the chloride plume than would be predicted by a constant averaged infiltration boundary.

Density-dependent flow was also found to significantly affect the 20-year chloride plume distribution in the preliminary transport model. After 20 years, the maximum chloride concentrations in the density-dependent flow simulation plume were approximately one half the maximum chloride concentrations of the non-density-dependent flow simulation plume. In addition, the maximum chloride concentration within the plume migrated to a much greater depth in the density-dependent flow simulation. This suggests density-dependent flow is an important mechanism causing additional dilution and spreading of the chloride plume in the vertical direction. Given the current chloride distribution at the

site, and the fact that the mean chloride concentration in the study area field at the time the facility was in operation was approximately 112,000 mg/L (AMEC Earth and Environmental, 2007), the density-dependent flow transport simulation with an initial NaCl release concentration of 200,000 mg/L (121,327 mg/L chloride) produces chloride distributions that are more similar to current site concentrations than non-density-dependent flow transport simulations with the same initial NaCl release concentration.

The tile drain simulation results indicate that tile drain systems do remove chloride from the shallow subsurface, which is corroborated by groundwater quality results from the tile drain collection sump. Short-term simulations showed that more closely spaced drainage lines remove more chloride mass per tile drain than drainage lines that are spaced further apart. The mass of chloride produced using 5 m tile drain spacing was just over four times the mass produced using 20 m tile drain spacing over the same area. This advantage in terms of chloride production must be balanced with the increased cost to install more drainage lines and deal with the additional saline produced water. Irrigation of freshwater over the tile drainage area can result in enhanced infiltration which increases the rate of chloride flushing in the unsaturated zone if the irrigation volume is sufficient to overcome any net water deficits at the site. Otherwise most of the irrigation water may be lost through evapotranspiration and thus provide no advantage in terms of chloride flushing. Simulation results suggest that if there were no net water deficit at the site, irrigating the tile drain field with 1,627 m^3/year of freshwater for a period of 4 years could reduce the chloride concentrations in the top 1 m of the model domain to concentrations similar to those after 25 years of operation of the tile drainage system with natural infiltration.

The results of the predictive simulations indicate that in the case of the tile drainage system installed at the study site with aquifer support from an underlying contaminated aquifer, remediation times for chloride in the unsaturated zone are long and likely greater than 100 years. This is due mainly to the low levels of precipitation available for

chloride flushing, the presence of upward hydraulic gradients at the site and the relatively low hydraulic conductivity of the soils.

A comparison of the predictive simulations with aquifer support from an underlying contaminated aquifer shows that tile drains do not appear to offer an advantage in terms of a quicker decrease in chloride concentrations over time versus natural attenuation. This is likely due to the fact that there are upward hydraulic gradients in the model domain at times of the year when the top flux boundary is negative which allows additional chloride mass to cross into the model domain at the bottom boundary. The steeper hydraulic gradient induced by the tile drain allows more chloride to enter the bottom corner of the model domain on the side of the tile drain than in the simulation without a tile drain. This resulted in similar chloride concentration profiles in the tile drain and natural attenuation simulations, even though the chloride outflux in the tile drain simulation was actually greater. The best case tile drain salt remediation scenario was one with water support from an underlying uncontaminated aquifer. The chloride concentrations in this scenario remained lower at depth than the other scenarios and decreased much more quickly over time in the unsaturated zone. This underlines the importance of quick response-time for salt releases. Density-dependent flow, which could not be incorporated in the tile drain simulations, may have the effect of reducing the total remediation time somewhat as salt would be expected to sink downward and dilute more rapidly than would be predicted by the non-density-dependent flow tile drain simulations performed in this study.

The results of the tile drain simulations illustrate that tile drainage systems are not necessarily a one-size fits all approach. Depending on the unique combination of meteorological and hydrogeological conditions at a particular site, tile drainage systems may not always offer significant advantages in terms of salt remediation times over natural attenuation.

8.3 Conclusions

8.3.1 Future Work

Although numerical modeling can be a useful tool to increase our understanding of hydrogeologic systems and contaminant transport within these systems, there is no substitute for good quality, long-term site monitoring data. It is recommended that monitoring well water levels, tile drainage system produced water volumes and analysis of major cations and anions in groundwater samples from the monitoring wells and the tile drain collection sump continue to be collected at the study site. The current and ongoing research conducted at the study site will prove much more valuable if tile drainage system monitoring is to continue for as long as the system remains in place. The long-term monitoring data could then be used to assess the actual effectiveness of tile drainage systems as a method of salt remediation in Alberta and give a much better idea of salt remediation time-frames. More accurate time-frames could act as an additional site management tool where more aggressive remediation options could be pursued if shorter remediation times are needed. More aggressive remediation options would include more extensive excavation of salt-impacted soil to remove more of the residual salt source in the subsurface prior to installation of the tile drainage system, more closely spaced tile drain lines, and/or irrigation of the site with freshwater to enhance salt flushing at sites with low levels of natural precipitation.

It would be useful if the tile drain simulations developed in this study could be re-run in density-dependent mode. Chloride transport at the site was found to be sensitive to density-dependent flow and it would be interesting to see the effect of density-dependent flow on the total remediation time estimated with the predictive simulations, in particular in relation to the behaviour of salt in the saturated zone, below the tile drain. The current numerical model could also be extended to include sodium-cation exchange processes to better understand the behaviour of sodium in the shallow subsurface. Sodium participates in cation exchange reactions which can ultimately cause the structure of medium and fine textured soils to degrade, especially if the EC of the soil is not also

correspondingly high. Better knowledge of the extent to which tile drainage systems can successfully remediate sodium would be an important advancement.

8.3.2 Site Management

Site remediation with tile drainage systems is generally a balance between the costs of installation, the costs of dealing with the associated produced saline water and the potential environmental benefit of restoring the original land-use capability of the soils. While closely spaced tile drain lines may produce more salt mass over time and therefore decrease the remediation time for the soils, they also produce greater volumes of saline water and have increased costs associated with materials, installation and disposal of the produced water. Irrigation was also shown to decrease total remediation time if the net water deficit at the site can be overcome; however, it would not be environmentally responsible to remove large quantities of valuable freshwater from the hydrosphere for this purpose since the saline water produced by the tile drainage system is ultimately deep-well injected. The water produced by the tile drain field could be treated onsite with reverse osmosis (RO) technology and re-used as irrigation water; however, this can also very expensive due to system energy requirements and RO conversion rates (the percentage of treated water obtained from incoming water) often range only between 10% and 50%. If the salt source has been removed and groundwater receptors are not threatened, tile drainage with passive infiltration may often be the most environmentally responsible, if not most time-efficient, management practice for shallow subsurface salt remediation.

REFERENCES

Agricultural and Rural Development Act, 1967. Edmonton - 83H, Soil Capability for Agriculture, Canada Land Inventory. Queen's Printer, Ottawa, Ontario.

Akhter, J., Mahmood, K., Malik, K.A., Ahmed, S. and Murray, R., 2003. Amelioration of a saline sodic soil through cultivation of a salt-tolerant grass *Leptochloa fusca*. Environmental Conservation, 30(2): 168-174.

Alberta Community Development, 2004. Alberta Natural Heritage Information Centre. Government of Alberta.

Alberta Energy and Utilities Board, 1998. Pipeline Performance in Alberta 1980-1997. Report 98-G, Calgary, Alberta.

Alberta Environment, 2001. Salt Contamination Assessment and Remediation Guidelines, Environmental Sciences Division - Alberta Environment, Edmonton, Alberta.

Alberta Environment, 2003. Water for Life: Alberta's Strategy for Sustainability. V955, Edmonton, Alberta.

AMEC Earth and Environmental, 2007. 04-05-50-26 W4M - Devon Alberta Recommendations for 2007, Edmonton, Alberta.

Anderson, M.P. and Woessner, W.W., 2002. Applied Groundwater Modeling: Simulation of Flow and Advective Transport. Academic Press, San Diego, California, 381 pp.

Appelo, C.A.J. and Postma, D., 1996. Geochemistry, Groundwater and Pollution. A.A. Balkema, Rotterdam, 536 pp.

Aringhieri, R. and Giachetti, M., 2001. Effect of sodium adsorption ratio and electrolyte concentrations on the saturated hydraulic conductivity of clay-sand mixtures. European Journal of Soil Science, 52: 449-458.

Baier, W. and Robertson, G.W., 1996. Soil moisture modelling - conception and evolution of the VSMB. Canadian Journal of Soil Science, 76: 251-261.

Bassil, E.S. and Kaffka, S.R., 2002. Response of safflower (*Carthamus tinctorius* L.) to saline soils and irrigation I. Consumptive water use. Agricultural Water Management, 54: 67-80.

Bevington, P.R., 1969. Data reduction and error analysis for the physical sciences. McGraw-Hill Book Company, New York.

Boivin, A., Simunek, J., Schiavon, M. and Van Genuchten, M.T., 2006. Comparison of Pesticide Transport Processes in Three Tile-Drained Field Soils Using HYDRUS-2D. Vadose Zone Journal, 5: 838-849.

Boufadel, M.C., Suidan, M.T. and Venosa, A.D., 1999. Numerical modeling of water flow below dry salt lakes: effect of capillarity and viscosity. Journal of Hydrology, 221: 55-74.

Bowser, W.E., Kjearsgaard, A.A., Peters, T.W. and Wells, R.E., 1962. Soil Survey of Edmonton: Sheet 83H, Bulletin No. SS-4, Alberta Soil Survey Report No. 21. University of Alberta, Edmonton, Alberta.

Canadian Association of Petroleum Producers, 2006. Alberta's Oil and Gas Royalties: How Alberta Gains from Higher Prices, Calgary, Canada.

Coquet, Y., Simunek, J., Coutadeur, C., van Genuchten, M.T., Pot, V. and Roger-Estrade, J., 2005. Water and Solute Transport in a cultivated silt loam soil: 2. Numerical Analysis. Vadose Zone Journal, 4: 587-601.

Croucher, A.E. and O'Sullivan, M.J., 1995. The Henry Problem for Saltwater Intrusion. Water Resources Research, 31(7): 1809-1814.

Davis, D.M., Gowda, P.H., Mulla, D.J. and Randall, G.W., 2000. Modeling Nitrate Nitrogen Leaching in Response to Nitrogen Fertilizer Rate and Tile Drain Depth or Spacing for Southern Minnesota, USA. Journal of Environmental Quality, 29: 1568-1581.

Domenico, P.A. and Schwartz, F.W., 1998. Physical and Chemical Hydrogeology. John Wiley and Sons Inc., New York, 506 pp.

Elder, J.W., 1967. Transient Convection in a Porous Medium. Journal of Fluid Mechanics, 27: 609-623.

Environment Canada, 2007a. Canadian Climate Normals 1971-2000. Environment Canada Weather Office.

Environment Canada, 2007b. Daily Data Report January 1984-October 2006, Calmar, Alberta.

Fetter, C.W., 2001. Applied Hydrogeology. Prentice Hall Inc., Upper Saddle River, New Jersey, 598 pp.

Freeze, R.A. and Cherry, J.A., 1979. Groundwater. Prentice Hall Inc., Englewood Cliffs, New Jersey, 604 pp.

Gee, G.W. and Bauder, J.W., 1986. Particle-size Analysis. Methods of Soil Analysis: Part 1. Physical and Mineralogical Methods, 9. American Society of Agronomy, Soil Science Society of America, Madison, Wisconsin, 1188 pp.

Gelhar, L.W., Welty, C. and Rehfeldt, K.R., 1992. A Critical Review of Data on Field-Scale Dispersion in Aquifers. Water Resources Research, 28(7): 1955-1974.

Groundwater Information Centre, 2007. Water Well Drilling Reports. Alberta Environment Groundwater Information Website.

Guan, J. and Aral, M.M., 1999. Optimal remediation with well locations and pumping rates selected as continuous decision variables. Journal of Hydrology, 221: 20-42.

Hallberg, G.R., Baker, J.L. and Randall, G.W., 1986. Utility of tileline effluent studies to evaluate the impact of agricultural practices on ground water, In Proceedings of Conference on Agricultural Impacts on Ground Water. National Water Well Association, Omaha, Nebraska.

Health Canada, 2006. Guidelines for Canadian Drinking Water Quality - Summary Table, Federal-Provincial-Territorial Committee on Drinking Water, Ottawa, Canada.

Henderson, T.H., Mayer, K.U., Parker, B.L. and Al, T.A., 2007. Development of a Three-Dimensional Multicomponent Reactive Transport Model of Density Driven Potassium Permanganate Oxidation of Trichloroethylene (in preparation).

Henry, H.R., 1964. Interfaces between salt water and fresh water in coastal aquifers, US Geological Survey Water-Supply Paper 1613-C, Sea Water in Coastal Aquifers: C35-C70.

Hitchon, B., Gunter, W.D. and Perkins, E.D., 1998. Introduction to Groundwater Chemistry and SOLMINEQGW. Geoscience Publishing Ltd., Sherwood Park, Alberta.

Hornbuckle, J.W., Christen, E.W. and Faulkner, R.D., 2007. Evaluating a multi-level subsurface drainage system for improved drainage water quality. Agricultural Water Management, 89: 208-216.

Kladivko, E.J., Frankenberger, J.R., Jaynes, D.B., Meek, D.W., Jenkinson, B.J. and Fausey, N.R., 2004. Nitrate Leaching to Subsurface Drains as Affected by Drain Spacing and Changes in Crop Production System. Journal of Environmental Quality, 33: 1803-1813.

Kladivko, E.J., Van Scoyoc, G.E., Monke, E.J., Oates, K.M. and Pask, W., 1991. Pesticide and nutrient movement into subsurface tile drains on a silt loam soil in Indiana. Journal of Environmental Quality, 20: 264-270.

Klute, A., 1986. Water Retention: Laboratory Methods. Methods of Soil Analysis: Part 1. Physical and Mineralogical Methods, 9. American Society of Agronomy Inc., Soil Science Society of America Inc., Madison, Wisconsin, 1188 pp.

Kolditz, O., Ratke, R., Diersch, H.-J.G. and Zielke, W., 1998. Coupled groundwater flow and transport: 1. Verification of variable density flow and transport models. Advances in Water Resources, 21(1): 27-46.

Kung, K.-J.S., Kladivko, E.J., Gish, T.J., Steenhuis, T.S., Bubenzer, G. and Helling, C.S., 2000. Quantifying preferential flow by breakthrough of sequentially applied tracers. Soil Science Society of America Journal, 64: 1296-1304.

Marr-Laing, T. and Severson-Baker, C., 1999. Beyond Eco-Terrorism: The Deeper Issues Affecting Alberta's Oilpatch. The Pembina Institute for Appropriate Development, Drayton Valley, Alberta.

Mayer, K.U., Frind, E.O. and Blowes, D.W., 2002. Multicomponent reactive transport modeling in variably saturated porous media using a generalized formulation for kinetically controlled reactions. Water Resources Research, 38(9): 2001WR000862.

Meadows, D.G., Young, M.H. and McDonald, E.V., 2005. A Laboratory Method for Determining the Unsaturated Hydraulic Properties of Soil Peds. Soil Science Society of America Journal, 69: 807-815.

Mohanty, B.P., Bowman, R.W. and Hendrickx, M.H., 1998. Preferential transport of nitrate to a tile drain in an intermittent-flood-irrigated field: Model development and experimental evaluation. Water Resources Research, 34(5): 1061-1076.

Mossop, G. and Shetsen, I., 1994. Geological Atlas of the Western Canada Sedimentary Basin. Canadian Society of Petroleum Geologists and the Alberta Research Council.

Nichols, W.E. and Freshley, M.D., 1993. Uncertainty Analyses of Unsaturated Zone Travel Time at Yucca Mountain. Ground Water, 31(2): 293-301.

Nosetto, M.D., Jobbagy, E.G., Toth, T. and Di Bella, C.M., 2007. The effects of tree establishment on water and salt dynamics in naturally salt-affected grasslands. Oecologia, 152: 695-705.

Oldenburg, C.M. and Pruess, K., 1995. Dispersive transport dynamics in a strongly coupled groundwater-brine flow system. Water Resources Research, 31(2): 289-302.

OMAFRA, 1996. Census of Agriculture and Policy and Programs Branch., Ontario Ministry of Agriculture, Food and Rural Affairs.

Prairie Farm Rehabilitation Administration, 1999. Leduc County, Part of the North Saskatchewan River Basin, Parts of Tp 047 to 051, R 21 to 28, W4M and R 01 to 04, W5M Regional Groundwater Assessment. Hydrogeological Consultants Ltd.

Province of Alberta, 1992. Environmental Protection and Enhancement Act. Ministry of Environment and Sustainable Resource Development, Queen's Printer, pp. 162.

Rausch, R., Schafer, W., Therrien, R. and Wanger, C., 2005. Solute Transport Modelling: An introduction to Models and Solutions Strategies. Gebruder Borntraeger Verlagsbuchhandlung, Stuttgart, Germany, 205 pp.

Richard, T.L. and Steenhuis, T.S., 1988. Tile Drain Sampling of Preferential Flow on a Field Scale. Journal of Contaminant Hydrology, 3: 307-325.

Richards, L.A., 1954. Diagnosis and improvement of saline and alkali soil, Department of Agriculture Agricultural Handbook 60.

Schaap, M.G. and Leij, F.J., 1998. Database-related accuracy and uncertainty of pedotransfer functions. Soil Science, 163(10): 765-779.

Schaap, M.G., Leij, F.J. and van Genuchten, M.T., 2001. ROSETTA: a computer program for estimating soil hydraulic parameters with hierarchical pedotransfer functions. Journal of Hydrology, 251: 163-176.

Scheidegger, A.E., 1957. The physics of flow through porous media. University of Toronto Press, Toronto, 313 pp.

Segol, G., 1994. Classic Groundwater Simulations - Proving and Improving Numerical Models. PTR Prentice Hall, Englewood Cliffs, New Jersey.

Shouse, P.J., Russell, W.B., Burden, D.S., Selim, H.M., Sisson, J.B. and Van Genuchten, M.T., 1995. Spatial variability of soil water retention functions in a silt loam soil. Soil Science, 159(1): 1-12.

Simpson, M.J. and Clement, T.P., 2003. Theoretical analysis of the worthiness of Henry and Elder problems as benchmarks of density-dependent groundwater flow models. Advances in Water Resources, 26: 17-31.

Simpson, M.J. and Clement, T.P., 2004. Improving the worthiness of the Henry Problem as a benchmark for density-dependent groundwater flow models. Water Resources Research, 40: W01504, 1-11.

Simunek, J., Hopmans, J.W., Nielsen, D.R. and van Genuchten, M.T., 2000. Horizontal Infiltration Revisited Using Parameter Estimation. Soil Science, 165(9): 708-717.

Skaggs, R.W., Breve, M.A. and Gilliam, J.W., 1994. Hydrologic and water quality impacts of agricultural drainage. Critical Reviews in Environmental Science and Technology, 24(1): 1-32.

Smettem, K.R.J., Trudgill, S.T. and Pickles, A.M., 1983. Nitrate loss in soil drainage water in relation to by-passing flow and discharge on an arable site. Journal of Soil Science, 34: 499-509.

Steefel, C.I. and Lasaga, A.C., 1994. A coupled model for transport of multiple chemical species and kinetic precipitation/dissolution reactions with application to reactive flow in single phase hydrothermal systems. American Journal of Science, 294: 529-592.

Sumner, M.E., 1993. Sodic Soils: New Perspectives. Australian Journal of Soil Research, 31: 683-750.

Therrien, R. and Sudicky, E.A., 1996. Three-dimensional analysis of variably-saturated flow and solute transport in discretely-fractured porous media. Journal of Contaminant Hydrology, 23: 1-44.

Tiedeman, C.R., Hill, M.C., D'Agnese, F.A. and Faunt, C.C., 2003. Methods for using groundwater model predictions to guide hydrogeologic data collection, with application to the Death Valley regional groundwater flow system. Water Resources Research, 39(1): 17p.

van Genuchten, M.T., 1980. A Closed-form Equation for Predicting the Hydraulic Conductivity of Unsaturated Soils. Soil Science Society of America Journal, 44: 892-898.

VanderKwaak, J.E., Forsyth, J.E., MacQuarrie, K.T.B. and Sudicky, E.A., 1997. WatSolv Sparse Matrix Iterative Solver - User's Guide. University of Waterloo, Waterloo, Ontario.

Voss, C.I. and Souza, W.R., 1987. Variable Density Flow and Solute Transport Simulation of Regional Aquifers Containing a Narrow Freshwater-Saltwater Transition Zone. Water Resources Research, 23(10): 1851-1866.

Wessolek, G., Plagge, R., Leij, F.J. and van Genuchten, M.T., 1994. Analysing problems in describing field and laboratory measured soil hydraulic properties. Geoderma, 64: 93-110.

Wilson, S., Griffiths, M. and Anielski, M., 2001. The Alberta GPI Accounts: Wetlands and Peatlands, The Pembina Institute, Drayton Valley, Alberta.

Wise, W.R., Clement, T.P. and Molz, F.J., 1994. Variably saturated modeling of transient drainage: sensitivity to soil properties. Journal of Hydrology, 161: 91-108.

WorelyParsons Komex, 2005a. 04-05-50-26 W4M Water Act Approval #00136300-00-00: 2004 Annual Report, WorelyParsons Komex, Calgary, Alberta.

WorelyParsons Komex, 2005b. 2004 Monitoring Program 04-05-50-26 W4M Drainage Field. E04600913-17, WorelyParsons Komex, Edmonton, Alberta.

Zhu, J. and Mohanty, B.P., 2002. Spatial Averaging of van Genuchten Hydraulic Parameters for Steady-State Flow in Heterogeneous Soils: A Numerical Study. Vadose Zone Journal, 1: 261-272.

APPENDIX A: GRAIN SIZE ANALYSIS DATA

CO4-01				
Depth (m)	% sand	% silt	% clay	Textural Class
0.5	24.0	58.0	18.0	Silt Loam
1.0	24.5	57.0	18.5	Silt Loam
1.5	28.5	56.5	15.0	Silt Loam
2.0	52.5	34.0	13.5	Loam
2.5	40.5	42.5	17.0	Loam

CO4-02				
Depth (m)	% sand	% silt	% clay	Textural Class
0.5	8.5	66.0	25.5	Silt Loam
1.0	44.5	46.5	9.0	Loam
1.5	35.0	44.5	20.5	Loam
2.0	39.0	45.5	15.5	Loam
2.5	41.5	44.0	14.5	Loam
3.0	39.5	33.5	27.0	Loam
3.5	43.0	41.0	16.0	Loam
4.0	55.5	35.0	9.5	Sandy Loam
4.5	9.5	70.5	20.0	Silt Loam
5.0	8.5	68.0	23.5	Silt Loam
5.5	6.0	74.0	20.0	Silt Loam

CO4-03				
Depth (m)	% sand	% silt	% clay	Textural Class
0.5	36.5	47.5	16.0	Loam
1.0	25.0	57.5	17.5	Silt Loam
1.5	27.0	52.0	21.0	Silt Loam
2.0	40.0	41.0	19.0	Loam
2.5	40.5	41.5	18.0	Loam

SWRC CORE SAMPLES				
Sample	% sand	% silt	% clay	Textural Class
1	11.27	65.77	22.96	Silt Loam
1D	10.66	68.86	20.48	Silt Loam
2	12.47	73.92	13.60	Silt Loam
2D	13.40	73.16	13.44	Silt Loam
3	19.38	59.91	20.71	Silt Loam
3D	20.38	65.84	13.78	Silt Loam
4	18.04	71.67	10.29	Silt Loam
4D	17.11	61.34	21.55	Silt Loam

APPENDIX A: GRAIN SIZE ANALYSIS DATA

CO6-01				
Depth (m)	**% sand**	**% silt**	**% clay**	**Textural Class**
1.40	19.85	66.40	13.75	Silt Loam
1.80	26.66	58.07	15.27	Silt Loam
2.50	38.88	49.98	11.14	Loam
3.00	37.87	49.70	12.43	Loam
3.80	44.19	45.82	10.00	Loam
4.40	38.73	51.43	9.83	Silt Loam
4.70	37.38	52.65	9.97	Silt Loam
5.30	32.17	54.75	13.09	Silt Loam
5.60	31.78	59.16	9.06	Silt Loam
6.20	32.09	57.01	10.90	Silt Loam

CO6-03				
Depth (m)	**% sand**	**% silt**	**% clay**	**Textural Class**
1.50	21.42	65.56	13.02	Silt Loam
2.00	22.20	67.57	10.23	Silt Loam
A	20.66	59.35	19.99	Silt Loam
B	22.83	61.11	16.06	Silt Loam
C	18.61	61.78	19.61	Silt Loam
D	33.22	63.68	3.10	Silt Loam
E	19.96	67.31	12.73	Silt Loam
F	19.00	57.20	23.80	Silt Loam

A	0.10 to 0.20 m section
B	Top of 1.5m
C	Section below 2.0m
D	0.38 - 0.46 m section
E	0-0.1 m section
F	0.20 m to 0.30 m section

CO6-05				
Depth (m)	**% sand**	**% silt**	**% clay**	**Textural Class**
1.50	9.87	75.15	14.98	Silt Loam
2.10	47.51	43.34	9.14	Loam
3.00	39.58	49.45	10.97	Loam
3.80	50.97	42.50	6.53	Loam
4.70	37.05	49.03	13.91	Loam
5.20	37.54	53.79	8.68	Silt Loam

APPENDIX A: GRAIN SIZE ANALYSIS DATA

CO6-02				
Depth (m)	**% sand**	**% silt**	**% clay**	**Textural Class**
1.50	49.07	45.33	5.59	Sandy Loam
2.00	41.97	43.20	14.83	Loam
3.00	40.93	49.35	9.72	Loam
4.00	31.77	57.64	10.59	Silt Loam
4.50	31.30	55.46	13.24	Silt Loam
5.00	38.70	50.98	10.32	Silt Loam

CO6-04				
Depth (m)	**% sand**	**% silt**	**% clay**	**Textural Class**
0.70	Insufficient soil for sampling			
1.30	Insufficient soil for sampling			
2.10	35.13	52.55	12.32	Silt Loam
2.90	41.13	46.48	12.40	Loam
3.20	41.15	45.55	13.30	Loam
4.00	50.68	40.54	8.78	Silt Loam
4.50	43.38	49.53	7.09	Loam
5.20	81.49	15.14	3.37	Loamy Sand
5.70	90.66	6.47	2.87	Sand
6.00	50.27	41.52	8.22	Loam
7.00	49.87	36.12	14.01	Loam
7.60	51.91	41.06	7.03	Loam

CO6-08				
Depth (m)	**% sand**	**% silt**	**% clay**	**Textural Class**
1.40	32.72	55.64	11.64	Silt Loam
2.30	26.58	57.79	15.64	Silt Loam
2.70	33.10	59.06	7.84	Silt Loam
3.80	41.88	52.50	5.63	Silt Loam

APPENDIX B: SOIL WATER RETENTION CURVE EXPERIMENTAL DATA AND ERROR ANALYSIS RESULTS

Sample	Suction Head (m)	Average Soil Height (cm)	Wet Weight (g)	Volumetric Water θ (m^3/m^3)	Estimated Error* $\Delta\theta$ (m^3/m^3)
1	saturated	3.60	62.8	0.574837	0.0731
	0.01	3.50	61.0	0.537780	0.0688
	0.17	3.40	59.5	0.507719	0.0654
	0.31	3.30	58.5	0.491592	0.0637
	0.61	3.22	57.4	0.468281	0.0611
	1.20	3.17	56.2	0.436301	0.0571
	2.26	3.10	55.3	0.415963	0.0548
	5.12	3.08	54.2	0.381524	0.0504
	10.00	3.04	53.4	0.359178	0.0476
	19.99	2.95	52.4	0.334885	0.0448
	45.00	2.85	50.8	0.288255	0.0390
	oven dry weight		42.9 g		
1D	saturated	3.80	71.2	0.574685	0.0724
	0.01	3.80	69.5	0.528163	0.0665
	0.17	3.70	68.3	0.508711	0.0644
	0.31	3.67	67.4	0.487368	0.0618
	0.61	3.63	66.1	0.455496	0.0579
	1.20	3.60	65.0	0.427517	0.0545
	2.26	3.52	63.9	0.404736	0.0518
	5.12	3.49	62.8	0.375439	0.0482
	10.00	3.41	62	0.359850	0.0464
	19.99	3.38	60.9	0.329201	0.0426
	45.00	3.32	59.9	0.303828	0.0395
	oven dry weight		50.2 g		
2	saturated	3.25	58.5	0.559950	0.0728
	0.01	3.21	56.1	0.489177	0.0638
	0.17	3.19	54.4	0.436826	0.0571
	0.31	3.17	53.7	0.416619	0.0546
	0.61	3.13	52.9	0.395364	0.0520
	1.20	3.09	51.9	0.366828	0.0484
	2.26	3.06	51.2	0.346635	0.0459
	5.12	3.00	50.4	0.325837	0.0434
	10.00	2.97	49.8	0.308120	0.0412
	19.99	2.92	49.3	0.295590	0.0397
	45.00	2.85	48.4	0.270011	0.0366
	oven dry weight		41.0 g		

APPENDIX B: SOIL WATER RETENTION CURVE EXPERIMENTAL DATA AND ERROR ANALYSIS RESULTS

Sample	Suction Head (m)	Average Soil Height (cm)	Wet Weight (g)	Volumetric Water θ (m^3/m^3)	Estimated Error* $\Delta\theta$ (m^3/m^3)
2D	saturated	2.90	53.4	0.552226	0.0738
	0.01	2.87	50.6	0.456544	0.0613
	0.17	2.86	49.5	0.418144	0.0562
	0.31	2.84	49.0	0.402781	0.0543
	0.61	2.83	48.6	0.390195	0.0527
	1.20	2.77	48.0	0.375417	0.0510
	2.26	2.75	47.5	0.359240	0.0489
	5.12	2.71	47.0	0.345356	0.0473
	10.00	2.67	46.6	0.334951	0.0461
	19.99	2.64	46.1	0.319062	0.0441
	45.00	2.55	45.3	0.297699	0.0416
	oven dry weight	38.0 g			
3	saturated	3.60	65.2	0.424628	0.0541
	0.01	3.45	64.3	0.415963	0.0534
	0.17	3.43	63.3	0.388070	0.0499
	0.31	3.40	63.0	0.382319	0.0493
	0.61	3.37	62.5	0.370293	0.0479
	1.20	3.31	62.0	0.361297	0.0469
	2.26	3.28	61.4	0.345579	0.0450
	5.12	3.21	60.7	0.330438	0.0432
	10.00	3.18	60.1	0.313934	0.0412
	19.99	3.15	59.4	0.293815	0.0387
	45.00	3.12	58.6	0.269976	0.0357
	oven dry weight	50.5 g			
3D	saturated	3.15	60.2	0.515001	0.0675
	0.01	3.10	57.4	0.429381	0.0565
	0.17	3.05	56.2	0.395505	0.0523
	0.31	3.04	55.7	0.379703	0.0503
	0.61	3.03	55.1	0.360959	0.0479
	1.20	3.00	54.5	0.343169	0.0456
	2.26	2.98	53.9	0.324535	0.0433
	5.12	2.96	53.2	0.302135	0.0404
	10.00	2.94	52.7	0.286505	0.0384
	19.99	2.93	52.3	0.273753	0.0368
	45.00	2.86	51.4	0.247250	0.0335
	oven dry weight	44.6 g			

**APPENDIX B: SOIL WATER RETENTION CURVE EXPERIMENTAL DATA
AND ERROR ANALYSIS RESULTS**

Sample	Suction Head (m)	Average Soil Height (cm)	Wet Weight (g)	Volumetric Water θ (m³/m³)	Estimated Error* $\Delta\theta$ (m³/m³)
4	saturated	3.35	63.2	0.465630	0.0602
	0.01	3.25	60.7	0.399964	0.0521
	0.17	3.22	59.6	0.368166	0.0481
	0.31	3.16	59.0	0.355411	0.0466
	0.61	3.14	58.5	0.341116	0.0449
	1.20	3.07	58.0	0.332499	0.0440
	2.26	3.04	57.6	0.321550	0.0427
	5.12	2.97	57.1	0.311622	0.0416
	10.00	2.95	56.7	0.299634	0.0401
	19.99	2.93	56.3	0.287483	0.0386
	45.00	2.90	55.5	0.261770	0.0353
		oven dry weight	48.2 g		
4D	saturated	3.60	66.1	0.415963	0.0530
	0.01	3.53	64.6	0.380022	0.0486
	0.17	3.49	63.5	0.351602	0.0451
	0.31	3.47	63.0	0.338644	0.0435
	0.61	3.43	62.6	0.330466	0.0426
	1.20	3.35	62.2	0.325941	0.0422
	2.26	3.32	61.8	0.316357	0.0411
	5.12	3.27	61.3	0.305294	0.0398
	10.00	3.23	60.9	0.296196	0.0387
	19.99	3.18	60.4	0.284503	0.0374
	45.00	3.10	59.7	0.268363	0.0355
		oven dry weight	51.7 g		

Notes:

*   calculated using the method of Bevington (1969).

APPENDIX C: HYDRAULIC HEAD DATA

Monitoring Well	Date	Groundwater Elevation (m)	Monitoring Well	Date	Groundwater Elevation (m)
Shallow Wells (installed 2003)			**Shallow Wells (installed 2003)**		
P04-1A	5-Aug-04	<722.66	P04-3A	5-Aug-04	723.67
	13-Sep-04	<722.66		13-Sep-04	723.20
	7-Oct-04	<722.66		7-Oct-04	723.04
	10-Nov-04	723.15		10-Nov-04	722.91
	30-Nov-04	723.04		30-Nov-04	722.92
	14-Apr-05	723.47		14-Apr-05	723.84
	9-May-05	723.07		9-May-05	723.67
	28-Jun-05	723.54		28-Jun-05	723.46
	19-Jul-05	723.15		19-Jul-05	723.28
	16-Aug-05	723.46		16-Aug-05	723.15
	15-Sep-05	723.80		15-Sep-05	723.25
	18-Oct-05	723.21		18-Oct-05	723.14
	22-Nov-05	723.39		22-Nov-05	723.06
	12-Dec-05	723.45		12-Dec-05	723.00
	24-Jan-06	723.04		24-Jan-06	722.84
	15-Feb-06	723.09		15-Feb-06	722.74
	7-Jun-06	723.34		7-Jun-06	722.71
	9-Aug-06	723.46		9-Aug-06	722.98
	13-Sep-06	723.76		13-Sep-06	722.82
	17-Oct-06	723.89		17-Oct-06	723.21
	15-Nov-06	---		15-Nov-06	---
	5-Dec-06	723.21		5-Dec-06	723.13
P04-2A	5-Aug-04	723.80	P04-4A	5-Aug-04	723.53
	13-Sep-04	723.55		13-Sep-04	723.08
	7-Oct-04	723.35		7-Oct-04	722.99
	10-Nov-04	723.12		10-Nov-04	722.92
	30-Nov-04	723.11		30-Nov-04	722.94
	14-Apr-05	724.23		14-Apr-05	---
	9-May-05	723.50		9-May-05	723.07
	28-Jun-05	723.48		28-Jun-05	723.13
	19-Jul-05	723.33		19-Jul-05	723.09
	16-Aug-05	723.24		16-Aug-05	723.07
	15-Sep-05	723.53		15-Sep-05	723.10
	18-Oct-05	723.27		18-Oct-05	723.07
	22-Nov-05	723.15		22-Nov-05	723.03
	12-Dec-05	723.09		12-Dec-05	723.01
	24-Jan-06	722.89		24-Jan-06	722.94
	15-Feb-06	722.79		15-Feb-06	722.87
	7-Jun-06	723.20		7-Jun-06	723.28
	9-Aug-06	723.15		9-Aug-06	723.00
	13-Sep-06	723.02		13-Sep-06	722.99
	17-Oct-06	723.47		17-Oct-06	723.27
	15-Nov-06	723.31		15-Nov-06	---
	5-Dec-06	723.38		5-Dec-06	723.05

Monitoring Well	Date	Groundwater Elevation (m)	Monitoring Well	Date	Groundwater Elevation (m)
Shallow Wells (installed 2003)			**Shallow Wells (abandoned 2003)**		
P04-5A	5-Aug-04	723.67	P98-1A	10-Nov-98	724.77
	13-Sep-04	723.38		21-Jan-98	723.90
	7-Oct-04	723.27		17-Feb-99	723.82
	10-Nov-04	723.09		1-Mar-99	723.71
	30-Nov-04	723.11		8-Mar-99	723.71
	14-Apr-05	723.26		29-Jun-99	724.81
	9-May-05	723.59			
	28-Jun-05	723.54	P98-2A	10-Nov-98	724.63
	19-Jul-05	723.41		21-Jan-98	724.00
	16-Aug-05	723.31		17-Feb-99	723.91
	15-Sep-05	723.40		17-Mar-99	723.76
	18-Oct-05	723.29		29-Jun-99	724.85
	22-Nov-05	723.20			
	12-Dec-05	723.16	P98-3A	10-Nov-98	724.75
	24-Jan-06	722.99		29-Jun-99	724.67
	15-Feb-06	722.87			
	7-Jun-06	723.53	P98-4A	10-Nov-98	724.06
	9-Aug-06	723.15		17-Feb-99	723.42
	13-Sep-06	723.00		1-Mar-99	723.33
	17-Oct-06	723.34		8-Mar-99	723.31
	15-Nov-06	723.05		29-Jun-99	724.11
	5-Dec-06	723.28			
			P98-5A	10-Nov-98	723.88
P04-6A	5-Aug-04	723.42		21-Jan-98	723.59
	13-Sep-04	723.10		17-Feb-99	723.38
	7-Oct-04	723.07		1-Mar-99	723.34
	10-Nov-04	723.02		8-Mar-99	723.29
	30-Nov-04	723.07		29-Jun-99	724.14
	14-Apr-05	723.29			
	9-May-05	723.33	P99-6A	8-Mar-99	723.45
	28-Jun-05	723.26		17-Mar-99	723.41
	19-Jul-05	723.19		29-Jun-99	724.37
	16-Aug-05	723.18			
	15-Sep-05	723.17	P99-6B	29-Jun-99	724.62
	18-Oct-05	723.12			
	22-Nov-05	723.15	P99-7A	8-Mar-99	723.61
	12-Dec-05	723.13		17-Mar-99	723.64
	24-Jan-06	722.99		29-Jun-99	724.70
	15-Feb-06	722.75			
	7-Jun-06	723.39			
	9-Aug-06	722.98			
	13-Sep-06	722.23			
	17-Oct-06	722.97			
	15-Nov-06	---			
	5-Dec-06	723.11			

Monitoring Well	Date	Groundwater Elevation (m)	Monitoring Well	Date	Groundwater Elevation (m)
Deeper Wells			**Deeper Wells**		
P04-2B	5-Aug-04	723.74	P99-8C	8-Mar-99	711.86
	13-Sep-04	723.42		17-Mar-99	711.73
	7-Oct-04	723.35		17-Mar-99	711.79
	10-Nov-04	723.18		29-Jun-99	711.96
	30-Nov-04	723.18		12-Nov-02	711.30
	14-Apr-05	723.35		30-Jul-04	710.96
	9-May-05	723.28		5-Aug-04	710.95
	28-Jun-05	723.31		13-Sep-04	710.96
	19-Jul-05	723.35		7-Oct-04	710.99
	16-Aug-05	723.29		10-Nov-04	710.74
	15-Sep-05	723.40		30-Nov-04	710.91
	18-Oct-05	723.32		14-Apr-05	710.97
	22-Nov-05	723.21		9-May-05	710.91
	12-Dec-05	723.16		28-Jun-05	710.84
	24-Jan-06	722.99		19-Jul-05	710.83
	15-Feb-06	722.91		16-Aug-05	710.76
	7-Jun-06	723.74		15-Sep-05	710.78
	9-Aug-06	723.17		18-Oct-05	710.81
	13-Sep-06	723.11		22-Nov-05	710.83
	17-Oct-06	723.44		12-Dec-05	710.85
	5-Dec-06	723.31		24-Jan-06	710.77
P99-8B	17-Jun-99	724.73		15-Feb-06	710.72
	29-Jun-99	724.85		7-Jun-06	710.72
	12-Nov-02	722.84		9-Aug-06	709.70
	30-Jul-04	724.53		13-Sep-06	710.70
	5-Aug-04	724.39		17-Oct-06	710.71
	13-Sep-04	724.72		15-Nov-06	---
	7-Oct-04	724.37		5-Dec-06	710.78
	10-Nov-04	724.27			
	30-Nov-04	724.17	P99-9C	8-Mar-99	721.56
	14-Apr-05	724.90		17-Mar-99	721.51
	9-May-05	724.66		17-Mar-99	723.83
	28-Jun-05	723.90		29-Jun-99	723.89
	19-Jul-05	724.50			
	16-Aug-05	724.32			
	15-Sep-05	724.71			
	18-Oct-05	724.50			
	22-Nov-05	724.30			
	12-Dec-05	724.13			
	24-Jan-06	723.71			
	15-Feb-06	723.48			
	7-Jun-06	724.37			
	9-Aug-06	723.96			
	13-Sep-06	723.69			
	17-Oct-06	724.50			
	5-Dec-06	724.30			

APPENDIX D: INFILTRATION DATA

Date	Top Boundary Infiltration (mm)	Date	Top Boundary Infiltration (mm)
Jan-84	0.00	Jan-87	0.00
Feb-84	0.00	Feb-87	0.01
Mar-84	12.82	Mar-87	5.29
Apr-84	-17.56	Apr-87	-15.97
May-84	36.49	May-87	28.52
Jun-84	-11.83	Jun-87	-26.61
Jul-84	-62.81	Jul-87	-24.80
Aug-84	-20.79	Aug-87	4.13
Sep-84	112.85	Sep-87	-1.55
Oct-84	0.70	Oct-87	-4.75
Nov-84	0.00	Nov-87	2.52
Dec-84	0.00	Dec-87	0.07
Total (mm/yr)	**49.87**	**Total (mm/yr)**	**-33.15**
Jan-85	0.00	Jan-88	-0.60
Feb-85	0.00	Feb-88	6.58
Mar-85	53.64	Mar-88	-0.13
Apr-85	15.70	Apr-88	-4.41
May-85	-7.81	May-88	-15.12
Jun-85	-19.07	Jun-88	13.67
Jul-85	-68.02	Jul-88	-24.14
Aug-85	11.20	Aug-88	24.34
Sep-85	23.60	Sep-88	38.76
Oct-85	4.81	Oct-88	-12.04
Nov-85	-1.82	Nov-88	-0.59
Dec-85	1.39	Dec-88	2.56
Total (mm/yr)	**13.63**	**Total (mm/yr)**	**28.91**
Jan-86	0.70	Jan-89	-0.08
Feb-86	2.44	Feb-89	0.00
Mar-86	4.60	Mar-89	0.00
Apr-86	11.13	Apr-89	-2.89
May-86	-6.00	May-89	32.04
Jun-86	-5.03	Jun-89	-13.12
Jul-86	25.14	Jul-89	-15.50
Aug-86	-76.59	Aug-89	7.64
Sep-86	77.47	Sep-89	-4.69
Oct-86	1.58	Oct-89	24.09
Nov-86	-0.12	Nov-89	8.95
Dec-86	0.00	Dec-89	0.30
Total (mm/yr)	**35.31**	**Total (mm/yr)**	**36.74**

Date	Top Boundary Infiltration (mm)	Date	Top Boundary Infiltration (mm)
Jan-90	0.00	Jan-93	0.00
Feb-90	0.00	Feb-93	0.09
Mar-90	0.22	Mar-93	24.19
Apr-90	20.13	Apr-93	4.63
May-90	-13.67	May-93	11.32
Jun-90	0.05	Jun-93	7.43
Jul-90	11.54	Jul-93	-33.54
Aug-90	-31.82	Aug-93	-22.21
Sep-90	-10.07	Sep-93	-3.24
Oct-90	20.78	Oct-93	2.18
Nov-90	-2.06	Nov-93	9.71
Dec-90	0.00	Dec-93	-0.43
Total (mm/yr)	**-4.90**	**Total (mm/yr)**	**0.14**
Jan-91	0.00	Jan-94	0.00
Feb-91	0.00	Feb-94	0.00
Mar-91	15.90	Mar-94	19.28
Apr-91	8.80	Apr-94	-20.60
May-91	67.87	May-94	12.93
Jun-91	21.19	Jun-94	7.06
Jul-91	-45.40	Jul-94	-29.81
Aug-91	-48.19	Aug-94	13.08
Sep-91	-10.50	Sep-94	15.78
Oct-91	6.23	Oct-94	0.32
Nov-91	2.39	Nov-94	0.81
Dec-91	0.00	Dec-94	0.00
Total (mm/yr)	**18.29**	**Total (mm/yr)**	**18.83**
Jan-92	0.00	Jan-95	0.00
Feb-92	0.14	Feb-95	0.00
Mar-92	101.57	Mar-95	2.44
Apr-92	2.61	Apr-95	-1.49
May-92	-5.02	May-95	-2.08
Jun-92	-62.21	Jun-95	-13.89
Jul-92	-26.78	Jul-95	10.87
Aug-92	-15.53	Aug-95	0.16
Sep-92	28.36	Sep-95	-33.76
Oct-92	-4.82	Oct-95	31.20
Nov-92	4.49	Nov-95	-0.61
Dec-92	-0.23	Dec-95	0.00
Total (mm/yr)	**22.55**	**Total (mm/yr)**	**-7.16**

Date	Top Boundary Infiltration (mm)	Date	Top Boundary Infiltration (mm)
Jan-96	0.00	Jan-99	0.00
Feb-96	0.00	Feb-99	0.00
Mar-96	3.15	Mar-99	0.00
Apr-96	21.73	Apr-99	17.64
May-96	9.26	May-99	33.88
Jun-96	31.18	Jun-99	-4.94
Jul-96	-27.63	Jul-99	8.01
Aug-96	-52.14	Aug-99	-27.45
Sep-96	32.48	Sep-99	-40.74
Oct-96	3.84	Oct-99	-2.22
Nov-96	-1.40	Nov-99	8.71
Dec-96	0.00	Dec-99	11.57
Total (mm/yr)	**20.47**	**Total (mm/yr)**	**4.46**
Jan-97	0.00	Jan-00	-0.05
Feb-97	0.00	Feb-00	0.00
Mar-97	18.05	Mar-00	10.53
Apr-97	78.11	Apr-00	-11.97
May-97	0.22	May-00	22.53
Jun-97	26.61	Jun-00	16.76
Jul-97	-41.07	Jul-00	15.10
Aug-97	-34.39	Aug-00	-55.05
Sep-97	20.55	Sep-00	6.50
Oct-97	19.23	Oct-00	-3.71
Nov-97	1.35	Nov-00	4.93
Dec-97	-0.45	Dec-00	0.20
Total (mm/yr)	**88.20**	**Total (mm/yr)**	**5.79**
Jan-98	-0.03	Jan-01	0.07
Feb-98	0.00	Feb-01	-0.94
Mar-98	0.16	Mar-01	7.23
Apr-98	-6.68	Apr-01	-13.17
May-98	3.10	May-01	-6.38
Jun-98	9.62	Jun-01	-1.22
Jul-98	-80.58	Jul-01	62.12
Aug-98	13.59	Aug-01	-64.82
Sep-98	28.75	Sep-01	2.95
Oct-98	34.92	Oct-01	5.17
Nov-98	0.02	Nov-01	9.78
Dec-98	0.00	Dec-01	0.00
Total (mm/yr)	**2.87**	**Total (mm/yr)**	**0.80**

Date	Top Boundary Infiltration (mm)	Date	Top Boundary Infiltration (mm)
Jan-02	0.00	Jan-05	0.00
Feb-02	0.00	Feb-05	0.00
Mar-02	0.00	Mar-05	11.16
Apr-02	20.67	Apr-05	-14.02
May-02	-20.28	May-05	5.75
Jun-02	-27.27	Jun-05	0.98
Jul-02	0.57	Jul-05	-40.69
Aug-02	-22.69	Aug-05	6.19
Sep-02	7.06	Sep-05	2.24
Oct-02	21.03	Oct-05	9.24
Nov-02	14.98	Nov-05	11.67
Dec-02	-0.44	Dec-05	1.61
Total (mm/yr)	**-6.38**	**Total (mm/yr)**	**-5.86**
Jan-03	0.53	Jan-06	-0.65
Feb-03	0.00	Feb-06	-3.47
Mar-03	13.98	Mar-06	0.00
Apr-03	37.19	Apr-06	5.12
May-03	-9.08	May-06	24.20
Jun-03	-8.68	Jun-06	-37.92
Jul-03	-51.61	Jul-06	-34.13
Aug-03	-5.92	Aug-06	-9.38
Sep-03	-1.65	Sep-06	62.94
Oct-03	6.45	Oct-06	29.29
Nov-03	-0.25	Nov-06	0.00
Dec-03	0.00	Dec-06	0.00
Total (mm/yr)	**-19.05**	**Total (mm/yr)**	**35.99**
Jan-04	0.00		
Feb-04	0.00		
Mar-04	70.66		
Apr-04	-6.12		
May-04	18.87		
Jun-04	-41.76		
Jul-04	-0.21		
Aug-04	-16.77		
Sep-04	36.14		
Oct-04	-5.89		
Nov-04	21.64		
Dec-04	0.20		
Total (mm/yr)	**76.77**		

APPENDIX E: 2004 TILE DRAINAGE WATER PRODUCTION

Date	Totaliser Meter Reading (m³)	Cumulative Volume (m³)	Comments
2-Apr-04	4.2	3488.1	
8-Apr-04	38.2	3522.1	
16-Apr-04	111.4	3595.3	
23-Apr-04	199.8	3683.7	
30-Apr-04	318.7	3802.6	
April Total	318.7		
7-May-04	427.1	3911.0	
14-May-04	504.2	3988.1	
21-May-04	550.1	4034.0	
27-May-04	619.5	4103.4	
May Total	300.8		
2-Jun-04	619.5	4103.4	
4-Jun-04	648.7	4132.6	
7-Jun-04	717.0	4200.9	System Shut In
June Total	97.5		
14-Jul-04	717.0	4200.9	System Shut In
16-Jul-04	744.5	4228.4	
19-Jul-04	756.1	4240.0	
21-Jul-04	776.5	4260.4	
23-Jul-04	777.9	4261.8	
26-Jul-04	777.9	4261.8	
28-Jul-04	783.9	4267.8	
30-Jul-04	832.0	4313.9	
July Total	115.0		
3-Aug-04	832.0	4315.9	
6-Aug-04	978.8	4462.7	
9-Aug-04	978.8	4462.7	
11-Aug-04	1078.0	4561.9	
13-Aug-04	1100.0	4583.9	
23-Aug-04	1100.0	4583.9	
25-Aug-04	1196.5	4680.4	
27-Aug-04	1210.5	4694.4	
30-Aug-04	1210.5	4694.4	
August Total	378.5		

Date	Totaliser Meter Reading (m³)	Cumulative Volume (m³)	Comments
1-Sep-04	1265.0	4748.9	
3-Sep-04	1277.1	4761.0	
7-Sep-04	1277.1	4761.0	
10-Sep-04	1283.0	4766.9	
20-Sep-04	1283.0	4766.9	
22-Sep-04	1318.7	4802.6	
24-Sep-04	1390.2	4874.1	
27-Sep-04	1390.2	4874.1	
29-Sep-04	1423.7	4907.6	
September Total	213.2		
1-Oct-04	1434.7	4918.6	
6-Oct-04	1464.8	4948.7	
8-Oct-04	1472.9	4956.8	
12-Oct-04	1472.9	4956.8	
15-Oct-04	1502.5	4986.4	
18-Oct-04	1502.5	4986.4	
20-Oct-04	1523.6	5007.5	
22-Oct-04	1531.5	5015.4	
25-Oct-04	1531.5	5015.4	
27-Oct-04	1549.6	5033.5	
29-Oct-04	1555.7	5039.6	
October Total	132.0		
1-Nov-04	1555.7	5039.6	
3-Nov-04	1570.2	5054.1	
5-Nov-04	1577.9	5061.8	
8-Nov-04	1577.9	5061.8	
10-Nov-04	1589.8	5073.7	
12-Nov-04	1595.4	5079.3	
15-Nov-04	1595.4	5079.3	
19-Nov-04	1616.4	5100.3	
22-Nov-04	1616.4	5100.3	
24-Nov-04	1621.3	5105.2	
26-Nov-04	1623.5	5107.4	
29-Nov-04	1623.5	5107.4	
November Total	67.8		
1-Dec-04	1647.5	5131.4	
3-Dec-04	1654.0	5137.9	
6-Dec-04	1654.0	5137.9	
7-Dec-04	1661.9	5145.8	System Shut In
December Total	38.4		
2004 Total	**1657.7**		